MANTLE XENOLITHS FROM THE ABRAHAMSKRAAL KIMBERLITE: A CRATON-MARGIN GEOTHERM

BY T.E. NOWICKI

This thesis is submitted in partial fulfilment of the requirements for the degree of Master of Science (Economic Geology) Rhodes University

October 1990

ABSTRACT

The Abrahamskraal kimberlite pipe (group I) occurs approximately 5 km to the south-west of the geophysically defined margin of the Kaapvaal craton in the central Cape Province, and contains a variety of crustal and mantle xenoliths. This study focusses on xenoliths of deep-seated origin (mantle and lower-crustal), and in particular on garnet-orthopyroxene bearing assemblages which are amenable to thermobarometric techniques. Four major types of deep-seated xenolith have been identified, i.e. peridotites, dunites, eclogites, and garnet pyroxenites. The petrographic features and mineral compositions of these xenoliths are described. Pressures and temperatures of equilibration have been calculated primarily using the garnet-orthopyroxene thermometer of Harley (1984), and the Al-in-enstatite barometer of Nickel and Green (1985).

The peridotites are coarse-textured (Harte, 1977), magnesium-rich rocks, and are typical examples of the common type I peridotites which generally dominate mantle xenolith suites in kimberlites. Garnet peridotite xenoliths define a geotherm which lies along a typical theoretical conductive geothermal gradient for shield areas (Pollack and Chapman, 1977), and which extends to a maximum pressure of 41 kb (~130 km). Comparison of the Abrahamskraal geotherm with that constructed for the northern Lesotho xenolith suite (calculated using the same thermobarometer couple), suggests that the lithosphere at the Namaqua/Kaapvaal boundary is not significantly thinner or hotter than that underlying the craton. Modelling of the craton boundary under the constraints provided by the Abrahamskraal geotherm, and by the distribution of diamond-bearing kimberlites in southern Africa, indicates that the Abrahamskraal kimberlite has sampled relatively thick, cool, Namaqua lithosphere. It is suggested that, in terms of diamond distribution, the age and magmatic history of the Namaqua lithosphere is of greater significance than its thickness.

Two varieties of dunite occur at Abrahamskraal. Coarse-textured dunites with Mg-rich olivine compositions similar to those of the peridotitic olivines, probably originated by similar (but perhaps more extreme) processes to those which formed the peridotites. A finer-grained and relatively Fe-rich variety of dunite may represent ultramafic cumulates formed by fractionation of basic or ultrabasic magmas within the mantle.

Two varieties of eclogite have been distinguished. Coarse-grained eclogites which yield relatively high temperature estimates, are believed to have originated from depths similar to those determined for the garnet peridotites, i.e. from the lower lithosphere. A distinctly finer grained variety of eclogite, yields significantly lower temperatures which may be based on frozen-in equilibria. A maximum depth of approximately 87 km (~27 kb) has been estimated for these xenoliths, but they may have originated from significantly shallower (possibly lower-crustal) levels.

The garnet pyroxenite xenoliths are generally orthopyroxene-rich rocks which contain varying amounts of garnet (8 to 33 %) and clinopyroxene (0 to 64 %). Textural features indicate that the garnet and possibly some of the clinopyroxene has exsolved from an originally Al-rich orthopyroxene. The rocks are significantly more Fe-rich than the peridotite xenoliths, and their constituent minerals show a wide range of Mg/Mg+Fe ratios. The pressure-temperature array defined by the garnet pyroxenites is approximately isothermal, and spans a depth range from approximately 30 to 95 km. It deviates strongly (to higher temperatures) from the ambient geothermal gradient at the time of kimberlite emplacement, as inferred from the garnet peridotite xenoliths. The pressures and temperatures calculated for the garnet pyroxenites are based on mineral equilibria which are believed to have been frozen-in during cooling from an intial high-temperature (probably molten) state. Qualitative modelling of possible cooling paths in pressure-temperature-composition space, indicates that the apparent depth range displayed by the garnet pyroxenites, approximates the true depth range over which these rocks were emplaced. However, the apparent pressures calculated from core compositions are significantly lower than the true pressures at which the original rocks formed. The garnet pyroxenite xenoliths appear to represent a major, possibly Namaqua-age (~1000-1400 Ma), magmatic event involving the emplacement of large amounts of mafic magma over a significant depth range in the shallow upper mantle.

CONTENTS

LIST OF FIGURES

LIST OF TABLES

LIST OF PLATES

1. INTRODUCTION

An increasing amount of evidence, both petrological and geophysical, suggests that old, stable, continental lithosphere forms a relatively thick, cool and rigid layer, which resists incorporation into the underlying convecting mantle (Harte and Hawkesworth, 1989). Kimberlites, generated near the base of the continental lithosphere by small degrees of partial melting of mantle peridotite (Wyllie, 1980, 1989; Eggler, 1989), intrude and sample the sub-continental lithosphere. Thus xenoliths of deep-seated origin included in kimberlites, provide Earth scientists with a direct means of studying this part of the Earth's mantle, as well as the lower-most portions of the continental crust. Other sources of deep-seated xenoliths include the alkali basalt-basanite-nephelinite series of igneous rocks (Menzies, 1983), and extremely alkaline continental volcanic rocks (e.g. minettes, monchiquites, alnoites, lamproites) related to kimberlites. Alkali basalts occur primarily in continental rift environments and their xenoliths reflect a thinner, hotter, and magmatically more active lithosphere than that represented by kimberlitic xenoliths (Harte and Hawkesworth, 1989).

This study deals with the deep-seated xenolith suite of the Abrahamskraal kimberlite pipe, and attention is focussed primarily on kimberlitic xenolith suites and the nature of the stable continental lithosphere. Diamonds are believed to be stable only in the lowermost portions of thick continental lithosphere, and hence this study is relevent to the understanding of the controls of diamond distribution, particularly in southern Africa.

1.1. Brief Overview of Deep-Seated Xenoliths in Kimberlites

Intensive study of mantle xenoliths from kimberlites, particularly over the last two decades, has revealed that the sub-continental lithospheric mantle is a heterogeneous body which has preserved evidence of a long and complex magmatic and metasomatic history (see Gurney and Harte, 1980; Harte, 1983; and Harte and Hawkesworth, 1989 for reviews).

The most abundant mantle xenoliths found in kimberlites are coarse, magnesium-rich peridotites (type I - Harte and Hawkesworth, 1989). These rocks are dominated by olivine and orthopyroxene, but commonly include minor amounts of garnet, clinopyroxene and/or Cr-rich spinel. Because of the relative abundance of type I peridotites, they are believed to constitute most of the lithospheric upper mantle. Their highly magnesian nature (Fo>91) , and strong depletion with respect to the basaltic components Ti, Al, Ca and Fe, suggests that these rocks are residues after extensive removal of basaltic and/or komatiitic partial melts from "fertile" peridotite (e.g. Nixon and Boyd, 1973a; Harte, 1983; Cox *et.al.*, 1987). In contrast to the major element data, many of the peridotites show enriched LREE patterns (e.g. Hawkesworth *et.al.*, 1983; Harte *et.al.*, 1987). These are believed to be the result of metasomatic events, some of which may have occurred as long ago as the late Archaean or early Proterozoic (Hawkesworth *et.al.*, 1983; Menzies *et.al.*, 1987). Other types of metasomatism which have affected the peridotites include: modal metasomatism, involving the introduction of new minerals such as phlogopite, amphibole and Fe-Ti oxides; and enrichment of the peridotites in major, minor and trace elements. In some cases the latter appears to be the result of chemical exchange between peridotitic mantle wall-rock and pyroxenitic intrusions (Harte *et.al.*, 1987).

A second group of peridotite xenoliths (type V - Harte and Hawkesworth, 1989) differ markedly, in terms of both texture and composition, from those described above. These xenoliths display textural features indicative of varying amounts of deformation and recrystallisation, and are enriched in basaltic components (particularly Ti) relative to the common type I xenoliths. In contrast to type I peridotite, xenoliths of type V peridotite generally show flat REE patterns (Harte, 1983). The origin of type V peridotite is a matter of some debate, but it is generally agreed that their distinctive textural and compositional features result from mechanical and chemical interaction between depleted lithospheric material, and the underlying asthenosphere or magmas derived therefrom (e.g. Nixon and Boyd, 1973a; Gurney and Harte, 1980; Harte, 1983).

Megacrysts of orthopyroxene, clinopyroxene, garnet, olivine and ilmenite occur in most kimberlite xenolith suites, and are occasionally very common

(Schulze, 1987). These are believed to represent phenocrysts, formed in a differentiating magma body at depths of 130 to 200km, and sampled (soon after their formation) by kimberlitic magmas (Harte, 1983; Schulze, 1987). In some cases however, megacrysts may form as a result of disaggregation of very coarse-grained peridotite xenoliths. Eclogite xenoliths are usually rare, but occasionally dominate kimberlitic xenolith suites (Dawson, 1980). The origin of the eclogites is uncertain, and current opinion is divided between magmatic and metamorphic models. Protagonists of a magmatic origin believe that the eclogites represent the high-pressure crystallisation products of mafic magmas (MacGregor and Carter, 1970; Hatton and Gurney, 1977; Hatton and Gurney, 1987), whereas others believe that they form as a result of subduction and metamorphism of oceanic crust (Helmstaedt and Doig, 1975; Ater *et.al.*, 1984; MacGregor and Manton, 1986).

Other xenoliths of presumed mantle origin include dunites, pyroxenites, and the relatively common MARID (mica-amphibole-rutile-ilmenite-diopside) suite of rocks. The latter are believed to have crystallised from magmas rich in incompatable elements (Dawson and Smith, 1977; Dawson, 1987a). Two varieties of dunite occur (Harte, 1983). Coarse magnesium-rich dunites are presumed to be depleted restites, while a finer-grained less magnesian variety are interpreted as cumulates or recrystallised megacrysts (Harte and Hawkesworth, 1989). Pyroxenites (usually garnet bearing) are generally rare in kimberlite xenolith suites. A notable exception is the Matsoku suite, where they occur as sheet-like intrusions cross-cutting metasomatised peridotite (Cox *et.al.*, 1973; Gurney *et.al.*, 1975; Harte *et.al.*, 1987).

Xenoliths of lower-crustal origin have not recieved as much attention as those from the mantle, largely due to their relative scarcity in kimberlite xenolith suites. In contrast to this, lower-crustal and shallow upper-mantle xenoliths appear to be relatively common in alkali basalts. Extensive study of these xenoliths indicates the presence, below areas affected by alkali basalt magmatism, of a transitional zone from an ultramafic upper-most mantle, to a mafic to intermediate lower crust (Griffin and O'Reilly, 1987). In southern Africa lower-crustal xenoliths are generally confined to kimberlites which occur close to the margin of the Kaapvaal craton (Griffin *et.al.*, 1979). In these areas the lower crust

appears to be dominated by mafic garnet granulites and eclogites (Griffin *et.al.*, 1979; Robey, 1981).

1.2. Thermobarometry of Kimberlite Xenoliths

A particularly important aspect of the study of kimberlite xenoliths is the use of mineral equilibria to establish the pressures and temperatures at which the xenoliths equilibrated (i.e. thermobarometry). In the case of mantle xenoliths, these pressures and temperatures are generally taken to represent the ambient conditions in the lower lithosphere prior to kimberlite eruption. This is based on two important assumptions:

1) That the minerals were in equilibrium at the ambient conditions prior to the kimberlite event.

2) That the mineral compositions were not affected by processes associated with entrainment in the kimberlite magma.

The validity of these assumptions is supported by a number of factors. Firstly, temperatures of equilibration for most mantle xenoliths are in excess of 800-850°C. At these temperatures diffusion rates are high enough to enable the reequilibration of minerals relatively soon after a thermal event (Harte *et.al.*, 1981). A second important factor is that kimberlite ascent rates are high, of the order of 10 to 30kmhr^{-1} (Eggler, 1989), and thus xenoliths do not have enough time to equilibrate to the changing conditions of pressure and temperature associated with entrainment in the kimberlite magma. The lack of inter- and intra-grain compositional variations in most mantle xenoliths, suggests that they are well equilibrated, and would appear to justify the above assumptions (Boyd and Finger, 1975; Harte *et.al.*, 1981).

Calculation of the ambient conditions at which xenoliths equilibrated enables the construction of pressure-temperature arrays for xenolith suites. These arrays represent the geothermal gradient (geotherm) in the portion of the lithosphere sampled by the kimberlite (Boyd, 1973). Geotherms have been constructed for a large number of kimberlite xenolith suites (eg. Finnerty and Boyd, 1987). The common type I xenoliths described

above generally define a "cool" geotherm which lies very close to that calculated from heat flow data for cratonic regions (Pollack and Chapman, 1977). The type V peridotites always plot at the high pressure end of the geotherm as defined by the group I xenoliths, but reflect temperatures which are significantly higher than what one would expect for a conductive geothermal gradient. These high temperatures are generally taken to reflect interaction with the underlying hot asthenosphere (e.g. Boyd, 1973; Harte, 1983).

Application of thermobarometric methods to lower-crustal and shallow upper-mantle xenoliths is more problematic, in terms of attainment of chemical equilibrium, than that described above. Temperatures in the lower crust and shallow upper-mantle below old stable continents are relatively low (<800°C), and diffusion rates in the anhydrous mineral assemblages which dominate these regions are likely to be extremely slow (Harte *et.al.*, 1981). Thus the xenoliths may not have been able to reequilibrate to the ambient conditions, and in many cases pressures and temperatures calculated for these xenoliths may not reflect steady state continental geotherms (Carswell and Griffin, 1981).

1.3. The Abrahamskraal Kimberlite and its Xenoliths

Most of the detailed xenolith studies conducted to date in southern Africa are of xenolith suites from kimberlites situated either on the Kaapvaal craton or a significant distance away from it. The results of these studies as well as heat flow modelling of the southern African lithosphere, have led to the generally held belief that the craton margin is marked by a thinning of the lithosphere and a steepening of the geothermal gradient towards the Namaqua-Natal mobile belt (e.g. Boyd and Gurney, 1986; Ballard and Pollack, 1987).

The Abrahamskraal kimberlite is situated approximately 5km to the southwest of the presumed boundary between the craton and the Namaqua mobile belt (Fig. 2.1.), and contains a varied suite of deep-seated xenoliths, many of which are suitable for thermobarometry. It therefore provides a good opportunity to study the transition between Archaean Kaapvaal lithosphere and that of the Proterozoic Namaqua mobile belt.

The petrographic features and mineral compositions of a representative range of xenoliths are described, with a view to establishing the nature of the lithosphere at the Kaapvaal/Namaqua boundary. However the main focus of this study is the determination of the geothermal gradient for this region at the time of kimberlite eruption. The significance of this geotherm in terms of current ideas on the nature of the Kaapvaal and Namaqua lithosphere is discussed in section 8.

Previous work on the Abrahamskraal kimberlite and its xenoliths includes a petrographic study by Callow (1988), and in-house reports of the Kimberlite Petrology Unit (DeBeers Consolidated; Grütter, 1987a,b). A regional study by Robey (1981), describes lower-crustal and upper-mantle xenoliths from the kimberlites of the central Cape Province, but does not include xenoliths from the Abrahamskraal pipe. A study of the isotopic characteristics of the craton-margin kimberlites of the northern Cape Province has been undertaken by Clarke *et.al.* (1988).

2. THE GEOLOGY OF THE ABRAHAMSKRAAL KIMBERLITE

The Abrahamskraal kimberlite pipe forms part of a large cluster of kimberlites which straddle the southwestern boundary of the Kaapvaal craton. Its position relative to the inferred margin of the craton is shown in Fig. 2.1. In this region the boundary between the Kaapvaal craton and the Namaqua mobile belt is buried beneath approximately 2.5km of Karoo sediments. Nevertheless DeBeer and Meyer (1984) show that this boundary can be relatively well constrained on the basis of geophysical evidence. The boundary has a distinctive gravity signature, and is marked by the truncation of on-craton magnetic features by northwest-southeast trending magnetic anomalies characteristic of the frontal zone of the Namaqua mobile belt (DeBeer and Meyer, 1984). In the Philipstown-Hanover region, the distribution of kimberlite pipes and the trends of associated dykes, lends support to the above defined craton margin (Fig. 2.2.; Grütter, 1987a). On-craton dykes show a NNW to NW trend, whereas those occurring to the southwest of the craton boundary trend in a northerly direction. The kimberlite pipes and associated dykes appear to lie along linear belts, the orientations of which are parallel to the dyke trends. These features suggest variations in the regional stress field within the Karoo rocks at the time of kimberlite intrusion, and probably reflect the nature of the underlying crust (Grütter, 1987a). The craton boundary shown in Fig. 2.2. is taken from Klinkert's (1982) interpretation of 1:250 000 aeromagnetic maps. The Abrahamskraal kimberlite is situated at the northern end of one of the off-craton kimberlite belts, approximately 5km to the southwest of the inferred craton margin. This suggests that the pipe has intruded the Namaqua mobile belt at the level of its suboutcrop position beneath the Karoo sediments. At depth the kimberlite may intrude either the mobile belt or the Kaapvaal craton, depending on the dip of the contact between the two.

The Abrahamskraal kimberlite forms a small irregular shaped intrusion with a longest dimension of approximately 60m. The pipe lies within a dolerite dyke which intrudes sandstones and shales of the Beaufort Group. Although the kimberlite is very poorly exposed at surface, samples were obtainable from prospecting pits and associated dumps. It is a typical group I monticellite kimberlite, and both diatreme and hypabyssal facies occur

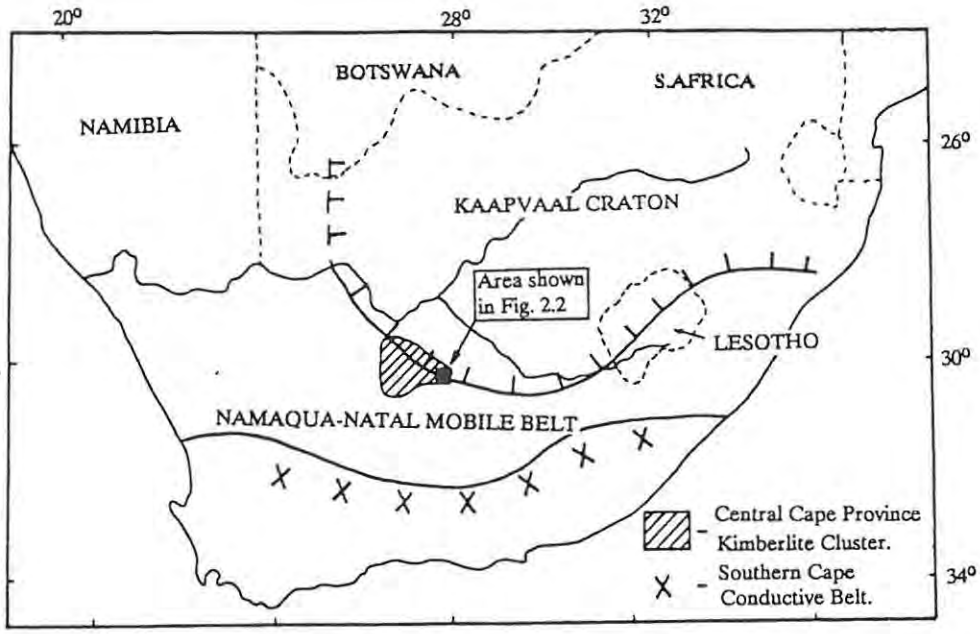

Fig.2.1: Map showing the position of the central cape province Kimberlite cluster in relation to the geophysically defined boundaries of the Namaqua-Natal mobile belt (modified after DeBeer and Meyer, 1984).

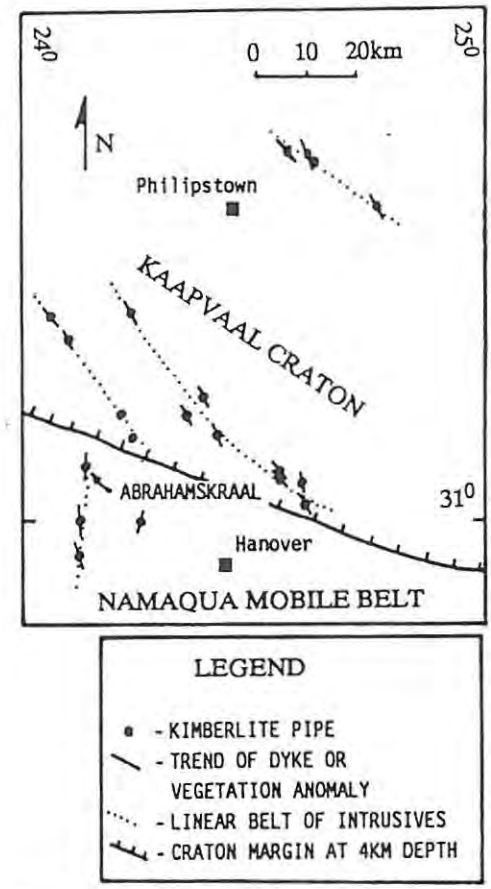

Fig. 2.2: Map of the Hanover-Philipstown area showing kimberlite localities and dyke trends in relation to the craton margin (after Grütter, 1987a). The position of the craton margin is taken from Klinkert's (1982) interpretation of 1:250 000 aeromagnatic maps.

(Grütter, 1987b). The presence of hypabyssal facies kimberlite indicates that significant erosion has occurred since the time of intrusion. An age of 81 ±2Ma has been determined for the Abrahamskraal pipe (Grütter, pers. comm., 1989).

Approximately two hundred and sixty xenoliths of both crustal and mantle origin have been collected from debris floors adjacent to the prospecting pits at Abrahamskraal. A list of the xenolith types and their abundances is given in table 2.1. The list cannot be taken to accurately represent the abundances of different types of xenoliths in the Abrahamskraal pipe, as sampling is likely to have been biased to a certain extent. Nonetheless it does give some indication of relative abundances, particularly of mantle and lower-crustal xenoliths. It is clear from table 2.1. that the xenolith suite is dominated by eclogites, harzburgites and dunites. Garnet peridotites, usually common in kimberlite xenolith suites, are relatively rare at Abrahamskraal (3%), possibly due to metasomatic replacement of garnet (see section 3.2). Garnet-bearing pyroxenite xenoliths on the other hand, are relatively abundant (5%). A large proportion of the xenoliths show evidence of modal metasomatism (>15%).

ORIGIN	ROCK TYPE	APPROXIMATE PROPORTION (%)	
UPPER/MID CRUSTAL	Amphibolite	2	6
	Biotite Gneiss	3	
	Leucocratic Gneiss	1	
LOWER CRUSTAL/ UPPER MANTLE ?	Eclogite	37	
	Kyanite Eclogite	<1	
SHALLOW UPPER MANTLE	Garnet Websterite	4	6
	Garnet Orthopyroxenite	1	
	Clinopyroxenite	1	
UPPER MANTLE	Metasomite	6	19
	Dunite	17	
	Spinel Lherzolite	<1	
	Spinel Harzburgite	1	
	Harzburgite	7	
	Metasomatised Harzburgite	9	
	Garnet Harzburgite	2	
	Garnet Lherzolite	1	
	Megacrysts	8	

Table 2.1.: Approximate proportions of different xenolith varieties at Abrahamskraal.

Forty-eight of the Abrahamskraal xenoliths were selected for the purposes of this study. The main selection criterion used was the suitability of the xenoliths for thermobarometry purposes, and hence all relatively fresh xenoliths containing both garnet and orthopyroxene were chosen (2 garnet lherzolites; 5 garnet harzburgites; 12 garnet pyroxenites). In addition, a representative number of eclogites, dunites and harzburgites were also selected. The full list of chosen xenoliths is given in appendix 1, together with their mineral assemblages. The xenoliths are small (longest dimension ≤5cm) and ovoid in shape. In many cases their outer rims have been altered by interaction with the kimberlite magma, however all xenoliths chosen for this study have fresh cores. Microprobe sections of all forty-eight xenoliths were prepared.

3. PETROGRAPHY

3.1. Introduction

The terms used to describe the textures in the xenoliths are based partly on the classification scheme of Harte (1977). The scheme applies primarily to peridotitic xenoliths which Harte subdivides into coarse, porphyroclastic, mosaic-porphyroclastic, and granuloblastic, on the basis of deformation textures. "Coarse" rocks lack features suggesting significant deformation, although mineral grains may show undulose extinction. The grains are generally equal to or greater than 2mm in average dimension, and show smoothly curved, straight or less regular grain boundaries. All of the Abrahamskraal peridotites display these coarse textures. Increasing deformation of the peridotites results in recrystallisation and the formation of small neoblasts (usually of olivine) which form a finer grained matrix (generally <1mm) surrounding coarse relic grains (porphyroclasts). The terms "porphyroclastic" and "mosaic-porphyroclastic" are used to describe rocks with relatively low (≤90%), and relatively high (>90%) proportions of recrystallised fine-grained matrix respectively. In "granuloblastic" rocks, porphyroclasts are very rare or absent, and "the grains of each mineral show a small size range and a granuloblastic texture" (Harte, 1977, p.283). The term "granuloblastic" is applied to some of the Abrahamskraal xenoliths (particularly the pyroxenites). It should be emphasised however, that it is used in a non-genetic sense to describe equigranular medium to coarse-grained rocks, and does not imply recrystallisation due to extensive deformation as is suggested by its usage in the scheme of Harte (1977).

A number of secondary events have affected the xenoliths from Abrahamskraal. In the discussion that follows these events are conveniently subdivided into two broad categories, i.e. "primary (or early) metasomatic", and "secondary". Primary metasomatism occurred in certain xenoliths as a result of the infiltration of metasomatic fluids prior to entrainment of the xenoliths in the kimberlite magma. The general features resulting from these processes are extensively described in the literature (for reviews see Harte, 1983; 1987, and Erlank *et.al.*, 1987) and will not be dealt with in depth here. Suffice to say that primary metasomatism may

result in the introduction of medium- to coarse-grained minerals (they may or may not be in textural equilibrium with the other primary phases) which are typically rich in certain components (eg. K, Ti and H_2O) not previously abundant in the rocks (Harte, 1983). Often the distinction between primary and primary metasomatic phases is unclear as the latter may be in textural equilibrium with the primary minerals in the rock. In the xenoliths of this study phases believed to be of primary metasomatic origin include phlogopite, Fe-Ti oxides, amphibole, Cr-spinel and clinopyroxene. Strictly speaking clinopyroxene does not fit into the above description of primary metasomatic minerals, however, in certain rocks it displays textures warranting its inclusion in this list. In this regard it should be noted that metasomatic clinopyroxene has been described from mantle xenoliths found at other localities (eg. Erlank *et.al.*, 1987; Dawson, 1987b).

Features which can clearly be regarded as the result of late stage processes have been categorised as "secondary". These include the presence of fine-grained phlogopite, spinel and amphibole, as well as a variety of very fine-grained alteration products. These features are believed to be associated with entrainment of the xenoliths in the kimberlite magma, and probably result from decompression reactions and the infiltration of kimberlite-derived fluids into the xenoliths. Evidence for partial melting, as described in several other kimberlite xenolith studies (e.g. Switzer and Melson, 1969; Robey, 1981), was not found in the Abrahamskraal xenoliths.

In the following discussion, the term "peridotite" refers to rocks with significant amounts of both olivine and orthopyroxene, and does not include dunites which are discussed separately. The term "lherzolite" is used here to refer to any olivine-orthopyroxene rocks which contain primary clinopyroxene, even if the latter only occurs in very small amounts (< 5%).

The mineral assemblages of the forty eight xenoliths selected for this study are listed in appendix 1, and their modal compositions are given in appendix 2.

3.2. Peridotites

The peridotites have been grouped into three different categories,viz. garnet lherzolite, garnet harzburgite, and harzburgite, based on the presence or absence of clinopyroxene and garnet. However, with the possible exception of sample 156 (garnet lherzolite), these rocks display very similar textures and it is believed that modal variations (Fig. 3.1) are primarily a function of the small size and coarse nature of the samples, while primary metasomatism may have been an important factor in some cases. Thus in the descriptions that follow these three rock types are regarded as a single group, the differences between them being discussed as variations rather than distinguishing features.

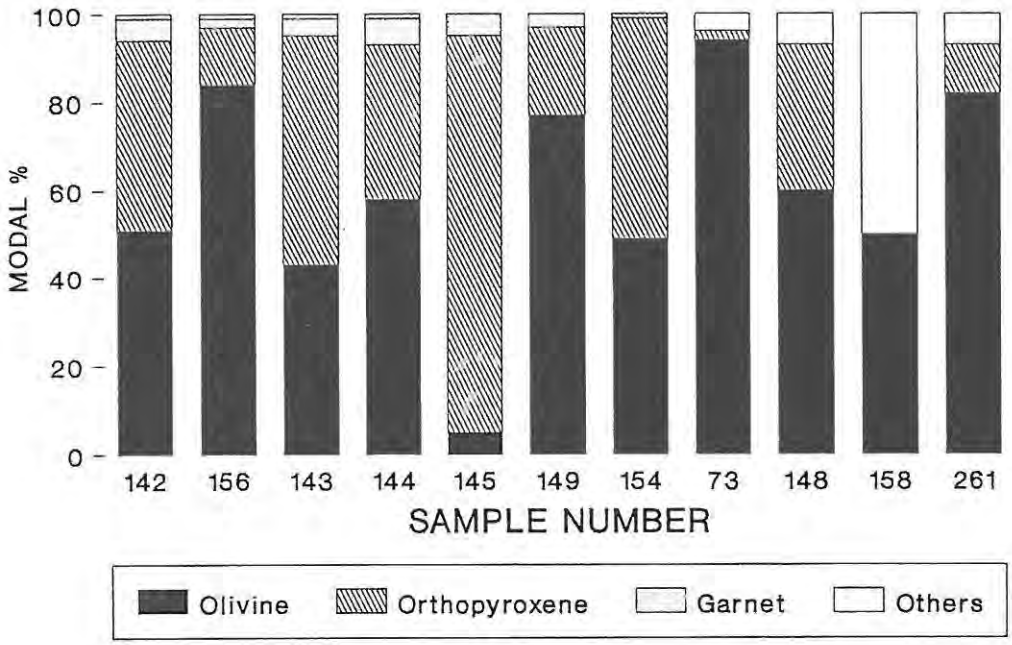

Fig. 3.1: Modal compositions of the Abrahamskraal peridotite xenoliths. "Others" includes minor amounts of primary clinopyroxene and Cr-spinel, metasomatic phases, and late-stage alteration.

It is clear from Fig. 3.1 that the peridotites are essentially olivine-orthopyroxene rocks which may contain minor amounts (usually < 5%) of garnet, clinopyroxene and spinel. Garnet is believed to have been present in all of the peridotites, its absence in the harzburgites possibly being accounted for by metasomatic replacement (see below). Primary clinopyroxene is only found in two of the samples (142 and 156) where it occurs in very

minor amounts (<1%). Cr-spinel occurs as a primary minor phase in three samples (73,156 and 143). In addition to these primary phases, some of the samples contain small amounts of primary metasomatic minerals, and late stage secondary minerals occur in varying amounts in all of the rocks examined. These are discussed in more detail below.

All of the peridotites are texturally coarse (Harte,1977), showing no signs of deformation (apart from minor undulose extinction). Grain sizes are variable (1-10mm), and grain boundaries are generally straight or smoothly curving, although in places they may be irregular where interlocking or "amoeboid" textures are developed (Plate 1). Olivine and orthopyroxene grains are generally equant but may be tabular in some cases. In one sample (144) tabular olivine grains show a vague parallel orientation. Garnet occurs as rounded to sub-angular grains which are usually smaller (1-3.5mm) than those of olivine and orthopyroxene. In all of the samples garnet is rimmed by kelyphitic material.

The textures in sample 156 (garnet lherzolite) differ somewhat from those described above. In this rock olivine and orthopyroxene display more uniform grain sizes, and textures tend towards granuloblastic-polygonal. Garnet is distinctly finer-grained (<0.5mm) than olivine and orthopyroxene and occurs as bead-like grains along the grain boundaries of these minerals. Occasional coarser-grained garnets (0.5-1mm) display intimate symplectitic intergrowths with Cr-spinel (Plate 2), suggesting perhaps that this xenolith equilibrated at conditions close to the boundary between spinel lherzolite - garnet lherzolite. The Cr-spinel in sample 143 occurs as small (<1mm) discrete rounded grains, while in sample 73 it is distinctly coarser grained (0.25-2mm).

In both of the garnet lherzolite samples clinopyroxene occurs as scattered, small (usually <0.5mm), discrete grains which appear to bein textural equilibrium with the other primary phases in the rock (Plate 3a) . In sample 142 clinopyroxene also occurs as an inclusion in garnet (Plate 3b), and on the margin of garnet grains where it has been partially replaced by kelyphite and is associated with phlogopite (Plate 3c). The latter variety of clinopyroxene grains may have originally been in equilibrium with the other primary phases, and been texturally modified by subsequent secondary processes.

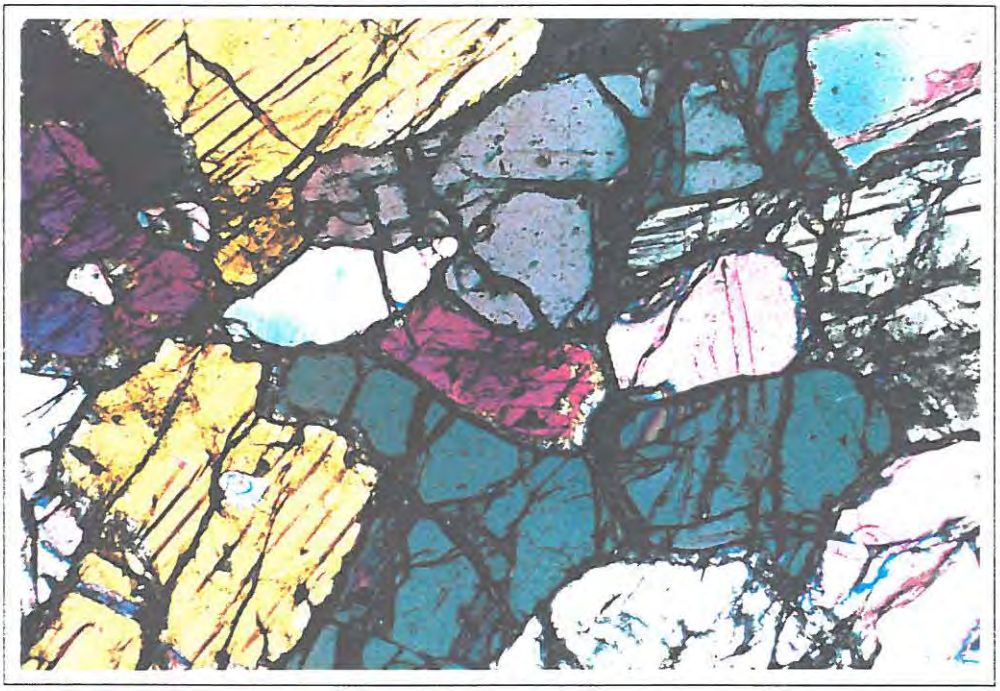

Plate 1: Coarse textures in garnet harzburgite. Plate shows coarse-grained olivine (high birefringence) and orthopyroxene (fractured, yellow-grey interference colours). Field of view (FOV) - 3.5 mm; Crossed polars.

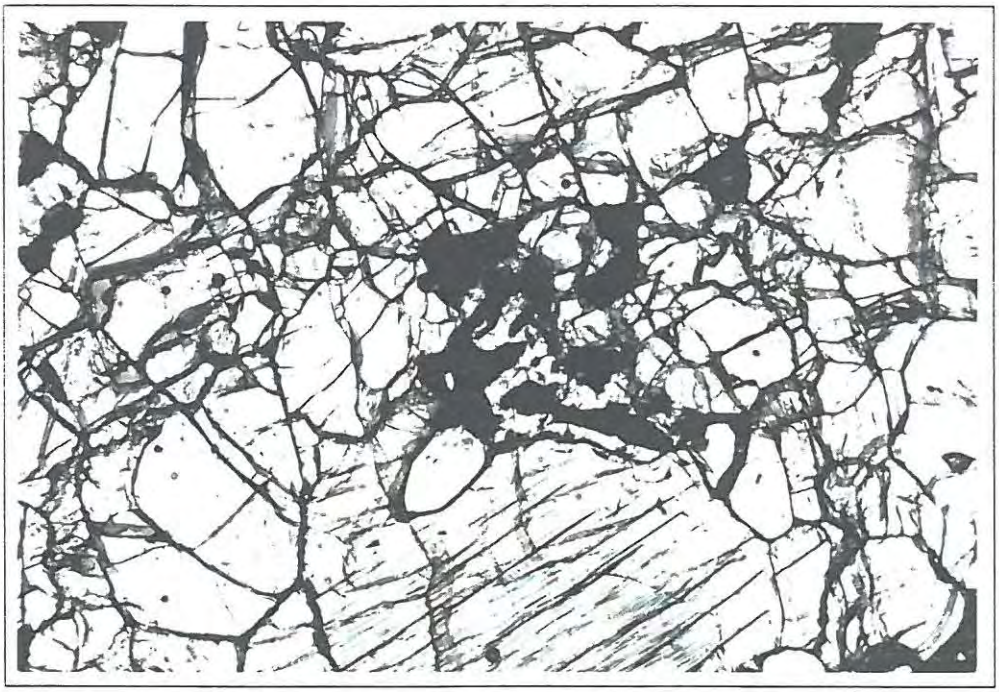

Plate 2: Intergrown garnet and Cr-spinel (opaque) in garnet lherzolite (156). The intergrowth (centre of plate) is surrounded by coarse textured olivine and orthopyroxene (bottom centre). FOV - 3.5 mm; Plane polarised light.

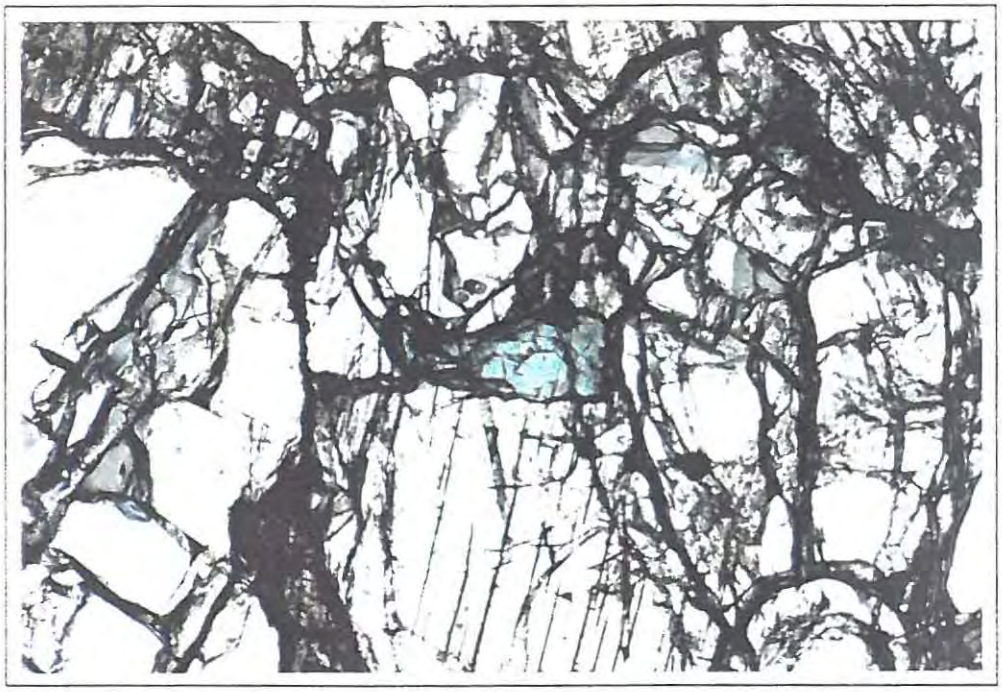

Plate 3a: Clinopyroxene grain in textural equilibrium with coarse-grained olivine and orthopyroxene (mineral with cleavage, e.g. bottom centre), in garnet lherzolite (142). FOV - 3.5 mm; Plane polarised light.

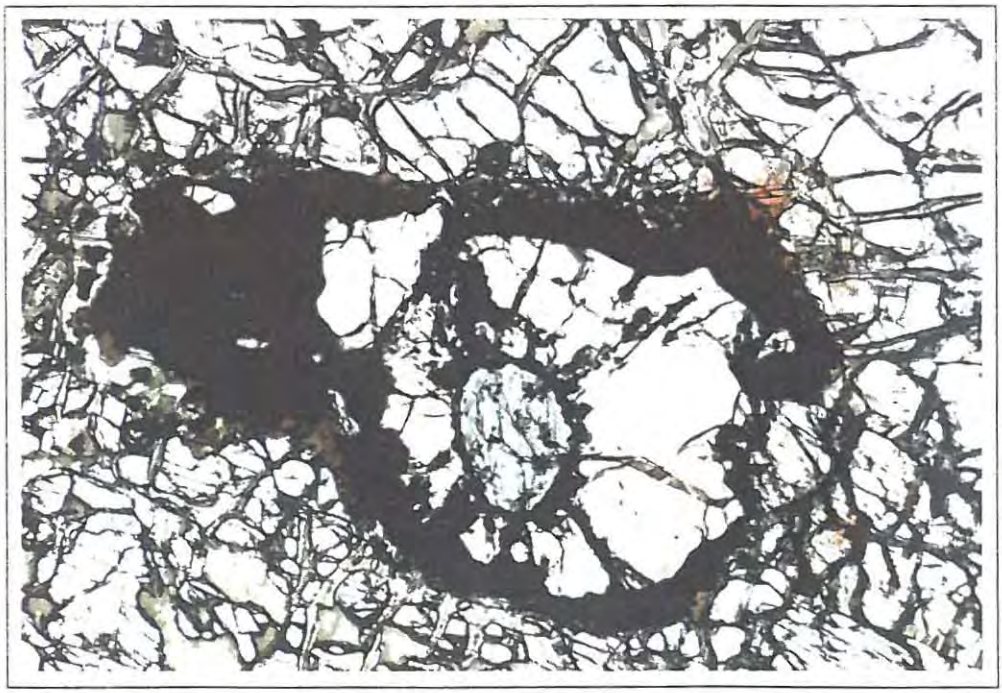

Plate 3b: Clinopyroxene inclusion in garnet within garnet lherzolite (142). Garnet is surrounded by kelyphite with minor secondary phlogopite and clinopyroxene. FOV - 3.5 mm; Plane polarised light.

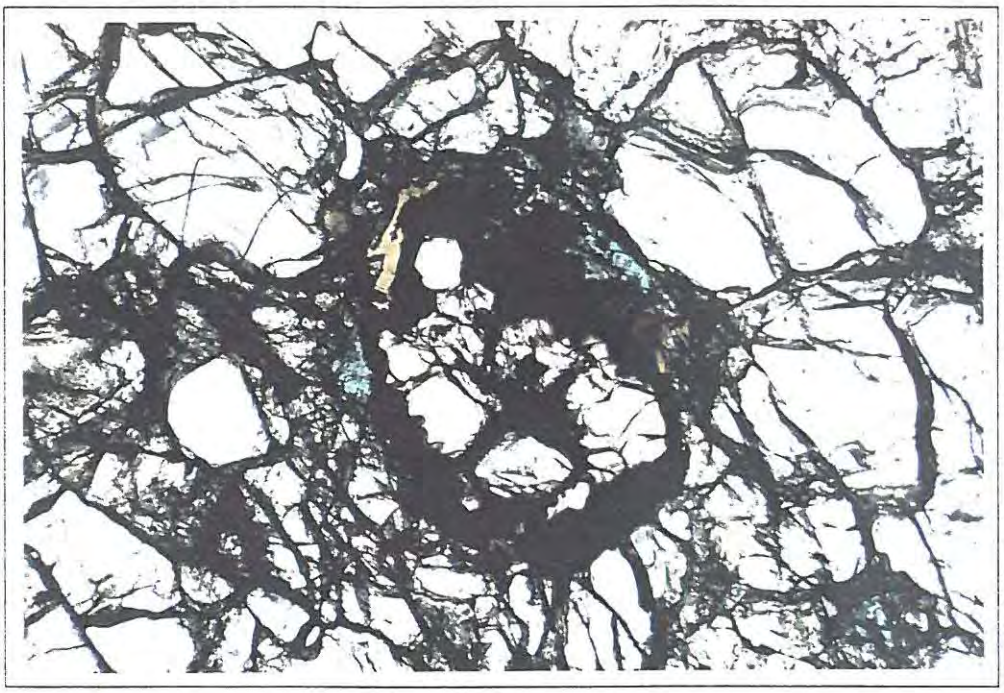

Plate 3c: Corroded clinopyroxene associated with phlogopite on rim of garnet grain (142). Garnet is surrounded primarily by coarse-grained olivine. FOV - 3.5 mm; Plane polarised light.

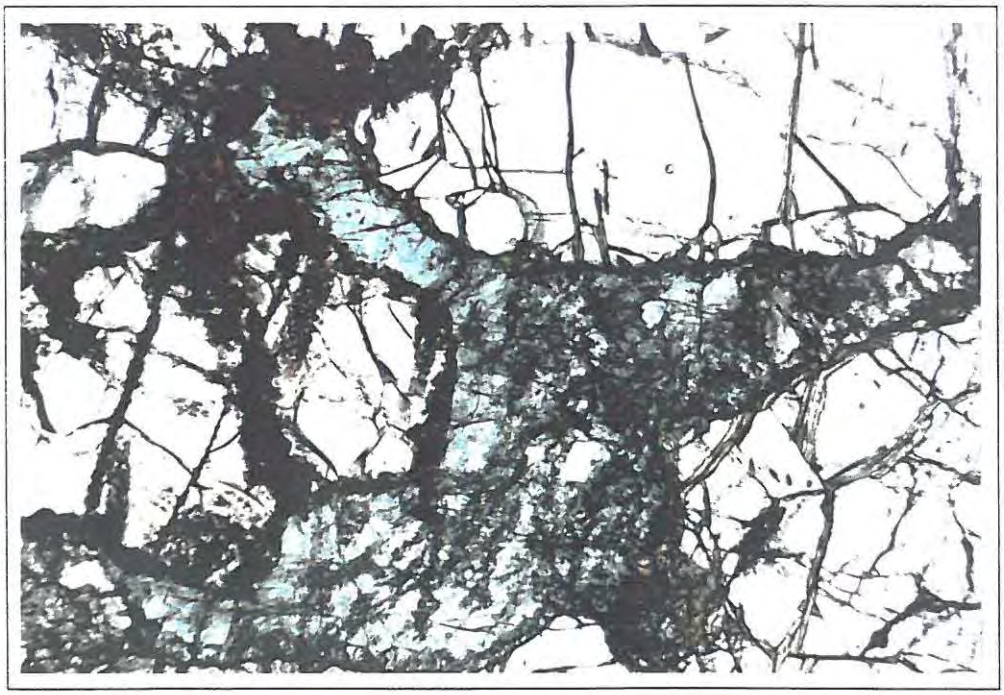

Plate 3d: Possible primary metasomatic clinopyroxene in garnet harzburgite (144). Clinopyroxene partially surrounds garnet and shows interstitial relationships with olivine and orthopyroxene (not shown). FOV - 3.5 mm; Plane polarised light.

Clinopyroxene also occurs in samples 143 and 144. In the latter sample it occurs as coarse (1-2mm) grains showing a close association with garnet. The clinopyroxene displays apparent interstitial relationships with olivine, orthopyroxene and garnet (Plate 3d), and in some cases it is seen to rim the garnet grains. In sample 143 clinopyroxene occurs as small corroded grains in alteration patches, where it is associated with other fine-grained alteration products. Although the evidence is not unequivocal, the clinopyroxene in both of these rocks is believed to be of primary metasomatic origin rather than part of the original assemblage. Pargasitic amphibole occurs in samples 143 and 154 as corroded remnants in patches of alteration.

The clinopyroxene and possibly the amphibole described above are the only primary metasomatic phases in the garnet-bearing peridotites. In contrast to this, metasomatic phlogopite, clinopyroxene and Cr-spinel are abundant in three of the four harzburgite samples (148, 158, and 261). These minerals are generally intergrown in vermiform or irregular aggregates occasionally developed along grain boundaries, but more commonly occurring dicretely in "patches" (1.5 - 3 mm; Plate 4a). The occurrence of these minerals as dicrete aggregates is suggestive of them having replaced a particular mineral. Erlank et.al. (1987) note a tendancy for metasomatic clinopyroxene and phlogopite to nucleate on and to replace garnet in many garnet peridotites. Spinel is produced to accomodate excess Al resulting from the breakdown of garnet. The textures described by Erlank et.al. (1987) are similar to those observed in the Abrahamskraal harzburgites, and it is suggested that the metasomatic patches may have originally been garnet grains. This is supported by the similarity in the size of the aggregates in the harzburgites to that of the garnet grains in the garnet harzburgites, as well as the rimming of garnet by metasomatic clinopyroxene in sample 144 (garnet harzburgite), and the low abundance of primary metasomatic minerals in the garnet bearing peridotites. In sample 73 (harzburgite) the secondary textures are somewhat different. Occasional aggregates of secondary material (Plate 4b) include phlogopite, dark brown turbid material, fine-grained spinel, and in places amphibole. The aggregates are often associated with coarse spinel.

The amount of metasomatic replacement and/or secondary alteration in the harzburgites is variable. In sample 73 less than 5% of the rock is made up of secondary material, while in sample 158, approximately 50% of the rock has been replaced by primary metasomatic minerals or late-stage alteration.

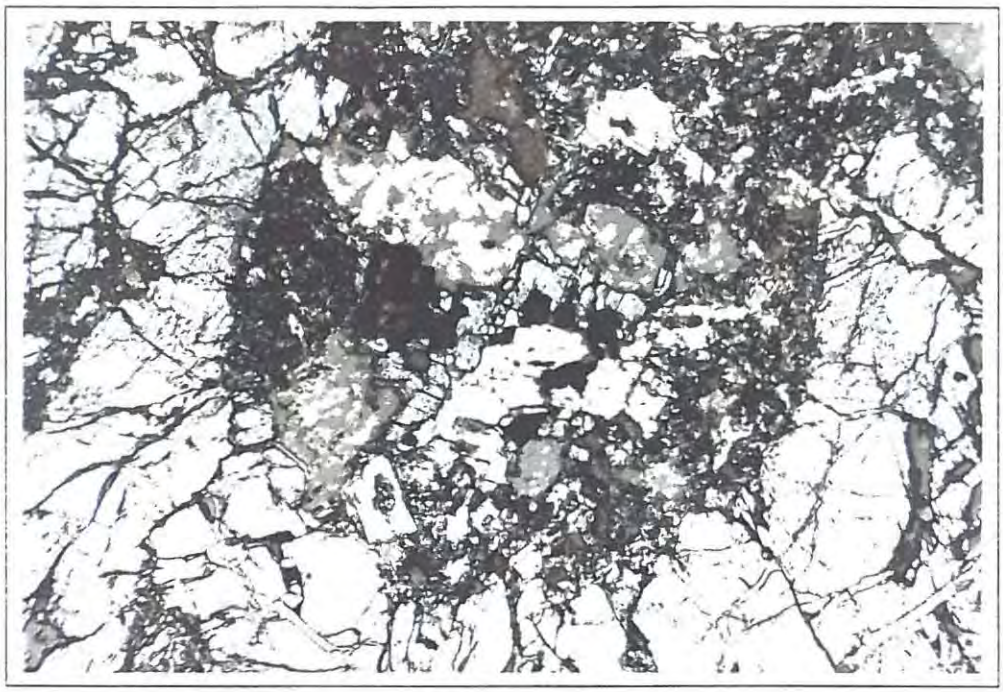

Plate 4a: Aggregate of clinopyroxene (pale green), phlogopite (pale yellow-brown), and spinel in harzburgite (261). The primary metasomatic minerals have been subject to late stage alteration (fine-grained dark brown material). The pale grey to brown-grey areas are holes covered with carbon coating. The aggregate is surrounded primarily by olivine. FOV - 3.5 mm; Plane polarised light.

Plate 4b: Aggregate of secondary material associated with spinel in harzburgite (73). The aggregate includes fine grained phlogopite, spinel, and minor amphibole. Surrounding minerals are olivine and orthopyroxene (centre left). FOV - 3.5 mm; Plane polarised light.

Late-stage secondary features in the peridotite xenoliths include kelyphite rims around garnet, fine-grained phlogopite and spinel, and very fine-grained alteration products of olivine and orthopyroxene (including serpentine). Kelyphite rims on garnet are generally made up of a narrow rim of dark brown turbid material. In most samples this inner rim is surrounded or partly surounded by fine-grained phlogopite- and/or spinel-rich material. The latter may also occur along grain boundaries where it is generally associated with very fine-grained alteration products. In sample 143 these minerals also occur in alteration "pools" which may include corroded remnants of primary metasomatic clinopyroxene as well as orthopyroxene and olivine. The formation of kelyphite rims is generally attributed to decompression reactions which occur during transport of the xenoliths in the kimberlite (Reid and Dawson, 1972; Garvie and Robinson, 1982), while the the very fine-grained alteration products, and possibly also the fine- grained phlogopite and spinel may result from the interaction of the xenolith with fluids derived from the kimberlite magma.

3.3. Dunites

Eleven dunite samples were examined. In samples 18 and 258 very minor amounts of garnet occur as small remnant grains surrounded by kelyphite. In sample 18 the garnet is particularly rare, and occurs only in an altered portion of the sample. In two of the samples (71 and 258) Cr-spinel occurs as rare discrete grains or as inclusions in olivine, and is believed to be primary. A range of primary metasomatic minerals occur in the dunites, and all of them have been serpentinised to some extent.

Two groups of dunite can be distinguished on the basis of grain size. Six of the samples studied are medium- to coarse-grained with the maximum grain size ranging from 1 to 3 mm (18,19a,19b,19c,99,263;see Plate 5a and 5b). The other samples (71,107,258,265,267) are very coarse-grained and show a much wider range of grain sizes (4 to 21 mm; see Plate 5c). Apart from undulose extinction observed in both dunite types, features suggestive of deformation are not evident. The finer-grained dunites can be divided into two subgroups. Three of the samples (19a,19b,99) are approximately equigranular (grain size $\geq$ 1mm; Plate 5a), while the other two samples (18,19a) show more variable grain sizes (0.2 - 3mm). Olivine grains in the latter variety are highly fractured (Plate 5b).

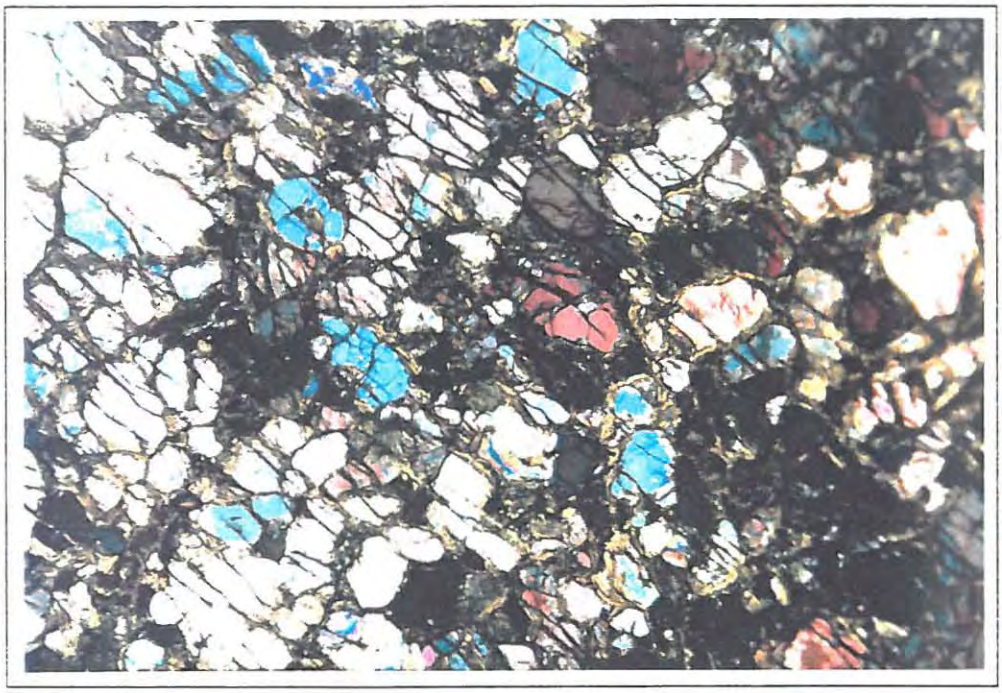

Plate 5a: Textures in the finer-grained, equigranular variety of dunite. Serpentinisation occurs along grain boundaries and fractures. FOV - 10mm; Crossed polars.

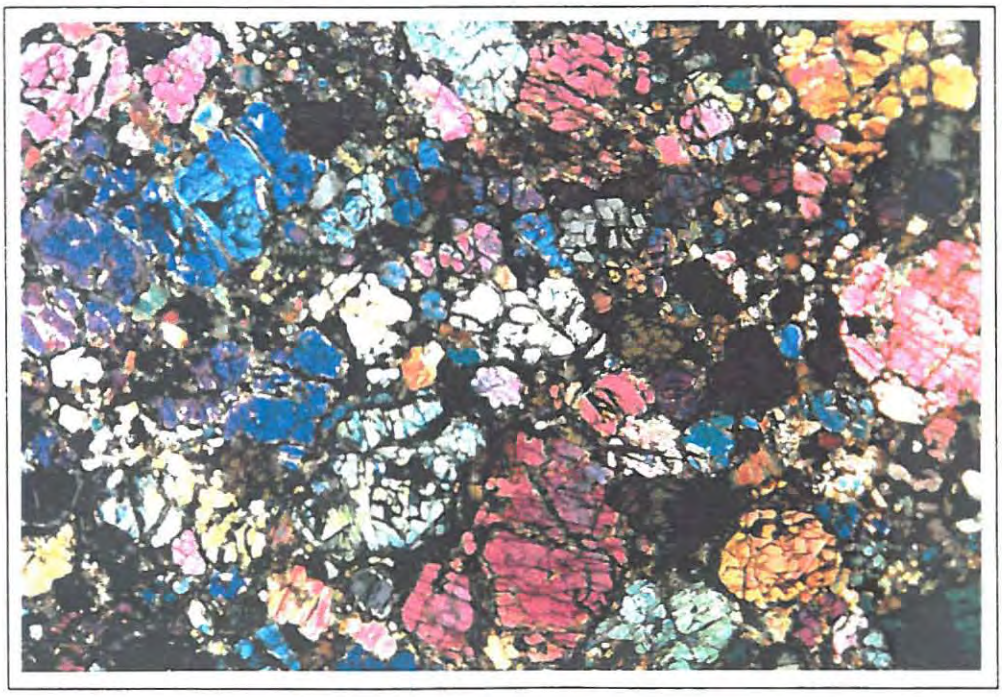

Plate 5b: Textures in the finer-grained, inequigranular variety of dunite. Olivine grains are highly fractured. Minor serpentinisation occurs along fractures and grain boundaries. FOV - 10 mm; Crossed polars.

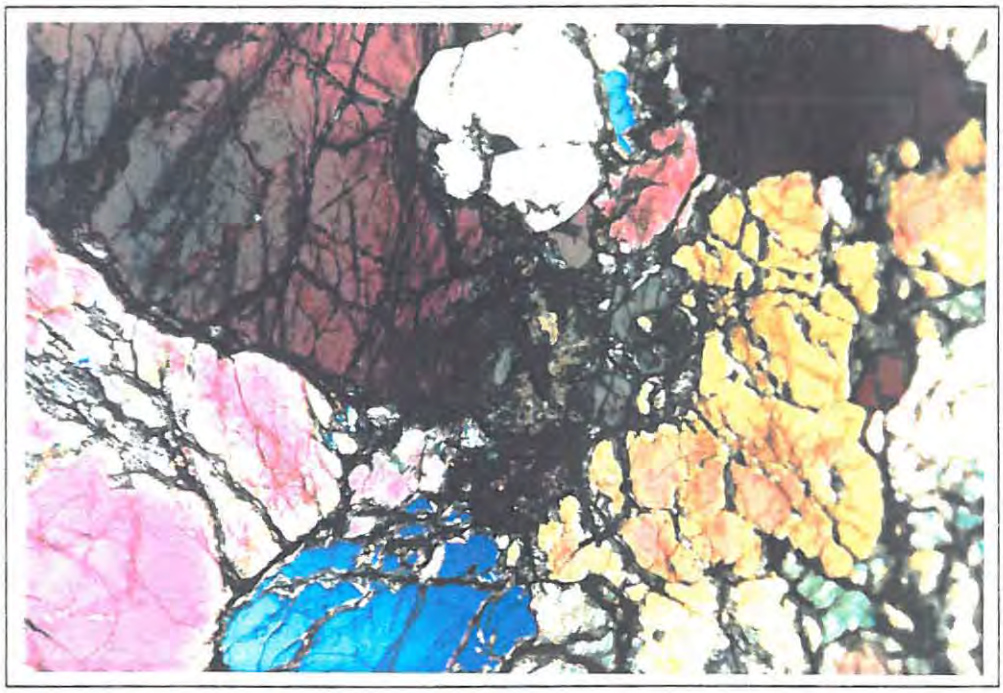

Plate 5c: Textures in a coarse-grained variety of dunite. Only minor serpentinisation occurs. FOV - 10mm; Crossed polars.

A range of primary metasomatic and secondary minerals and textures are developed in the dunites. The minerals include phlogopite, clinopyroxene, Cr-spinel, potassic-richterite and serpentine. Phlogopite is present in all of the samples except for 71 and 258. It occurs both as scattered discrete medium-sized grains, and in coarse aggregates where it may be intergrown with spinel and clinopyroxene (Plate 6a). The discrete phlogopite grains often show equilibrium textures, but occasional cross-cutting and interstitial textural relationships, and the coarse phlogopite aggregates, support a primary metasomatic origin. Clinopyroxene (found in 19C,107,267) also occurs as scattered medium-sized to fine grains but is more commonly found in intergrowths with phlogopite and Cr-spinel. This intergrown clinopyroxene may be coarse and poikilitic (267) or finer-grained (107). K-richterite occurs in a similar fashion to phlogopite, i.e. as discrete medium-sized to coarse grains (Plate 6b), as well as in coarse aggregates. Both of the K-richterite bearing samples (18,19b) are rich in phlogopite and have obviously undergone extensive metasomatism. K-richterite does not occur in any of the clinopyroxene-bearing samples, and it is only found in samples of the finer-grained variety of dunite.

Spinel is present in all of the dunites except for sample 258. It generally occurs in the centers of the coarse phlogopite aggregates where it is

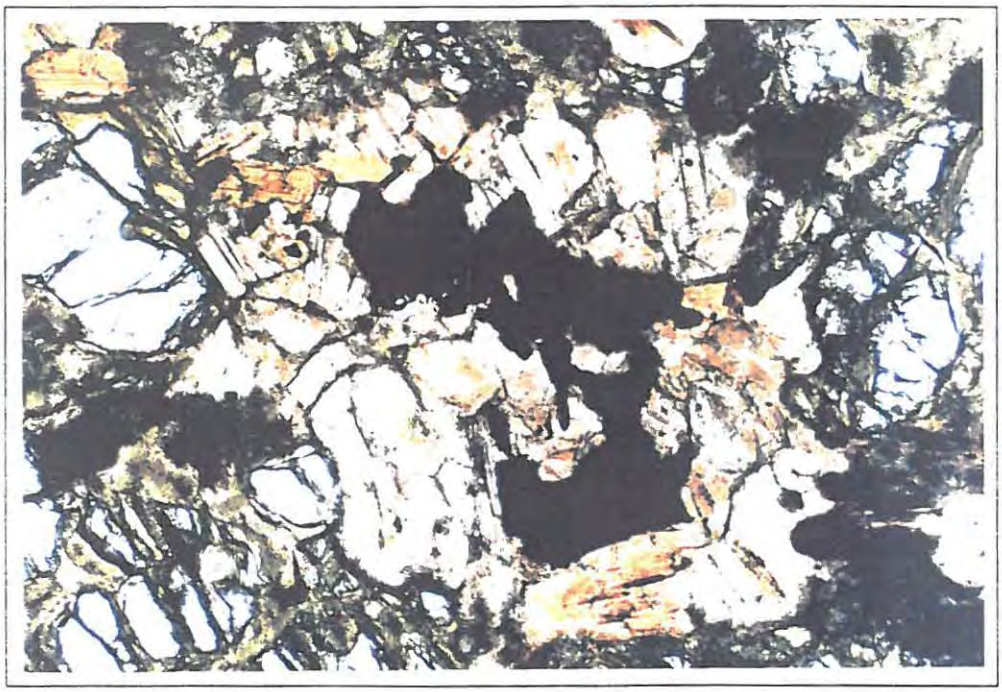

Plate 6a: Phlogopite-spinel intergrowth in dunite. Clear mineral is olivine. Khaki-yellow coloured material is serpentine. FOV - 3.5 mm; Plane polarised light.

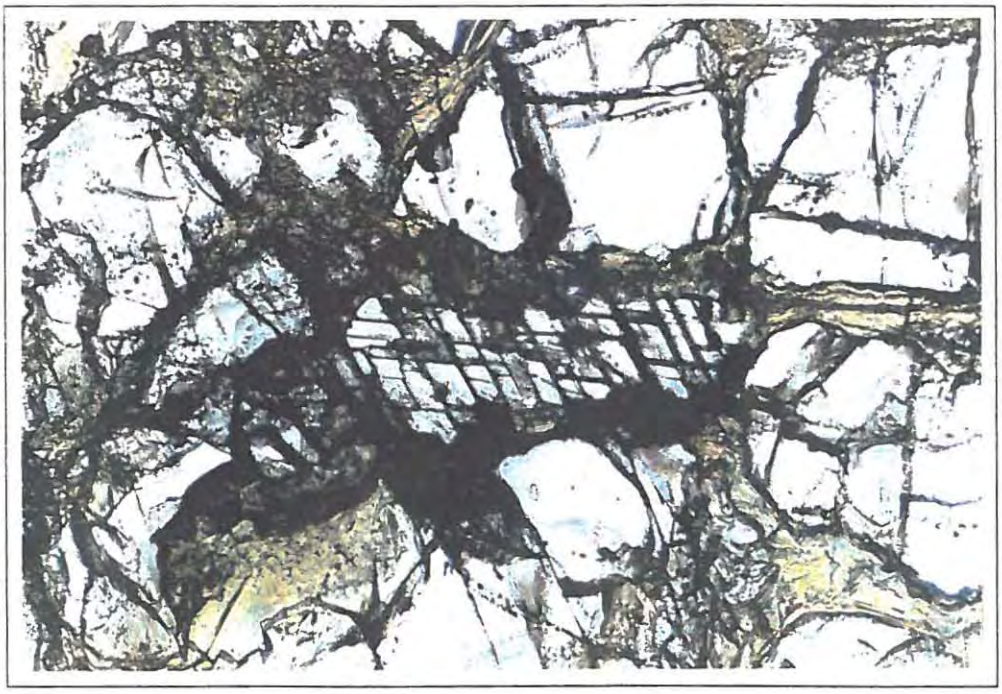

Plate 6b: Discrete grain of K-richterite (with cleavage) in dunite (19b). Yellowish material is serpentine. FOV - 1mm; Plane polarised light.

partly replaced by the phlogopite (Plate 6a), but it is also found as small grains scattered throughout the rock. It is not clear whether the spinel is of primary metasomatic origin, or whether it formed part of the original assemblage and was subsequently involved in metasomatic proceses.

The extent of metasomatism in the dunites varies considerably. In sample 258 no metasomatic phases are present, while in other samples (18,19b,263,267) they form up to 20% of the rock. Serpentinization ranges in intensity from minor alteration along grain boundaries and fractures, to near pervasive alteration (olivine forms small remnants surrounded by serpentine).

3.4. Pyroxenites

Three varieties of pyroxenite occur in the Abrahamskraal xenolith suite. The most common variety is garnet websterite (9 samples), only one sample of which contains olivine (4 modal% in sample 283). The other varieties are garnet orthopyroxenite (3 samples), and spinel-bearing clinopyroxenite of which only one sample has been found (266). A fourth variety of pyroxenite may be present in the form of three altered garnet-clinopyroxene rocks (160,260,273). In these rocks very fine-grained yellow to khaki brown alteration has replaced mineral grains believed to have been orthopyroxene. Thus although these rocks presently contain an eclogitic assemblage, they were probably originally pyroxenites (they have similar mineral compositions to the garnet websterites; see section 4.3 and appendix 3).

3.4.1. Garnet (± Sp) Websterites

The garnet websterites all contain the primary assemblage orthopyroxene, clinopyroxene and garnet. Modal variations in the garnet websterites are illustrated in Fig. 3.2. Most of the samples are orthopyroxene-rich (>50% orthopyroxene), and contain significantly greater amounts of clinopyroxene and garnet than the peridotites. Cr-spinel (in sample 274) , magnetite ± Ti-magnetite and acsessory rutile occur as apparently primary phases in some of the samples. Although these minerals are in textural equilibrium with the major primary phases in the rocks, some of them (particularly the Ti-bearing minerals) may be of primary metasomatic origin. Other discrete phases present in the garnet websterites are phlogopite (197,257,264,274,280), pargasitic amphibole (264,280,283), and Fe-Ni sulphide (257,259).

The garnet websterites are coarse-grained(although finer than the peridotites) with orthopyroxene generally ranging to coarser grain sizes (up to 3.5mm) than clinopyroxene (usually <1.5mm) and garnet (<1mm). The opaque minerals display similar size ranges to garnet (0.1 to 1.5mm) while rutile forms fine (<0.5mm) bead-like grains. Amphibole occurs as coarse (up to 2mm) subhedral grains, and phlogopite may be coarse- (up to 3mm) or fine-grained (<0.5mm).

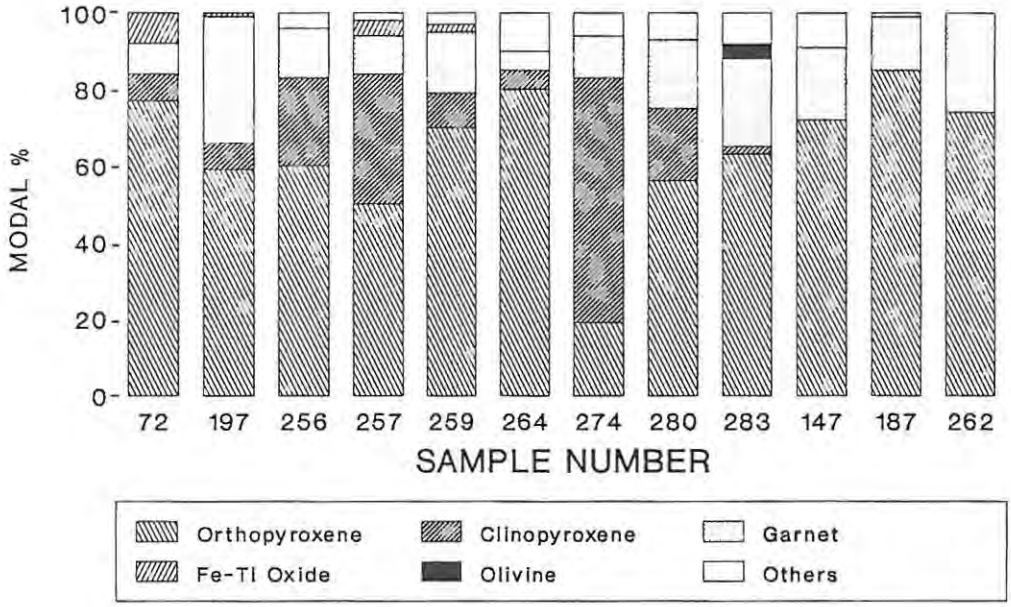

Fig. 3.2: Modal compositions of the Abrahamskraal garnet pyroxenite xenoliths. "Others" includes phlogopite, amphibole and late-stage alteration.

A range of primary textures are developed in the garnet websterite samples. These textures are believed to reflect different degrees of reequilibration of garnet and clinopyroxene, which appear in turn to have been exsolved from orthopyroxene. In the least equilibrated rocks (72,256), relatively fine-grained garnet and to a lesser extent clinopyroxene occur along orthopyroxene grain boundaries. In places garnet grains form continuous "strings" of elongate bead-like grains, often almost entirely surrounding coarse orthopyroxene grains, and giving rise to the so-called "necklace" texture (Plate 7a). On the opposite end of the spectrum, samples 280 and 274 display very well equilibrated granuloblastic-polygonal textures involving all three major primary phases (Plate 7b). This equigranular texture is only disrupted by occasional coarse orthopyroxene grains which display irregular grain boundaries (as opposed to the straight and smoothly curving grain boundaries in the polygonal areas), and contain fine-grained exsolution lamellae and tabular inclusions (clinopyroxene and/or an opaque

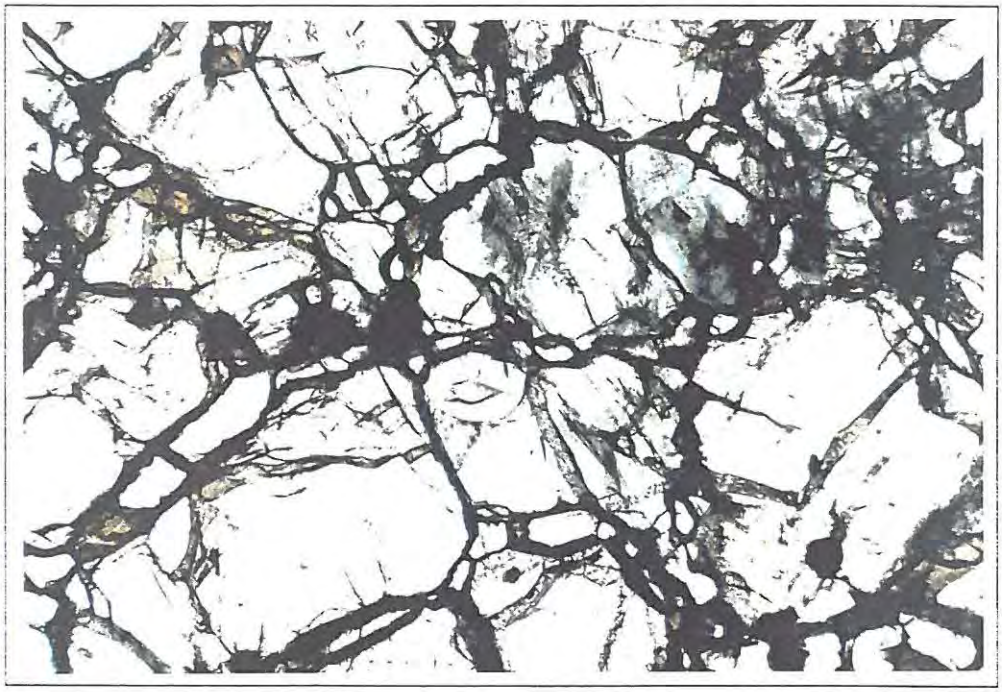

Plate 7a: Necklace texture in garnet websterite. Small, bead-like or elongate grains of garnet (clear mineral with dark rims) surround large grains of orthopyroxene (large grains with very fine exsolution features). Clinopyroxene (pale green) occurs as intermediate-sized grains. FOV - 3.5 mm; Plane polarised light.

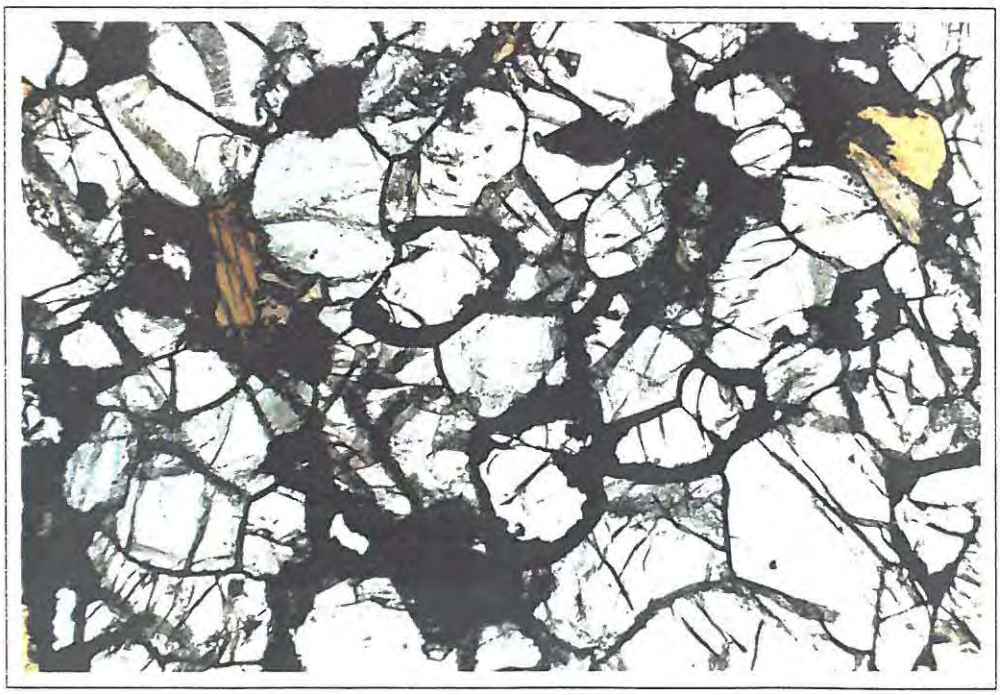

Plate 7b: Granuloblastic-polygonal textures in garnet websterite. Plate shows equigranular garnet (pale pink with dark rims), orthopyroxene (colourless), and clinopyroxene (pale green), as well as minor primary metasomatic phlogopite. Dark material is kelyphite. FOV - 3.5 mm; Plane polarised light.

phase). These may be relics of earlier igneous orthopyroxene. In other samples one usually finds both of the above textures developed to varying degrees. In these rocks "necklace" textures are preserved in parts of the sample which are rich in coarse orthopyroxene, while well-equilibrated clinopyroxene-orthopyroxene-garnet aggregates occur interstitially to coarse orthopyroxene (259), and as relatively large (± 8mm) polygonal-textured "pools" (259). In certain samples, bands of garnet (197,259) and clinopyroxene (197) occur in large orthopyroxene grains, supporting an exsolution origin for garnet and clinopyroxene (Plate 7c).

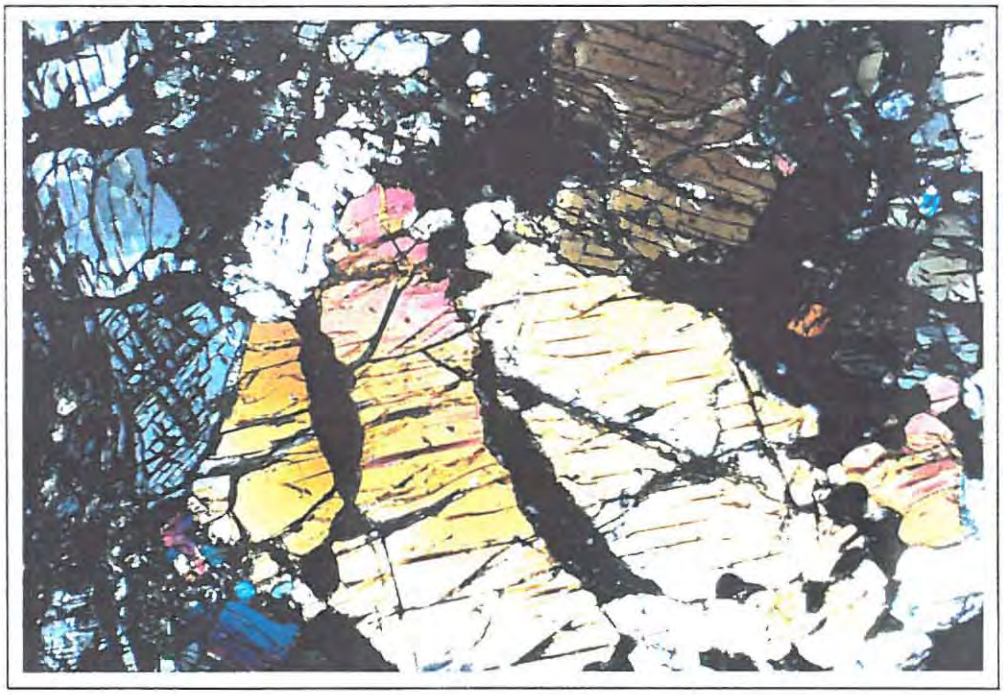

Plate 7c: Bands of exsolved garnet (black) in large orthopyroxene grain, within garnet websterite. FOV - 3.5 mm; Crossed polars.

It has already been mentioned above that the distinction between primary and primary metasomatic phases is not very clear in the case of the Fe-Ti oxides. This also applies to coarse-grained amphibole which occurs in three of the xenoliths. In sample 264 amphibole occurs as corroded grains in a small veinlet of secondary material (Plate 8a), and clearly predates the other finer grained alteration products. These include a narrow selvage of fine-grained (<0.5mm) phlogopite, and very fine-grained yellow/green and khaki-coloured alteration products of orthopyroxene amd clinopyroxene. In samples 280 and 283 amphibole occurs as coarse subhedral grains which do not display clear secondary textures (Plate 8b). Sample 280 is also the only garnet websterite xenolith which contains coarse phlogopite. The

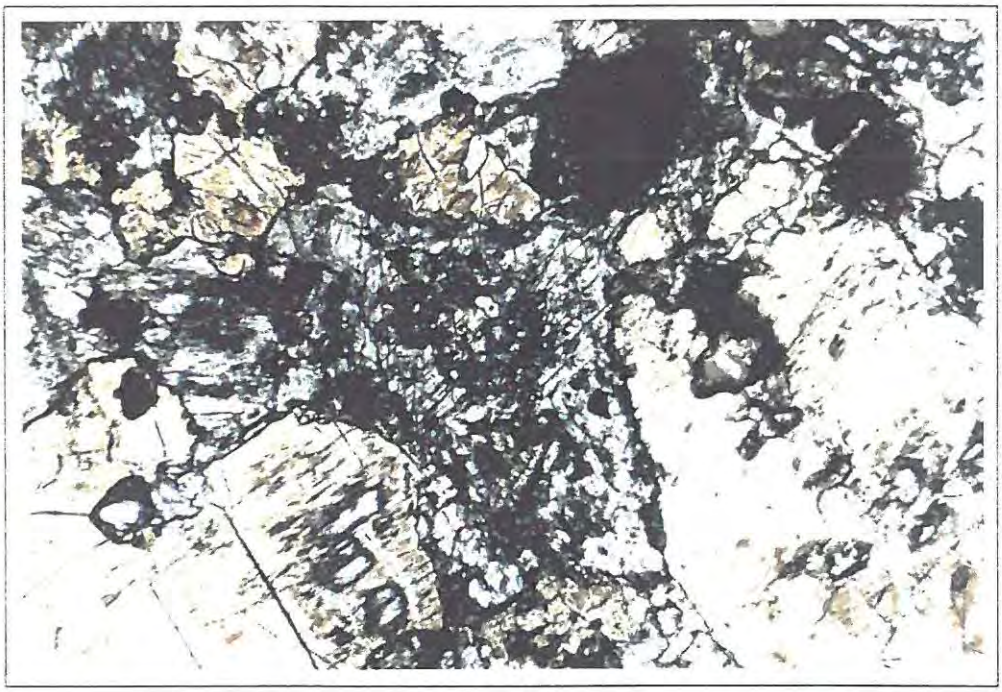

Plate 8a: Coarse-grained amphibole (pale brown) in alteration veinlet within garnet websterite (280). Yellow material is v.fine-grained alteration after orthopyroxene. FOV - 3.5 mm; Plane polarised light.

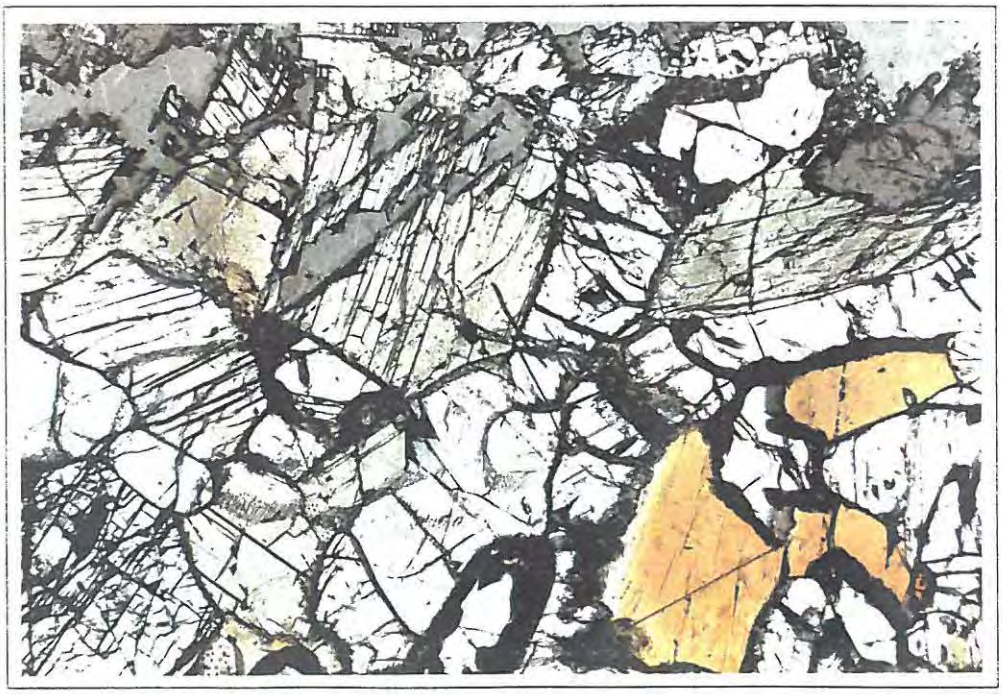

Plate 8b: Coarse-grained pargasitic amphibole (pale brown) and phlogopite (orange-brown) in garnet websterite (280). Other minerals are orthopyroxene (colourless, with cleavage), garnet (rimmed by dark kelyphite), and clinopyroxene (pale green). FOV - 3.5 mm; Plane polarised light.

phlogopite forms large (up to 3mm) laths which often show cross-cutting textures (Plate 8c), suggesting a primary metasomatic origin for this mineral. In contrast to this, many of the samples contain small amounts (<1%) of fine-grained secondary phlogopite (<0.5mm) which occurs in association with kelyphite (rims around garnet) and other fine-grained alteration products. Fe-Ni sulphide (257,259) occurs as rather rare interstitial grains scattered throughout the samples.

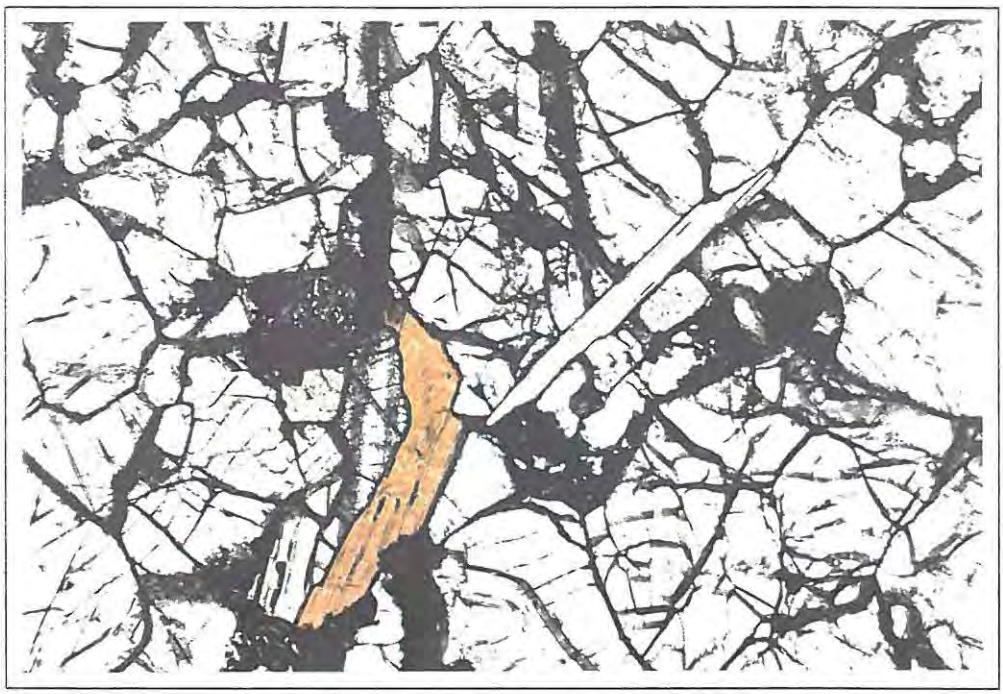

Plate 8c: Cross-cutting phlogopite grains in garnet websterite (280). The rock consists primarily of orthopyroxene, with lesser fine-grained garnet (rimmed or replaced by dark kelyphite), and clinopyroxene (pale green). FOV - 3.5 mm; Plane polarised light.

Kelyphite is developed to varying degrees in all of the garnet websterites studied. It consists of dark brown turbid material and very fine-grained opaque phases, and occurs either as rims around garnet or as small patches presumed to have originally been garnet grains. Other very fine-grained alteration products probably result from the breakdown of orthopyroxene and clinopyroxene caused by late stage infiltration of fluids from the kimberlite magma.

3.4.2. Garnet Orthopyroxenites

Apart from the absence of clinopyroxene, the garnet orthopyroxenite samples are very similar to the well-equilibrated garnet websterites. Garnet occurs

as relatively fine grains (usually <1mm) which form between 14 and 26 percent of the rocks (Fig.3.2), orthopyroxene generally being slightly coarser- grained (0.5 -2mm). Accessory phases include rutile (187,262), Ti-magnetite (187), and Fe-Ni sulphide (187). Apart from kelyphite rims around garnet and minor khaki-brown alteration along grain boundaries in samples 147 and 187, secondary minerals and alteration products are absent indicating that these rocks have not been subject to primary metasomatism or extensive late stage alteration.

Because of the fresh nature of the rocks, primary textures are well-preserved. Although garnet is generally finer-grained than orthopyroxene, the poorly equilibrated exsolution textures observed in the garnet websterite samples do not occur in the garnet orthopyroxenites. The rocks generally display granuloblastic-polygonal textures, suggesting that they have reached textural equilibrium. In contrast to some of the garnet websterite samples, coarse "relic" orthopyroxene grains are not observed. Rutile and the opaque minerals occur as scattered grains which appear to be in textural equilibrium with orthopyroxene and garnet.

Kelyphite rims on garnet are made up of dark very fine grained material with small aluminous spinel grains concentrated in the outer part of the rim (Plate 9).

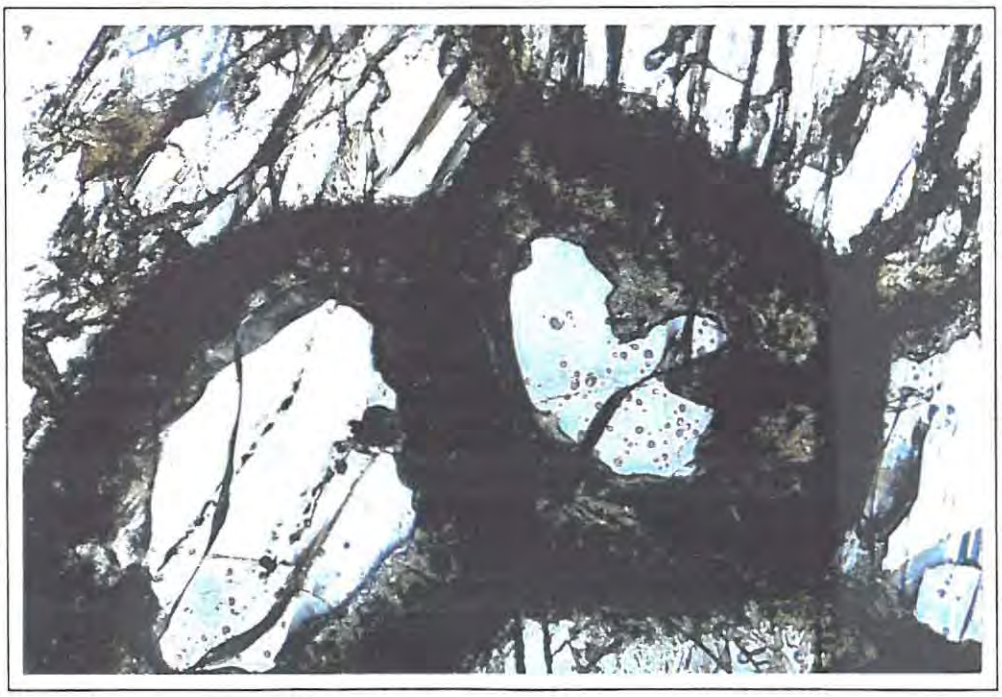

Plate 9: Kelyphite rimming garnet in garnet orthopyroxenite (262). An inner rim of very fine-grained khaki-brown alteration is surrounded by dark, spinel-rich material. Surrounding mineral is orthopyroxene. FOV - 1 mm; Plane polarised light.

3.4.3. Spinel Clinopyroxenite

This is a coarse-grained granuloblastic rock with medium- to coarse-grained pale green amphibole. Chrome-spinel occurs as scattered small (<0.5mm) rounded grains, and as inclusions in clinopyroxene. Late stage fine-grained brown and yellow-brown alteration affects both clinopyroxene and amphibole along grain boundaries.

3.5. Eclogites

Nine eclogite samples from Abrahamskraal were studied. Garnet/clinopyroxene ratios vary from 63:37 to 24:76 (see Fig. 3.3). Accesory rutile occurs in six of the samples, and primary sulphides (Fe-Ni) occur in sample 229. Rutile and sulphide grains are usually small (<0.5mm) but occassional coarse grains occur (up to 1mm). Phlogopite occurs in varying amounts in all but three of the eclogites, but its mode of occurrence is highly variable (see below). Other minerals believed to be of primary metasomatic or secondary origin are hornblende, minor amounts of sulphide, and intergrown fine- grained spinel and orthopyroxene which occurs as outer rims on garnet. Very fine-grained alteration products include turbid brown alteration of clinopyroxene, and dark brown kelyphite rims on garnet. Small amounts of carbonate occur in samples 229 and 269.

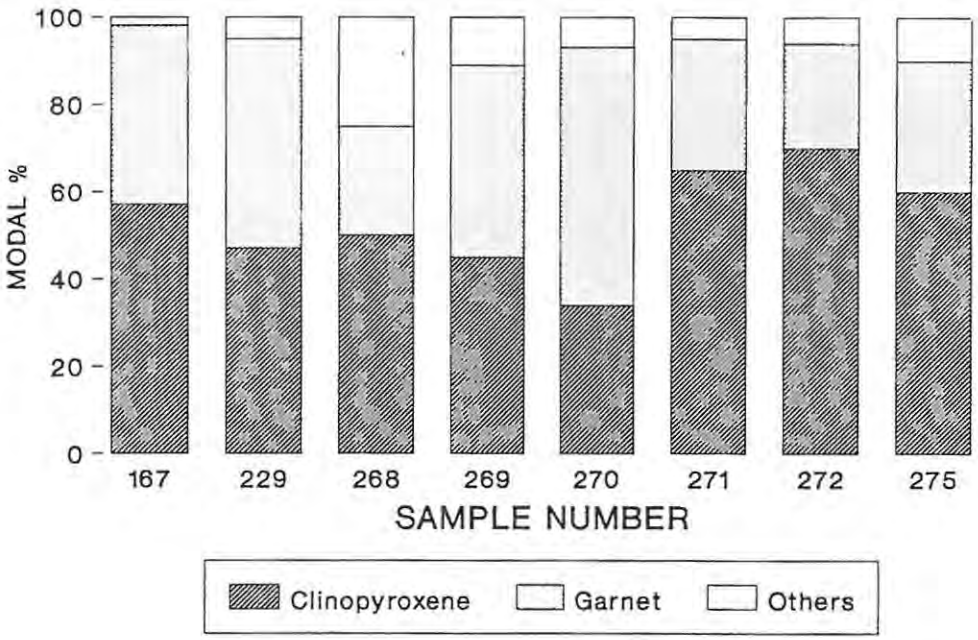

Fig. 3.3: Modal compositions of the Abrahamskraal eclogite xenoliths. "Others" includes rutile, various opaque phases, and late-stage alteration. Due to extensive alteration, the modal composition of sample 284 could not be reliably estimated.

Two textural varieties of eclogite, i.e. coarse- (0.5-6mm) and fine-grained (≤1mm), can be distinguished. Primary textures in the coarse-grained eclogites vary according to the ratio of garnet and clinopyroxene in the rock. Where the samples are rich in garnet, clinopyroxene occurs as relatively small interstitial grains in coarse garnet aggregates which display a granuloblastic textures (Plate 10a). In more clinopyroxene-rich areas however, garnet usually occurs along grain boundaries (where it forms embayments in the clinopyroxene), at triple junctions between coarse clinopyroxene grains, or as inclusions in clinopyroxene. The clinopyroxene in these areas is usually coarser-grained, and displays interlocking textures which tend towards granuloblastic-polygonal (e.g. 271, Plate 10b). Garnet inclusions in clinopyroxene are present in all but one (275) of the samples studied, while clinopyroxene is very rarely found as inclusions in garnet. The interstitial clinopyroxene, and the abundant garnet inclusions in clinopyroxene may be remnants of earlier igneous textures, although the evidence is by no means conclusive. The finer-grained eclogites (229,284) are equigranular and show granuloblastic-polygonal textures.

Phlogopite occurs as very coarse-grained cross-cutting plates (268); fine- to medium-grained laths also showing discordant textural features in places (273); as rims around garnet (and kelyphite; 160,271,273); as medium- to fine-grained aggregates in veinlets or aggregates (279); and as small grains along the grain boundaries of clinopyroxene and garnet. Hornblende occurs as small grains (≤0.5mm) in association with the very coarse phlogopite in sample 268, and minor amounts occur in the phlogopite-rich veinlets and aggregates in sample 270. In samples 167 and 275 hornblende forms fine- to medium-grained aggregates rimming and in some cases entirely replacing garnet. With the exception of the medium- and coarse-grained phlogopite which is probably of primary metasomatic origin, all of the above described minerals are believed to be the result of secondary processes occurring after entrainment of the xenoliths in the kimberlite magma.

Kelyphite rims are developed on garnets in all of the samples studied, although in some cases they are very thin (<0.1mm). They consists of an inner rim of very fine-grained dark brown material which may in turn be rimmed by fine-grained intergrown spinel, and orthopyroxene, phlogopite and/or hornblende. Brown turbid material partially replaces the clinopyroxene rims in most of the samples and in some cases partially or completely replaces the clinopyroxene grains. This is believed to be a result of exsolution of small amounts of sodic plagioclase from the

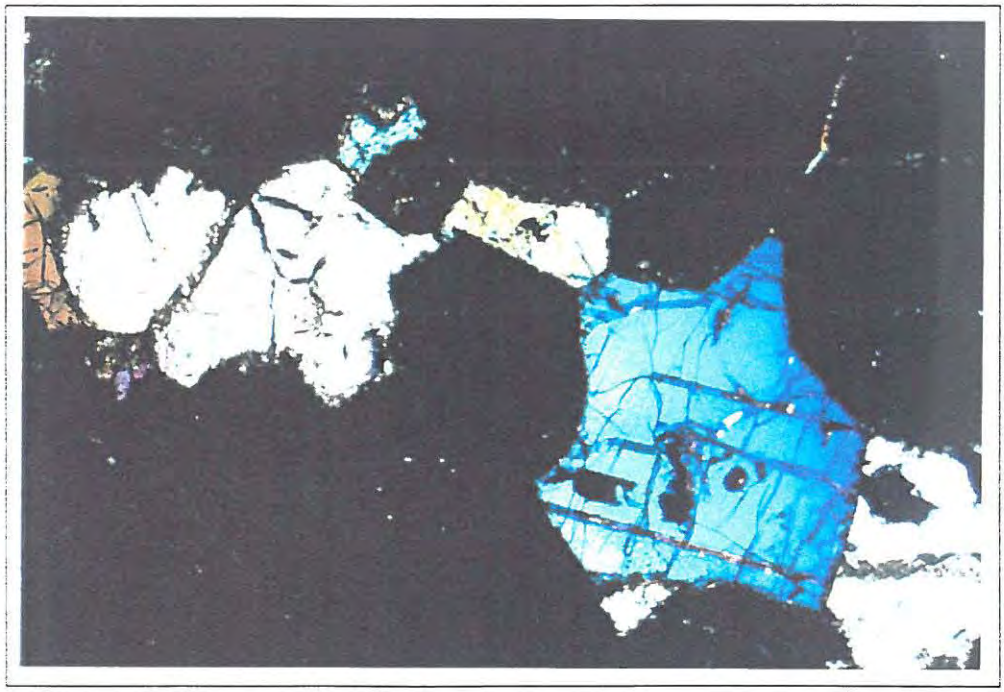

Plate 10a: "Interstitial" clinopyroxene in garnet-rich (black mineral) portion of eclogite (269). Garnet displays granuloblastic-polygonal textures. FOV - 3.5 mm; Crossed polars.

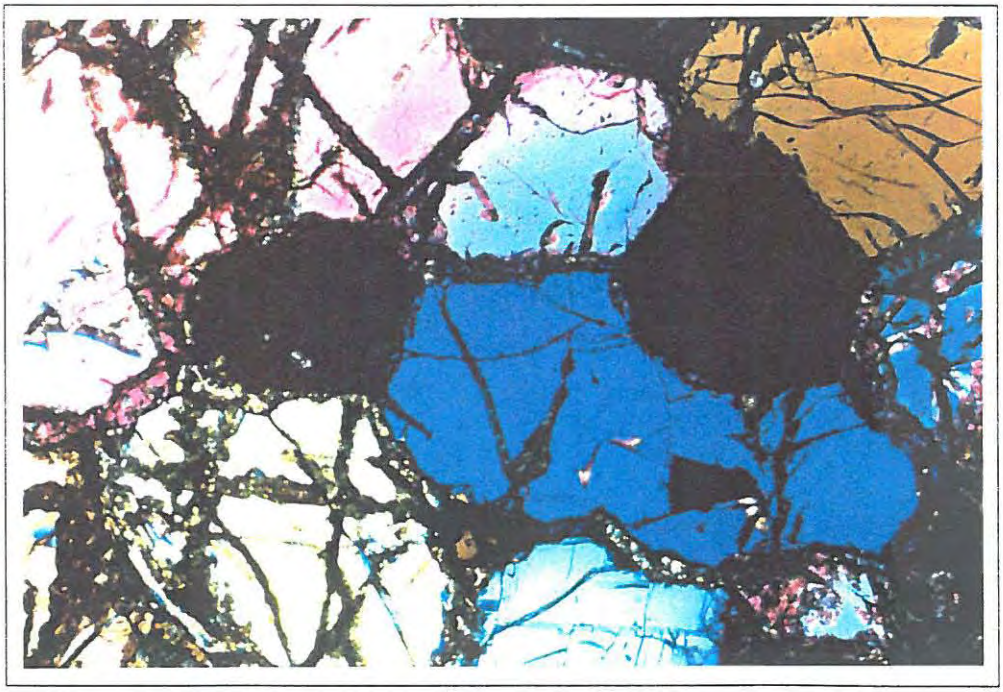

Plate 10b: Granuloblastic textures in clinopyroxene-rich portion of eclogite (271). FOV - 3.5 mm; Crossed polars.

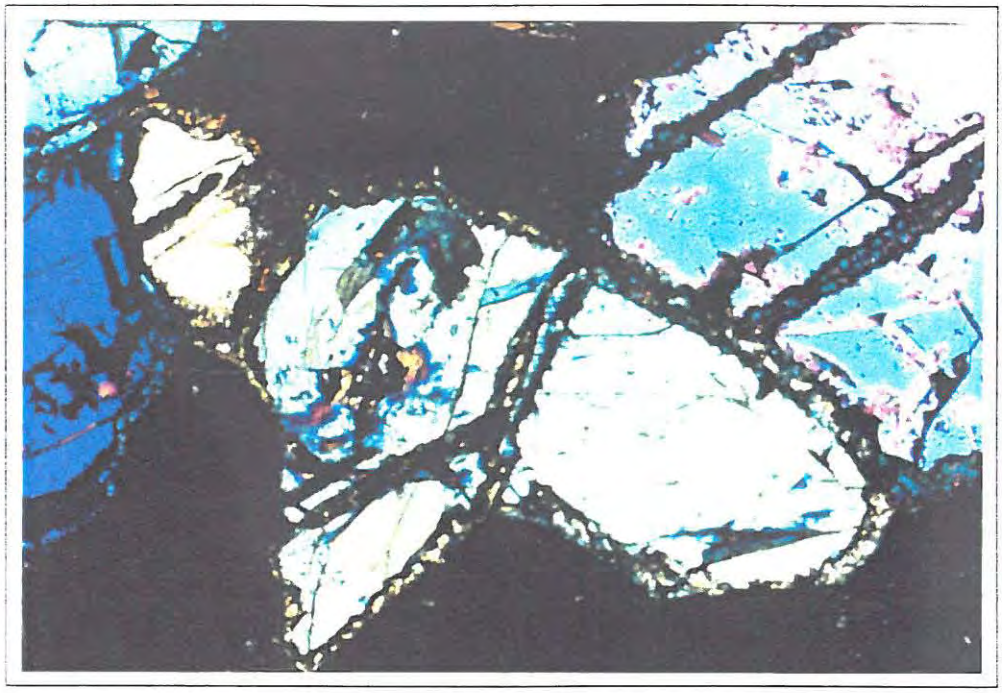

Plate 11: Na-poor secondary clinopyroxene rims on primary clinopyroxene in eclogite. The narrow rims are in optical continuity with the primary grains, but have a slightly different birefringence. FOV - 3.5 mm; Crossed polars.

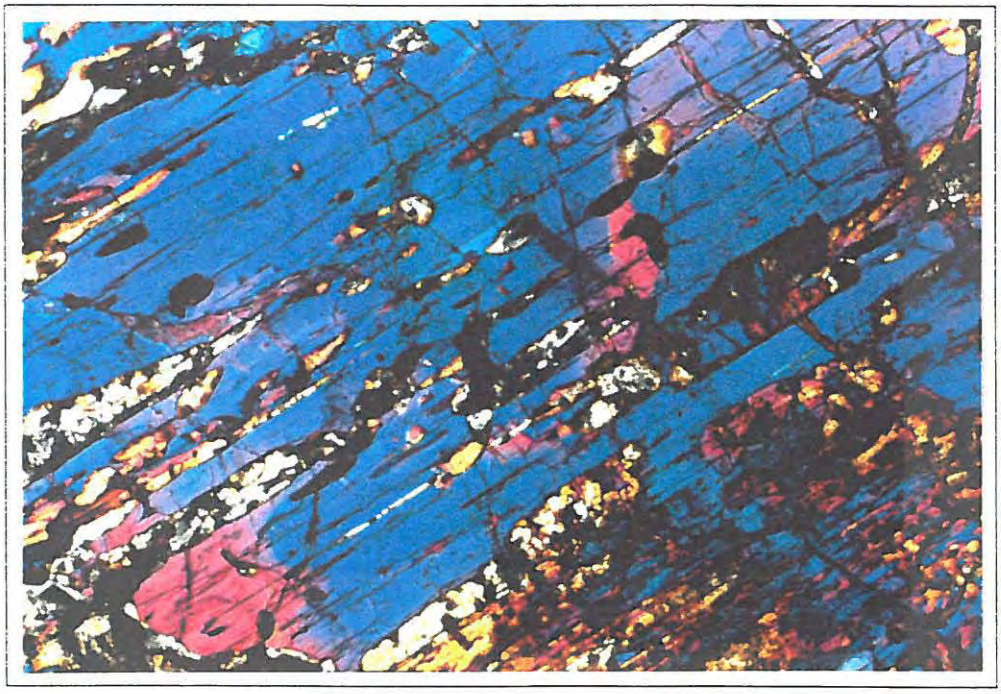

Plate 12: Garnet blebs (black) and orthopyroxene lamellae (white to yellow) in clinopyroxene megacryst (217). FOV - 3.5 mm; Crossed polars.

clinopyroxene during decompression, and occurs due to the inability of clinopyroxene to accomodate significant amounts of Na at low pressures. In many cases this results in the formation of sodium-poor clinopyroxene rims around primary clinopyroxene grains (Plate 11). In sample 178 large patches of intergrown fine grained albite occur. The origin of these patches is not clear, but they may have formed by the complete breakdown of Na-rich clinopyroxene.

6. Clinopyroxene Megacryst

A single clinopyroxene megacryst from Abrahamskraal was examined. The megacryst is approximately 2cm in diameter and has exsolved both orthopyroxene and garnet (Plate 12). Orthopyroxene occurs as irregular patches (up to 1mm in diameter) and lamellae which reach up to 0.2mm in thickness. Garnet has been exsolved as small blebs which in some cases are elongated along the principle cleavage direction in the clinopyroxene grain. Rutile occurs as small (<1mm), angular inclusions in the clinopyroxene.

4. MINERAL CHEMISTRY

4.1. Analytical Procedure

Minerals in the Abrahamskraal xenoliths were analysed using a JEOL Superprobe (model 733). Analyses were done using a 15 kV accelerating voltage, and a sample current of 25 nA. Peak and backround positions were counted for twenty and ten seconds respectively. Natural and synthetic standards were used, and the ZAF method was used for the correction of raw data.

Multiple analyses of single grains were carried out in order to determine analytical precision, which was found to be better than ± 2% for major elements (> 10 wt%), and ± 10% for minor elements (< 2 wt%). In order to asses inter- and intra-grain variations in mineral composition, multiple analyses (usually more than 3 points) of both cores and rims were carried out on several grains (≥ 3 grains in each sample) of each mineral. In most cases inter-grain variations in core compositions for any particular sample were within analytical error, suggesting chemical equilibrium between the primary minerals. Zoning was observed in several of the samples, and is discussed below. With the exception of the sections on zoning, the following discussion is based on average core compositions. Average core and rim compositions for the primary (and some of the secondary) minerals are given in appendix 3.

In the sections on garnet composition, reference is made to the classification scheme of Dawson and Stephens (1975). These authors have classified kimberlitic garnets into twelve groups on the basis of mineral composition. Their scheme is based on statistical (cluster) analysis of 352 analyses of garnets from kimberlites and their xenoliths.

4.2. Peridotites and Dunites

The mineral compositions of the peridotite xenoliths from Abrahamskraal are typical of those of the common Mg-rich, coarse, peridotite xenoliths, well documented from kimberlites world-wide (see Harte, 1983, and Gurney and Harte, 1980 for reviews). The compositions of the peridotitic minerals are graphically represented in terms of their Ca, Mg and Fe contents in Fig. 4.1. All the minerals are very Mg-rich and display restricted compositional variations.

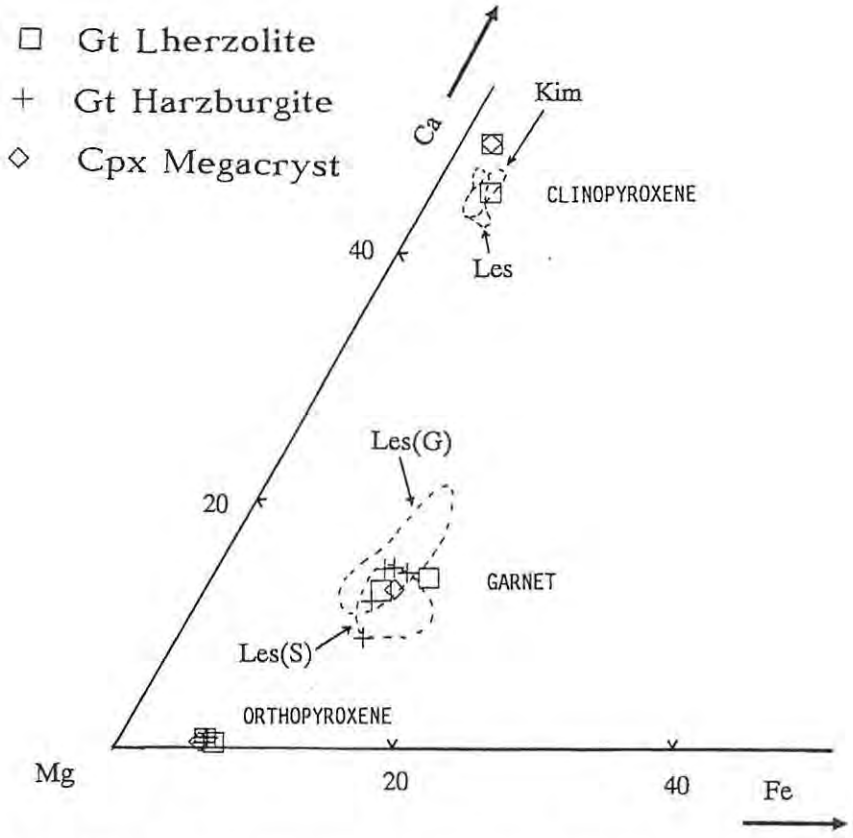

Fig. 4.1: A portion of a ternary CMF diagram showing the compositions of the Abrahamskraal peridotite xenoliths in relation to those from the northern Lesotho (Les), and Kimberley (Kim) kimberlites. Data for northern Lesotho and Kimberley were obtained from Nixon and Boyd (1973a), and Boyd and Nixon (1978) respectively. G - granular; S - sheared.

4.2.1. Garnet

Garnets from the garnet peridotites are all chrome-pyropes (group 9 of Dawson and Stephens, 1975), and show a high degree of compositional overlap with peridotitic garnets from other kimberlites (Fig. 4.1 and 4.2). No systematic differences in composition occur between garnets from garnet lherzolites and those from garnet harzburgites. Mg/Mg+Fe ratios and Cr_2O_3 values range from 0.839 to 0.899, and 2.16 to 5.10 respectively, and they are all very Ti-poor (< 0.1 wt% TiO_2). In sample 156, discrete garnet grains have the same composition as those intergrown with spinel.

Exsolved garnet in the clinopyroxene megacryst sample has slightly lower chrome (1.82 wt% Cr_2O_3), but is otherwise very similar to the peridotitic garnets (Fig. 4.3). It is enriched in chrome and magnesium relative to garnets from the common Cr-poor megacryst suites (Fig. 4.3), but contains considerably less chrome than the Cr-rich megacrysts from the Colarado-Wyoming kimberlites, which range from 3 to 13 wt% Cr_2O_3 (Schulze, 1987).

Cr_2O_3 - CaO variations in the peridotitic garnets are illustrated in Fig. 4.4. Apart from a single, slightly subcalcic, harzburgitic garnet, they all plot within the garnet lherzolite trend established by Sobolev *et.al.* (1973), suggesting that the rocks are Ca saturated and that all of the garnets equilibrated in the vicinity of clinopyroxene (as well as orthopyroxene and olivine). The apparent absence of clinopyroxene from most of the peridotite samples, may be due to sampling problems associated with the coarse-grained nature and small sample size of the xenoliths.

4.2.2. Orthopyroxene

Orthopyroxene compositions in the peridotites are very restricted (see Fig. 4.1 and 4.5). They are all enstatites with Mg/Mg+Fe ratios varying from 0.934 to 0.941, and CaO contents between 0.20 and 0.49 wt%. The Al_2O_3 content of the orthopyroxenes is low (1.02 to 0.83 wt%), in keeping with their presumed high pressure origin (see section 6). These compositional ranges are comparable to those displayed by orthopyroxenes from peridotitc xenoliths in both on- and off-craton kimberlites (Fig. 4.5). Differences in

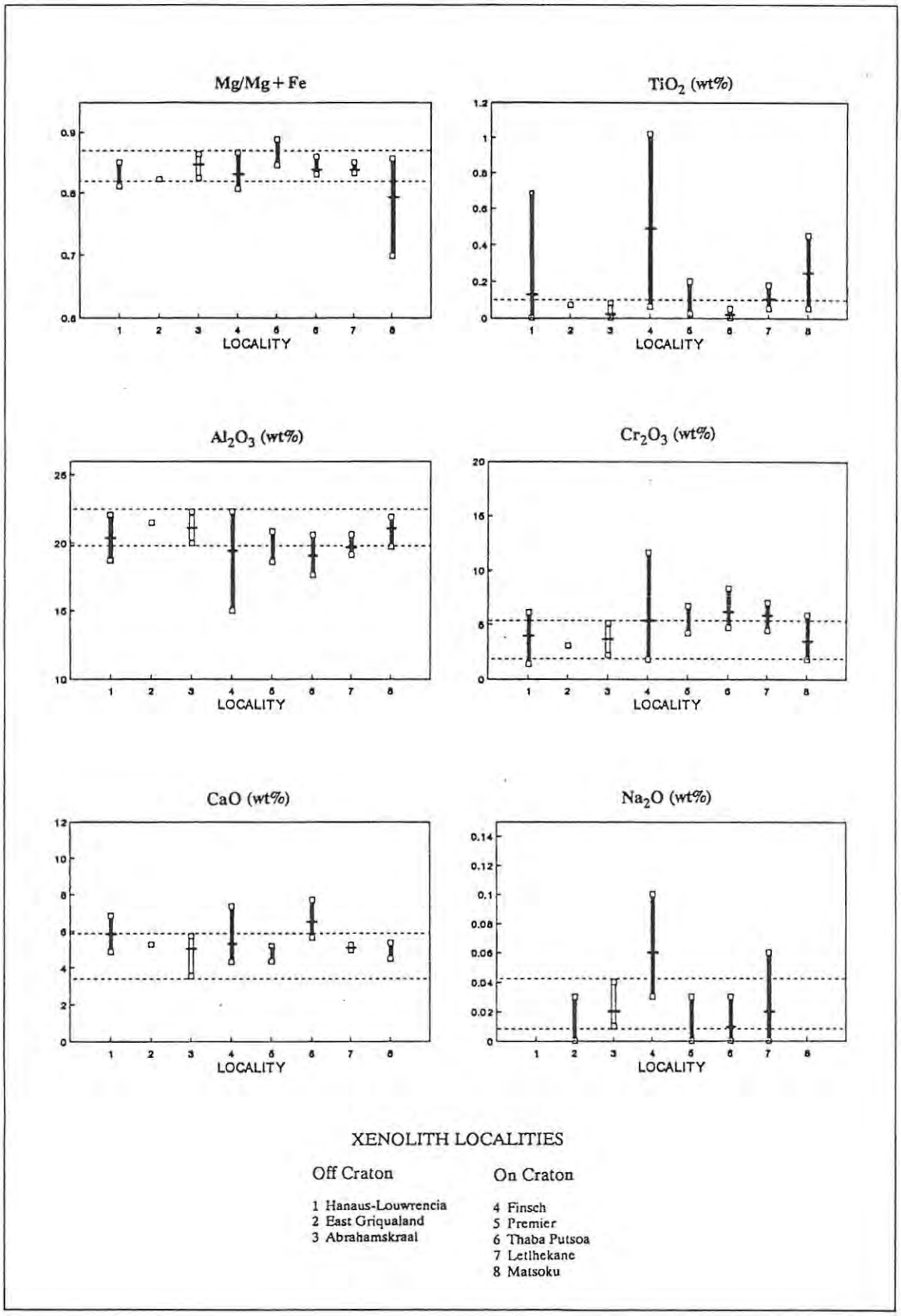

Fig. 4.2: Diagrams showing the compositional ranges displayed by peridotitic garnets from a number of on- and off-craton kimberlites. The dashed line delineates the range displayed by Abrahamskraal peridotitic garnet. ╋ - average value. Data for the various localities were obtained from: 1 - Mitchell (1984); 2 - Nixon (1987); 4 - Skinner (1989); 5 - Danchin (1979); 6 - Nixon and Boyd (1973a); 7 - Shee (1978); 8 - Cox et.al. (1973).

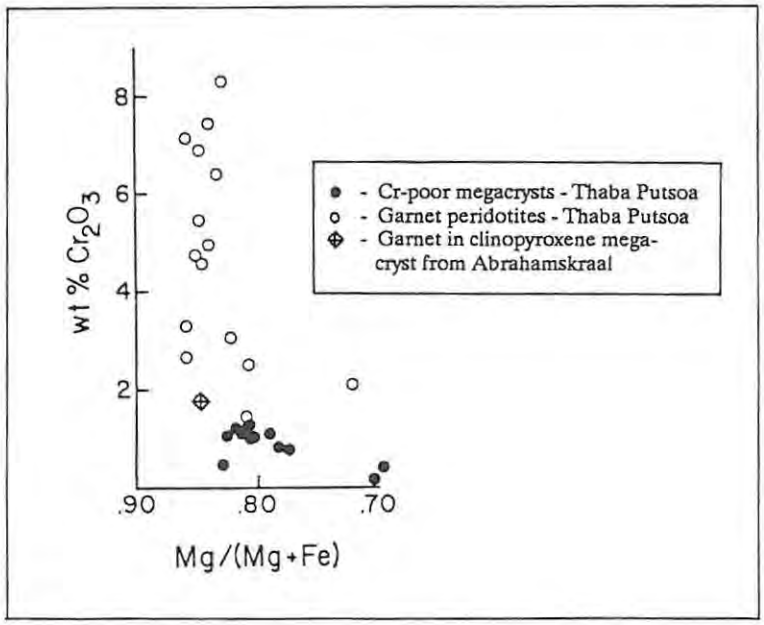

Fig. 4.3: Plot of wt% Cr_2O_3 vs Mg/Mg+Fe showing the composition of exsolved garnet in the Abrahamskraal clinopyroxene megacryst in relation to garnets from the Thaba Putsoa (N.Lesotho) Cr-poor megacryst and garnet peridotite suites (after Schulze, 1987). Data from Nixon and Boyd (1973a,b).

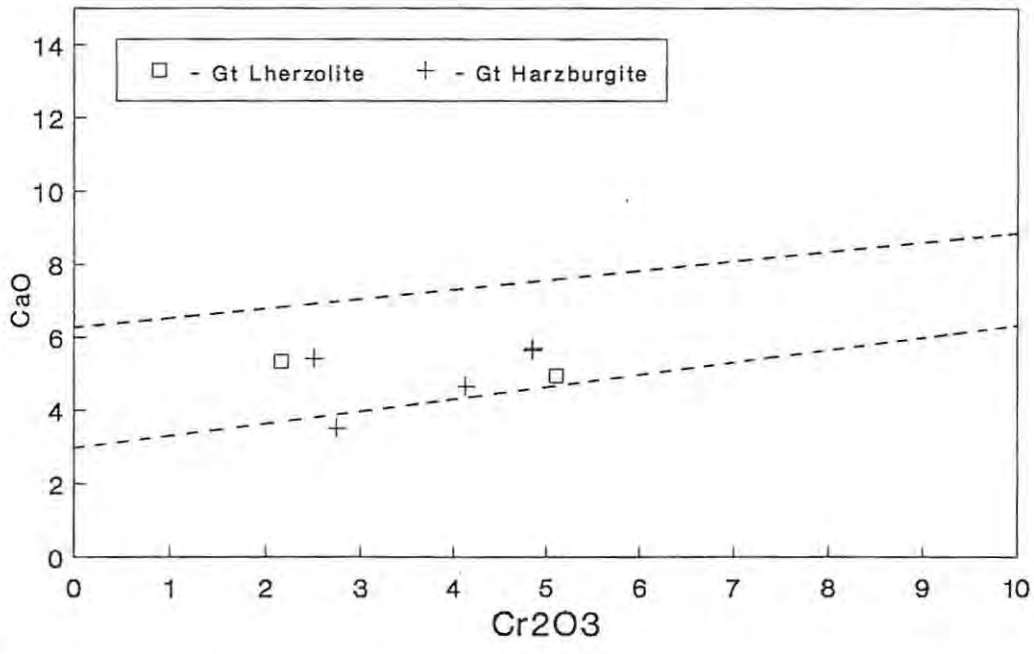

Fig. 4.4: Plot of wt% CaO vs Cr_2O_3 in peridotitic garnets from Abrahamskraal. Dashed lines delineate the lherzolite trend of Sobolev et.al. (1973).

Al_2O_3 content are a function of varying depths of equilibration, and it is interesting to note that in terms of the Al_2O_3 content of peridotitic orthopyroxenes, the off-craton kimberlites at Hanaus and Louwrencia, as well as the Abrahamskraal kimberlite, show considerable overlap with several of the on-craton kimberlites.

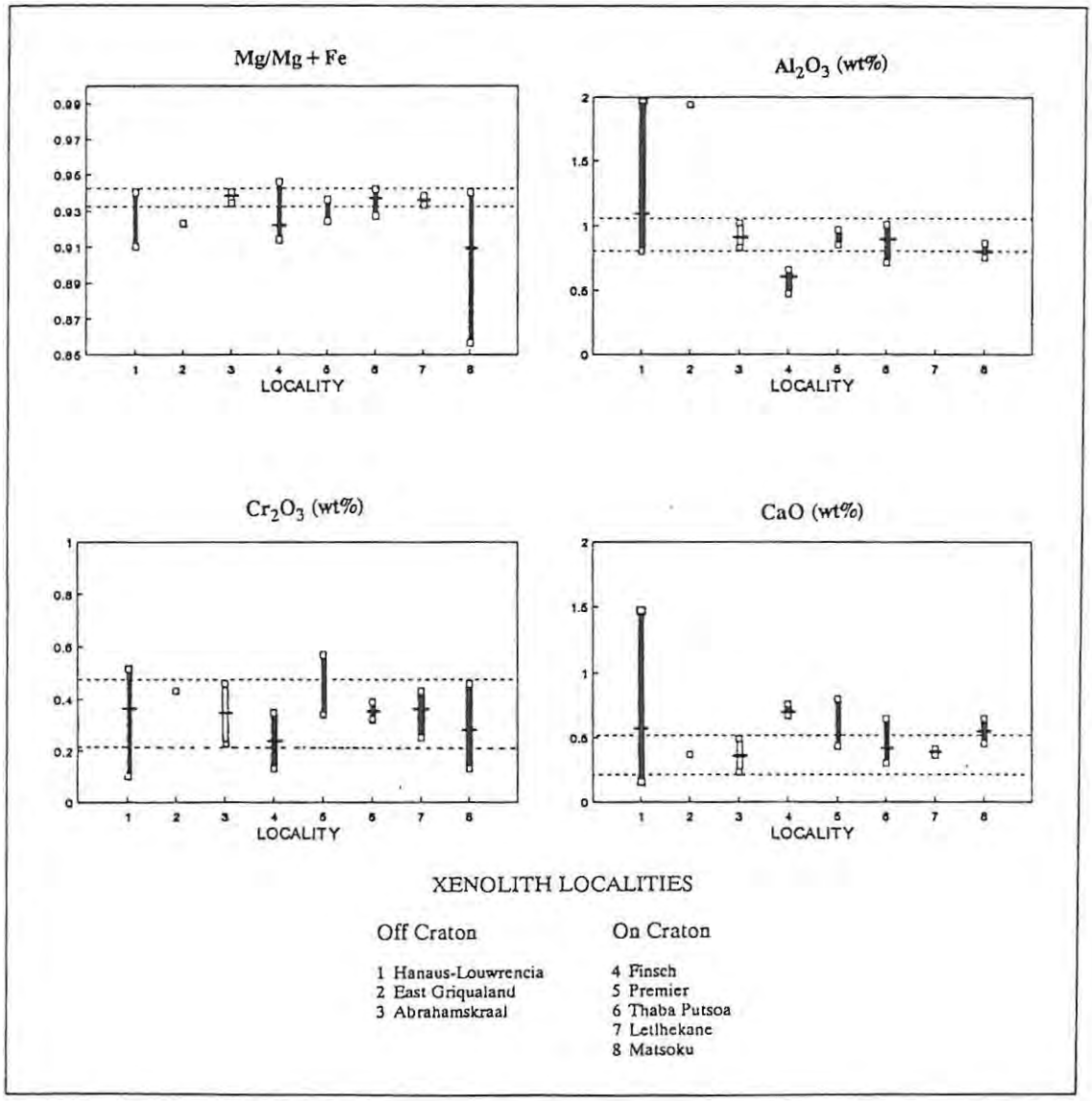

Fig. 4.5: Diagrams showing the compositional ranges displayed by peridotitic orthopyroxenes from a number of on- and off-craton kimberlites. The dashed line delineates the range displayed by Abrahamskraal peridotitic orthopyroxene. ╪ - average value. Data for the various localities were obtained from: 1 - Mitchell (1984); 2 - Nixon (1987) ; 4 - Skinner (1989); 5 - Danchin (1979); 6 - Nixon and Boyd (1973a); 7 - Shee (1978); 8 - Cox et.al. (1973).

On the basis of mineral composition, exsolved orthopyroxene in the clinopyroxene megacryst is indistinguishable from primary peridotitic orthopyroxene.

4.2.3. Olivine

Forsterite contents of olivines from the peridotites range from 92 to 93, and are typical of depleted Mg-rich peridotite xenoliths from other localities (Fig. 4.6; Harte, 1983; Gurney and Harte, 1980). The olivines from the dunites however are more variable in composition (Fig. 4.7). With the exception of sample 267 (in which olivine has Fo = 90), olivines in the coarse dunites (see section 3.3) have forsterite contents greater than or equal to 91. On the other hand, olivines in the medium- to fine-grained dunites range from Fo-86 to Fo-91, suggesting a different origin for these rocks, possibly by cumulus processes (see section 7.1).

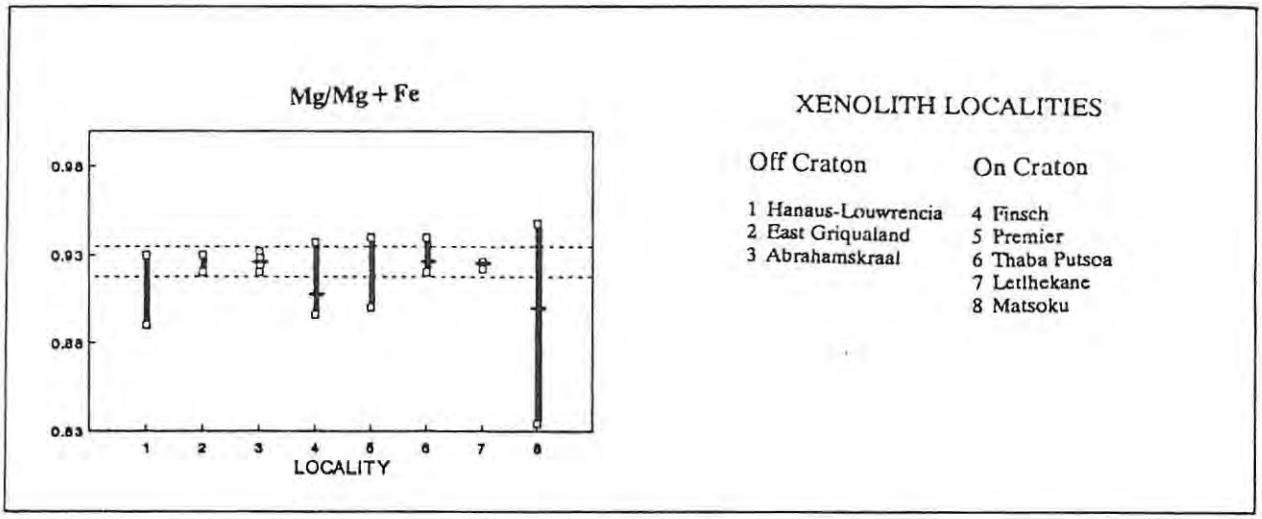

Fig.4.6: Diagram showing Mg/Mg+Fe ratios of olivines from a number of on- and off-craton kimberlites. The dashed line delineates the range displayed by Abrahamskraal peridotitic olivine. ⊣⊢ - average value. Data for the various localities were obtained from: 1 - Mitchell (1984); 2 - Nixon (1987); 4 - Skinner (1989); 5 - Danchin (1979); 6 - Nixon and Boyd (1973a); 7 - Shee (1978); 8 - Cox et.al. (1973).

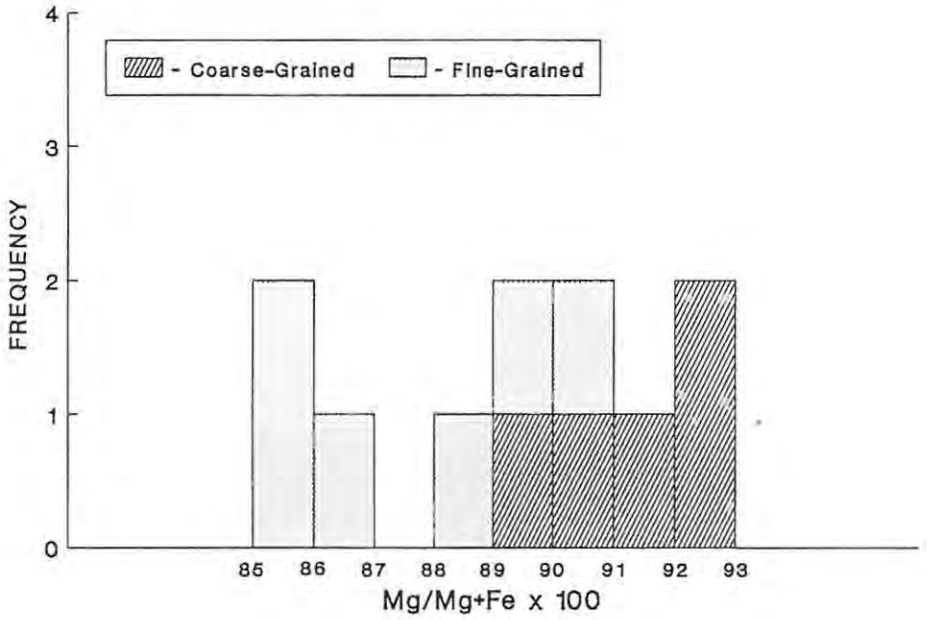

Fig. 4.7: Histogram showing the range in Mg/Mg+Fe ratios displayed by the two textural varieties of dunite (i.e. coarse- and fine-grained, see section 3.3).

4.2.4. Clinopyroxene

In contrast to the other minerals from the peridotite xenoliths, the compositions of clinopyroxene from the two garnet lherzolite samples (142,156) are significantly different from each other (Fig. 4.1 and 4.8). They are magnesium-rich (Mg/Mg+Fe = 0.928 and 0.958 respectively) and have relatively high Ca/Ca+Mg ratios (0.460 and 0.491 respectively), reflecting comparatively low temperatures of origin (i.e. they do not belong to the high temperature group of peridotitic xenoliths described from several kimberlite pipes, e.g. Nixon and Boyd, 1973a; Boyd, 1974; Harte and Gurney, 1982, see section 1.1). The two clinopyroxenes differ considerably in terms of the concentrations of several oxides, including: Al_2O_3 (3.28 and 1.48 wt%), Cr_2O_3 (3.07 and 0.80 wt%), CaO (18.69 and 23.57 wt%), and Na_2O (3.06 and 0.86 wt%). However, despite these differences, in most cases both of the Abrahamskraaal peridotitic clinopyroxenes show some overlap with those from at least one of the other kimberlite localities shown in Fig. 4.8. Apart from its Al_2O_3 content (5.18 wt%), the composition of metasomatic clinopyroxene is intermediate between those of the "primary" clinopyroxenes discussed above.

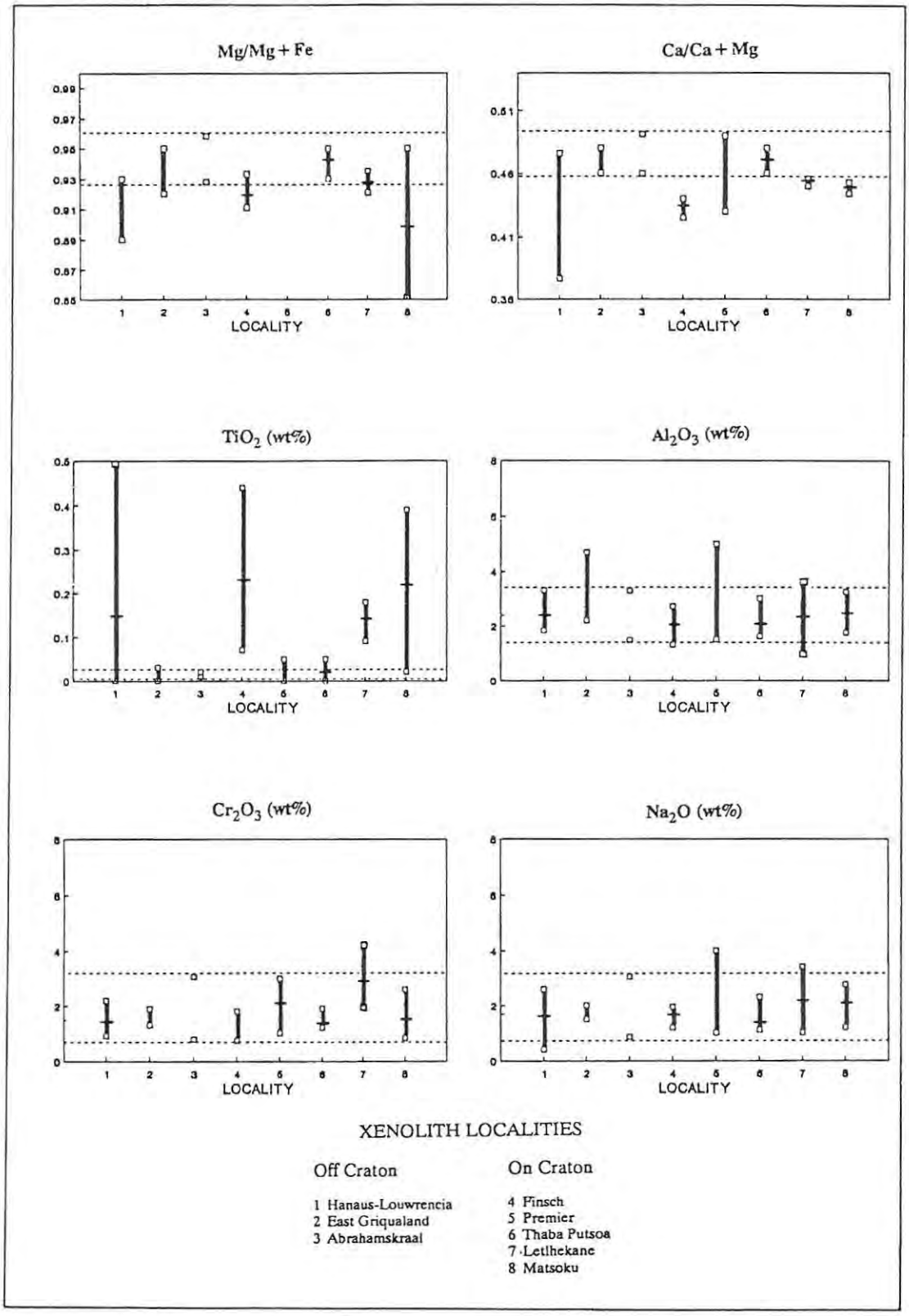

Fig. 4.8: Diagrams showing the compositional ranges displayed by peridotitic clinopyroxenes from a number of on- and off-craton kimberlites. The dashed line delineates the range displayed by Abrahamskraal peridotitic clinopyroxene. ╫ - average value. Data for the various localities were obtained from: 1 - Mitchell (1984); 2 - Nixon (1987); 4 - Skinner (1989); 5 - Danchin (1979); 6 - Nixon and Boyd (1973a); 7 - Shee (1978); 8 - Cox et.al. (1973).

As with garnet and orthopyroxene, the composition of the clinopyroxene megacryst is essentially the same as that in the Abrahamskraal lherzolites. The Abrahamskraal megacryst is more Ca- and Mg-rich than clinopyroxenes from Cr-poor and Cr-rich megacryst suites found elsewhere (Fig. 4.9).

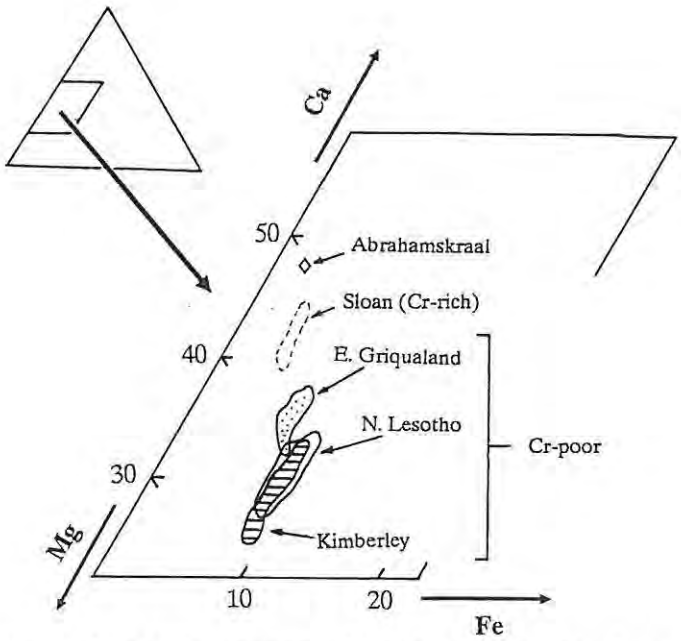

Fig.4.9: Portion of a CMF ternary diagram showing the composition of the Abrahamskraal clinopyroxene megacryst in relation to Cr-poor and Cr-rich megacryst suites from other localities. Data for Sloan from Schulze (1987). Data for Cr-poor suites from Nixon (1987).

4.2.5. Spinel

Primary Cr-spinel occurs in three peridotite samples (156, 143 and 261). Inter-sample variations in spinel chemistry are large, with Mg/Mg+Fe ratios ranging from 0.640 to 0.703, and Cr/Cr+Al ratios ranging from 0.685 to 0.462. With the exception of sample 261 (8.88 wt% Fe_2O_3), the spinels are relatively Fe_2O_3-poor (<5 wt%). In sample 156 discrete spinel grains have the same compositions as spinel occurring in intimate symplectite-like intergrowths with garnet.

Secondary spinels occurring in kelyphite rims around garnet are Al-rich, while those occurring in intergrowths with phlogopite and clinopyroxene in the harzburgites and dunites are Cr-rich (Cr/Cr+Al > 0.9), and have high

Fe_2O_3 contents (7.22 to 11.28 wt%).

4.2.6. Zoning

Apart from garnet, most of the minerals in the peridotite xenoliths are zoned to some extent. In all cases the chemical variation applies only to the outer 20 to 40 microns of the grains, and the absence of zoning in the garnet may be due to the replacement of this outer rim by late stage kelyphite. In orthopyroxene and clinopyroxene, zoning towards the rims involves increases in Al, Fe, Ti and to a lesser extent Ca, and decreases in Mg (Table 4.1). Variations are highly erratic and often are most extreme in the vicinity of secondary minerals such as Al-spinel and phlogopite. In one orthopyroxene grain, zoning was observed adjacent to a fracture. The elements involved in zoning (rims are richer in those elements which are normally associated with metasomatic enrichment events; Gurney and Harte, 1980; Harte, 1983), and its erratic nature suggest that the zoning may be a result of metasomatic processes rather than disturbances in the pressure-temperature regime.

	142 (Gt lherzolite)		149 (Gt harzburgite)	
	Core	Rim	Core	Rim
SiO_2	57.59	55.09	57.65	56.08
TiO_2	0.00	0.28	0.00	0.37
Al_2O_3	1.02	3.19	0.83	2.07
Cr_2O_3	0.46	1.05	0.36	0.63
FeO	4.09	4.98	4.21	5.49
MnO	0.10	0.17	0.09	0.13
NiO	0.12	0.09	0.11	0.14
MgO	36.05	33.79	36.09	33.92
CaO	0.40	1.19	0.43	1.06
Na_2O	0.17	0.24	0.08	0.21
Total	99.90	100.08	99.86	100.07

Table 4.1: Core and rim compositions of orthopyroxene in two garnet peridotites.

4.2.7. Summary

The compositions of peridotitic minerals are typical of those found in the coarse magnesium-rich xenoliths which generally dominate kimberlite

xenolith suites (Fig. 4.2, 4.5 and 4.8), and they clearly reflect the highly depleted nature of these rocks. Clinopyroxenes from the two lherzolite samples differ from the other peridotitic minerals in that they show relatively major intersample compositional variations. Although their compositions overlap with those of clinopyroxenes from other kimberlite-hosted garnet lherzolites (Fig. 4.8), they plot at opposite ends of the ranges displayed by these rocks. It is difficult to assertain the significance of these chemical variations, but the fact that they are not coupled with variations in the compositions of other phases may suggest that the clinopyroxene is not of primary origin.

The textural distinction between coarse- and finer-grained dunite varieties is corroborated by the olivine composition data. The finer-grained dunites show a wider compositional range (Fo86 - Fo91) than the coarser variety, which are restricted to highly magnesian compositions (≥Fo90).

4.3. Garnet Websterites and Orthopyroxenites

In contrast to the minerals from the peridotitic xenoliths, those from the garnet websterites and orthopyroxenites show very wide ranges in composition, primarily reflected in their Mg/Mg+Fe ratios (Fig. 4.10 and 4.11). Apart from a slight overlap in the case of clinopyroxene, the minerals in the garnet websterites and orthopyroxenites are more Fe-rich than those in the peridotites.

Coexisting minerals in the garnet websterites and orthopyroxenites are plotted on CMF and AFM diagrams in Fig. 4.10 and 4.11 respectively. The near-absence of crossing tie-lines between coexisting phases on the CMF diagram indicates consistent Fe-Mg partitioning between the minerals. This is strongly suggestive ofchemical equilibrium. However, the minerals (particularly garnet and orthopyroxene) can be subdivided into a Mg-rich and an Fe-rich group, and there does appear to be a significant difference in garnet-clinopyroxene Fe-Mg partitioning between the two. This is more clearly illustrated on the AFM diagram (Fig. 4.11), where garnet-clinopyroxene tie-lines from the two groups intersect each other in several places. Within the groups all the tie-lines are parallel. These features appear to result from the fact that clinopyroxene in the Mg-poor

websterites does not show Fe-enrichment trends equivalent to those seen in garnet and orthopyroxene. Garnet-orthopyroxene tie-lines are in all cases approximately parallel (no intersections), indicating equilibrium between these two minerals.

In Fig. 4.10 the compositions of minerals in the Abrahamskraal garnet websterites and orthopyroxenites are compared to those of similar xenoliths from the northern Lesotho kimberlites and from the Mesozoic and Cenozoic basaltic rocks of eastern Australia.

4.3.1. Garnet

Garnets from the garnet websterites and orthopyroxenites of this study fall into two groups distinguished by their Mg/Mg+Fe ratios. Although the Mg-rich garnets fall into group 9 of Dawson and Stephens (1975), they are more Fe-rich than the peridotitic garnets, and have distinctly lower Cr_2O_3 contents. The most Cr-rich garnet occurs in the Cr-spinel-bearing sample 274 (1.86 wt%), whereas those without primary Cr-spinel all contain less than 0.32 wt% Cr_2O_3. The Fe-rich variety of garnets fall into group 3, i.e. that of the "common eclogites" (Dawson and Stephens, 1975). Apart from the Mg/Mg+Fe ratios, no systematic differences exist between the two varieties of garnet. Their Al_2O_3 (21.22 to 22.66 wt%) and CaO (4.8 to 5.9 wt%) contents are higher but less variable than those in the peridotitic garnets.

The compositional variations shown by the Abrahamskral pyroxenitic garnets are similar to those for pyroxenite xenoliths from eastern Australia and northern Lesotho (Fig. 4.10). The Ca-contents of garnets from all three localities are approximately equal, and show minimal variation. The Mg/Mg+Fe ratios of the garnets are however highly variable, and the range shown by the Abrahamskraal garnets overlaps with those from Australia and northern Lesotho. Garnets from the northern Lesotho pyroxenite xenoliths extend to more Fe-rich compositions than those from Abrahamskraal.

4.3.2. Orthopyroxene

Orthopyroxenes of the garnet websterites and orthopyroxenites from

Abrahamskraal fall into two separate groups which correspond to the two groups of websteritic garnets found in these rocks (Fig. 4.10). As would be expected under equilibrium conditions, orthopyroxenes coexisting with group 9 garnets are more magnesian than those coexisting with group 3 garnets.

Both groups of orthopyroxene are distinguishable from peridotitic orthopyroxenes by their lower Mg/Mg+Fe ratios (0.900 to 0.732), and Cr_2O_3 contents (0.34 to 0.04 wt%). They show very limited intersample variation in CaO content (0.15 to 0.26 wt%), and are generally more Ca-poor than the peridotitic orthopyroxenes. Al_2O_3 contents (0.91 to 2.47 wt%) overlap with those from peridotites but extend to more Al-rich compositions reflecting shallower depths of equilibration (see section 6).

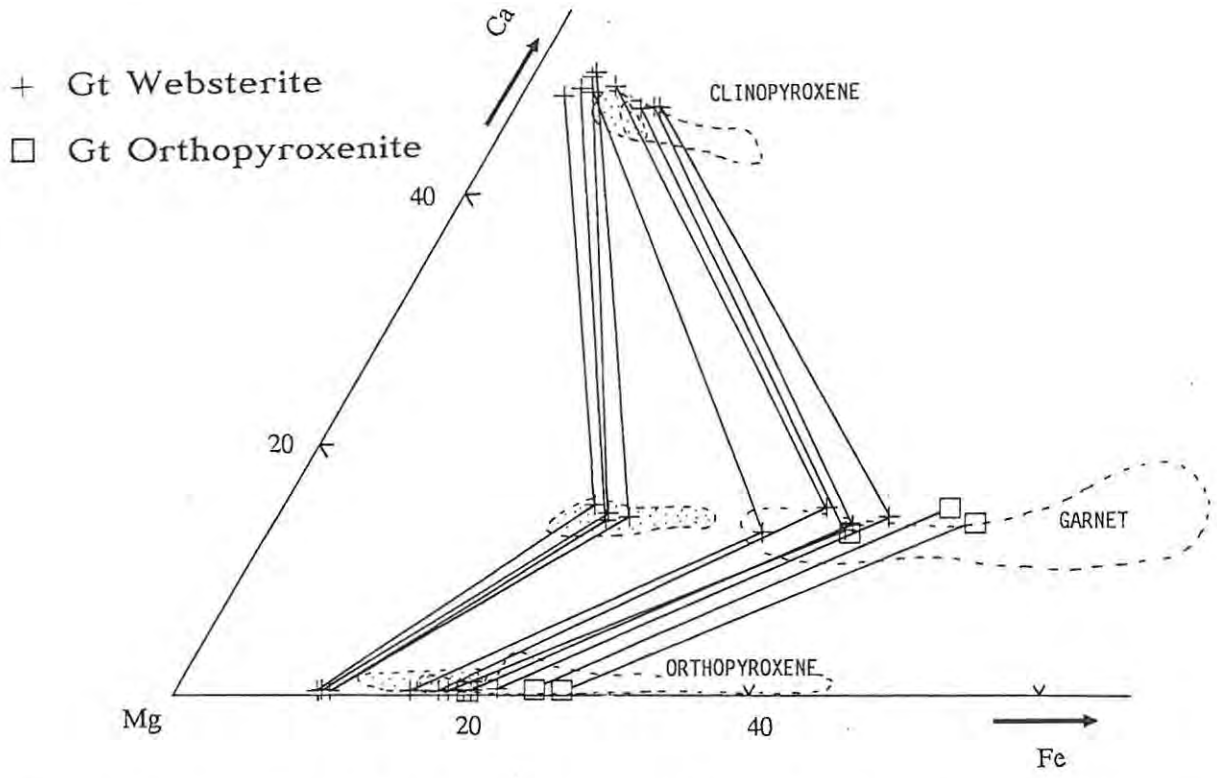

Fig. 4.10: Portion of a CMF ternary diagram showing the compositions of coexisting garnet, orthopyroxene, and clinopyroxene in the Abrahamskraal garnet pyroxenites. Also shown are the compositional fields for pyroxenitic minerals from the northern Lesotho kimberlites (dashed line; Griffin et.al., 1979) and from the alkali basalts of eastern Australia (stippled field; Griffin et.al., 1984).

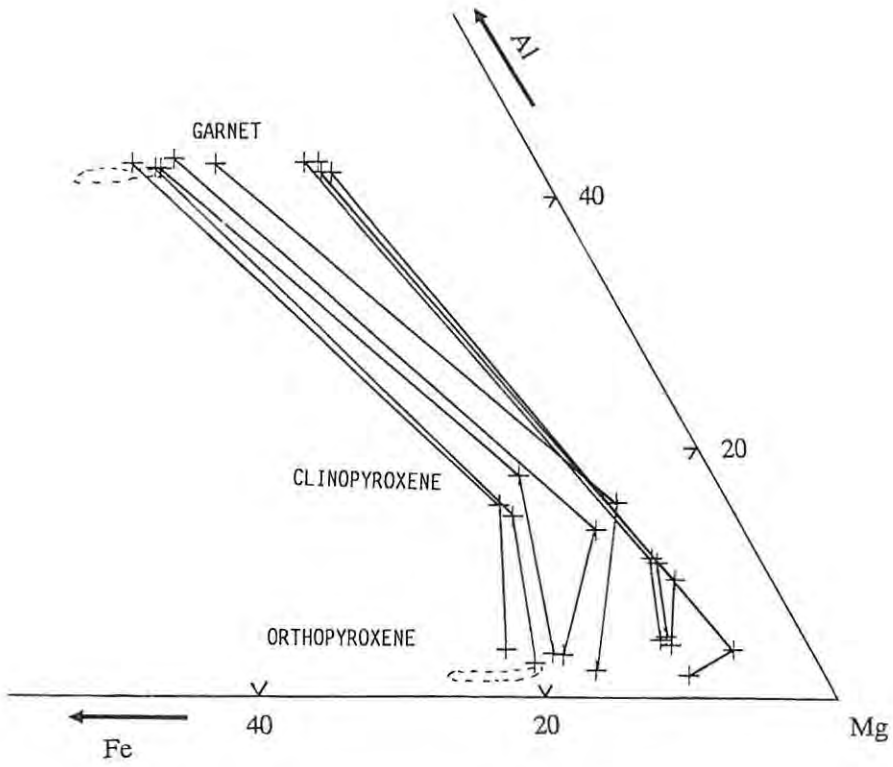

Fig. 4.11: Portion of an AFM ternary diagram showing the compositions of coexisting garnet, orthopyroxene, and clinopyroxene in the Abrahamskraal garnet websterites. Also shown are the compositional fields for garnet and orthopyroxene from the Abrahamskraal garnet orthopyroxenites (dashed line).

The compositional ranges shown by pyroxenitic orthopyroxenes from Abrahamskraal, eastern Australia and northern Lesotho correlate well with those displayed by coexisting garnet (Fig. 4.10). However orthopyroxene from the eastern Australian pyroxenite xenoliths appears to be slightly richer in Ca than that from Abrahamskraal. Although the northern Lesotho orthopyroxenes extend to more Fe-rich compositions, their Ca contents are approximately equal to those from Abrahamskraal, and there is a considerable amount of overlap between the compositional fields for the two localities.

4.3.3. Clinopyroxene

The websteritic clinopyroxenes show a more restricted range of Mg/Mg+Fe ratios than coexisting garnet and orthopyroxene, and unlike the latter two minerals, they are not clearly separable into two groups (Fig. 4.10). In keeping with the trends shown by garnet and orthopyroxene, websteritic clinopyroxene is generally more Fe-rich and Cr-poor (0.13 to 0.61 wt% Cr_2O_3) than that from the garnet lherzolite samples, although there is some overlap of Mg/Mg+Fe ratios (0.809 to 0.944).

As for garnet and orthopyroxene, clinopyroxene compositional trends are very similar for the three localities shown in Fig. 4.10, and the same patterns of Fe-enrichment are evident. In contrast to garnet and orthopyroxene however, clinopyroxene shows a slight decrease in Ca-content with decreasing Mg/Mg+Fe ratio. This trend is displayed by clinopyroxenes from the Abrahamskraal and the northern Lesotho pyroxenites, and highlights the compositional similarities between the two rock suites.

4.3.4. Olivine

Olivine in the single olivine-bearing garnet websterite of this study (283) is slightly Fe-rich (Fo-89) relative to the peridotitic olivines, and coexists with minerals at the more Mg-rich end of the range displayed by the garnet websterite assemblages.

4.3.5. Opaques

Six of the garnet websterite xenoliths of this study contain an apparently primary opaque phase. In five of these rocks (72,257,259,264,283) the dominant phase is magnetite with exsolved lamellae of Ti-magnetite (ulvospinel ?). One of the samples (274) contains Cr-spinel with a Mg/Mg+Fe ratio of 0.487, and a Cr/Cr+Al ratio of 0.654.

4.3.6. Zoning

Zoning in the garnet websterites is observed in orthopyroxene and clinopyroxene but not in garnet (probably for the same reasons as outlined

in section 4.2.6.). The zoning patterns in the garnet websterites and orthopyroxenites are different to those observed in the peridotites. Zoning in orthopyroxene and clinopyroxene (Table 4.2) involves a decrease in Al, and to a lesser extent Fe and Ca (in clinopyroxene only), and inreases in Mg towards the rims (this is exactly opposite to what is observed in the peridotites). The variations are not as erratic as those in the peridotites, and do not appear to be dependant on proximity to secondary phases. Thus the zoning may reflect partial reequilibration of the minerals under changing pressure-temperature conditions. The significance of the zoning patterns is discussed further in section 6.

	257				280			
	Opx		Cpx		Opx		Cpx	
	Core	Rim	Core	Rim	Core	Rim	Core	Rim
SiO_2	54.23	54.59	52.28	52.55	54.62	55.32	52.68	53.08
TiO_2	0.05	0.04	0.35	0.26	0.02	0.02	0.31	0.21
Al_2O_3	1.83	1.28	3.96	3.42	1.71	1.28	4.56	4.54
Cr_2O_3	0.13	0.10	0.38	0.39	0.15	0.12	0.54	0.60
FeO	14.44	14.19	5.87	5.43	12.58	12.52	4.95	4.45
MnO	0.21	0.20	0.10	0.10	0.14	0.12	0.07	0.04
NiO	0.03	0.03	0.03	0.03	0.13	0.12	0.06	0.06
MgO	28.49	29.06	13.99	14.32	30.43	30.78	13.99	13.87
CaO	0.26	0.19	21.11	21.56	0.19	0.14	20.39	20.48
Na_2O	0.03	0.01	2.23	2.05	0.03	0.03	2.41	2.70
Total	99.69	99.68	100.31	100.11	100.00	100.44	99.96	100.02

Table 4.2: Core and rim compositions of orthopyroxene and clinopyroxene from two garnet websterites.

4.4. Eclogites

Garnet and clinopyroxene from the Abrahamskraal eclogites display compositional ranges which, although showing a large degree of overlap with websteritic minerals, form distinctive fields on CMF (Fig. 4.12) and AFM (Fig. 4.13) diagrams. Although several crossing tie-lines occur on the CMF diagram, the slopes of the tie-lines appear to vary as a functon of the Fe/Mg ratio of coexisting phases, suggesting that the minerals maintained approximately consistent partitioning of Fe, Mg and Ca. On the AFM diagram however (Fig. 4.12), a different situation is evident. Coexisting minerals on this diagram define two distinct groups showing significantly different

partitioning ratios. In one group (229,269,270) relatively Mg-rich garnet coexists with Al-poor clinopyroxene, while in the other (178,268,271, 272,275,284), relatively Fe-rich garnet coexists with Al-rich clinopyroxene. Within each group partitioning is reasonably consistent (parallel tie-lines), although some of the tie-lines do intersect at low angles. The only consistent petrographic difference between the two groups

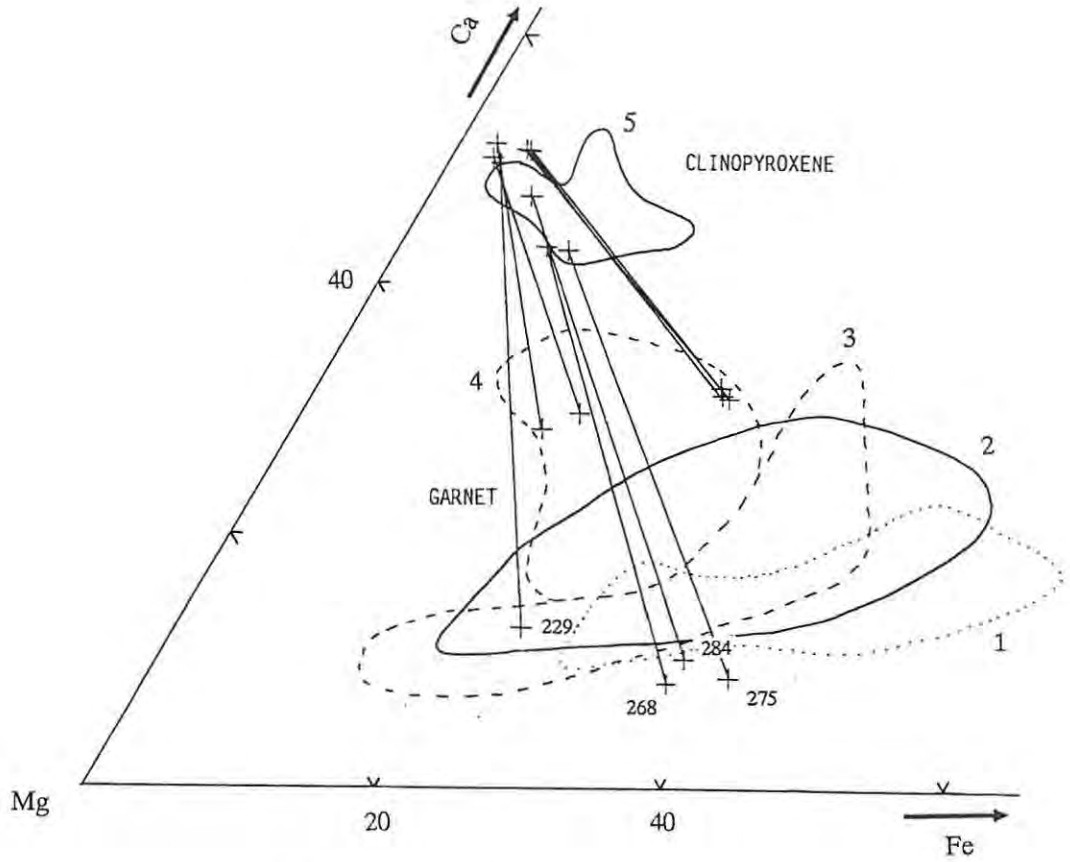

Garnet Fields

1 - Lower-crustal eclogites - N. Lesotho (Griffin *et.al.*, 1979)
2 - Lower-crustal eclogites - Central Cape Province (Robey, 1981)
3 - Eclogites - main trend Roberts Victor (Hatton, 1978)
4 - Ca-rich eclogites - Roberts Victor (Hatton, 1978)

Clinopyroxene Field

5 - Lower-crustal eclogites - Central Cape Province (Robey, 1981)

Fig. 4.12:Portion of a CMF ternary diagram showing the compositions of coexisting garnet and clinopyroxene in the Abrahamskraal eclogite xenoliths. Also shown are the compositional fields of eclogitic minerals from various other localities. Sample numbers are given for the Ca-poor garnets.

is that the samples with Al-poor clinopyroxene are distinctly richer in garnet than the others (Fig. 4.14).

In Fig. 4.12 the compositions of eclogitic minerals from Abrahamskraal are compared to those from the extensively documented Roberts Victor (RV) suite, as well as from the kimberlites of northern Lesotho, and of the central Cape Province. The Roberts Victor eclogites are presumed to be of mantle origin (e.g. Dawson, 1980) while those from northern Lesotho and the central Cape Province are believed to originate in the lower crust (Griffin *et.al.*, 1979; Robey, 1981).

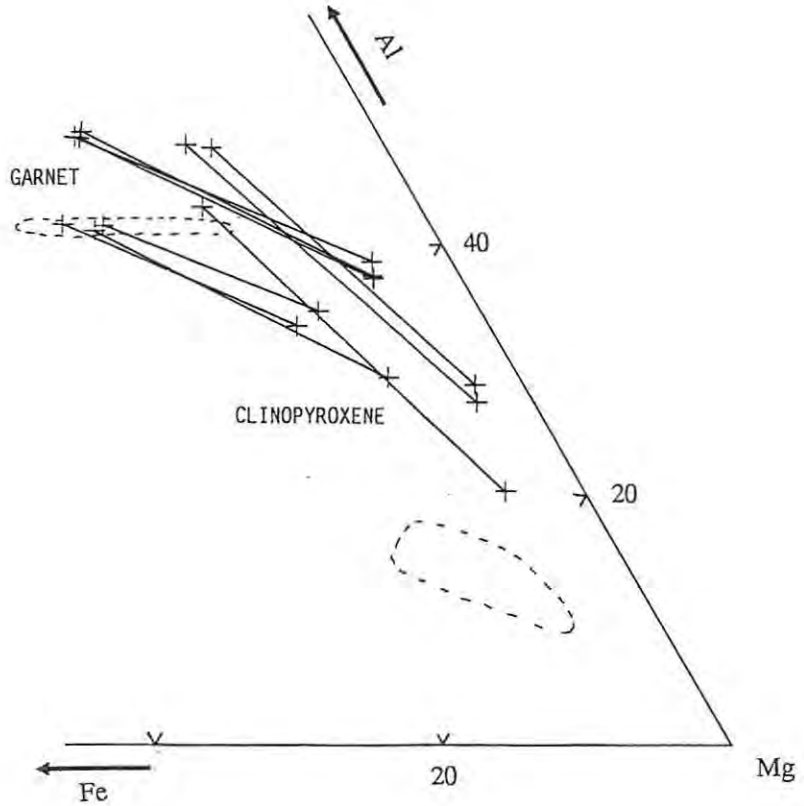

Fig. 4.13: Portion of an AFM diagram showing the composition of coexisting garnet and clinopyroxene in the Abrahamskraal eclogite xenoliths. Also shown are the compositional fields for websteritic garnet and clinopyroxene from Abrahamskraal (dashed lines).

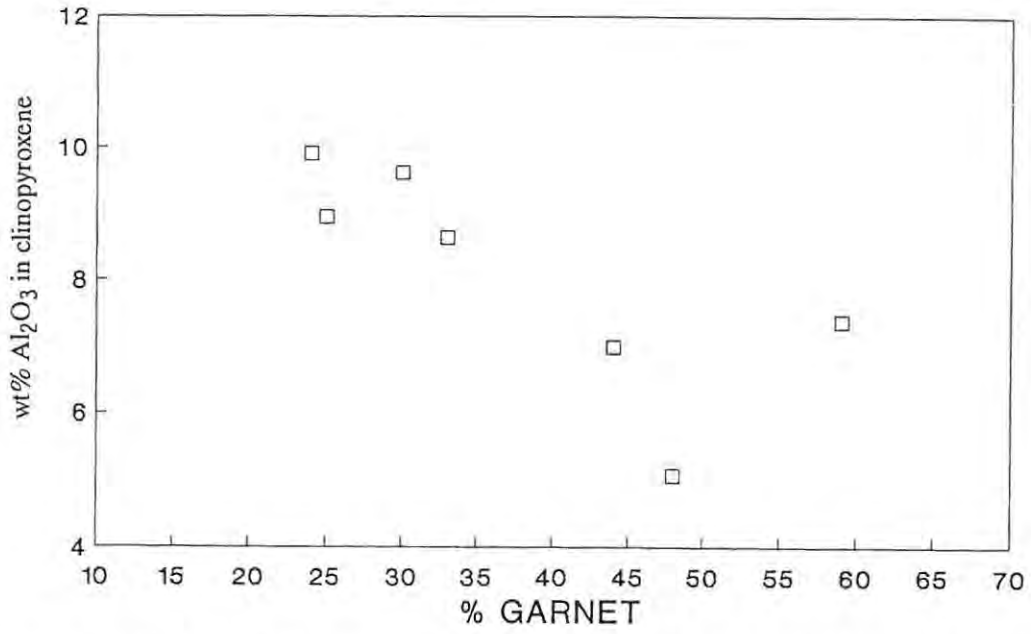

Fig. 4.14: Plot of Al in clinopyroxene vs % garnet in the Abrahamskraal eclogites.

4.4.1. Garnet

Eclogitic garnets of this study fall into two distinct groups, distinguished by large differences in Ca and Al content (Fig. 4.12 and 4.13). In the low-Ca, low-Al group (3.18 to 4.93 wt% CaO), three of the four garnets fall into group 3 (that of the "common eclogites", Dawson and Stephens, 1975), but appear to be slightly poorer in Ca than the eclogitic garnets from RV, northern Lesotho and the central Cape Province (Fig. 4.12). The fourth low-Ca garnet (229) is significantly more Mg-rich (group 9) than the other three, and falls within the compositional fields of eclogitic garnets from the localities mentioned above. It is interesting to note that the eclogites of presumed lower-crustal origin from the central Cape Province and northern Lesotho are not clearly distinguishable on the basis of the Ca, Mg and Fe content of their garnets, from the mantle-derived eclogites found at Roberts Victor (Fig. 4.12).

The Ca- and Al-rich garnets (11.06 to 11.97 wt% CaO) fall into group 6 of Dawson and Stephen's classification scheme, and plot within the field of garnets from the Roberts Victor Ca-rich eclogites (Fig. 4.12). Dawson and Stephens (1975) note that group 6 garnets are commonly found in kyanite

eclogites. This is not the case for the garnets of this study, none of which coexist with kyanite, and no systematic petrographic differences between the Ca-poor and Ca-rich varieties of eclogite were observed (although both finer-grained eclogites contain Ca-poor garnet).

Both groups (Ca-rich and Ca-poor) of eclogitic garnet from Abrahamskraal show Fe-enrichment trends similar to those displayed by the garnet websterites. However, significant variations in Ca content also occur (not seen in the websterites). In the case of the low-Ca garnets, these do not appear to be correlated with Mg/Mg+Fe variations, while the group 6 garnets show a slight increase in Ca content with decreaseing Mg/Mg+Fe (Fig. 4.12). It should be mentioned however, that the number of samples analysed and plotted is rather small, and hence the trends must be regarded with a certain amount of circumspection. Nevertheless, a similar negative correlation between Ca and Mg/Mg+Fe has been observed in the kyanite-bearing eclogites and granulites of the central Cape Province, while the kyanite-free eclogites from the same region show more "subdued and non-definative Ca-enrichment trends" (Robey, 1981).

Variations in garnet compositions are believed to reflect whole-rock variations. However, garnet groups distinguished on the basis of their Ca and Al content do not coincide with the two groups distinguished on the basis of Fe-Mg partitioning between garnet and clinopyroxene (Fig. 4.13). The reasons for this are not clear.

4.4.2. Clinopyroxene

In terms of the CFM components, the eclogitic clinopyroxenes from Abrahamskraal show much less variation than their coexisting garnets (Fig. 4.12). The distinction between Ca-poor and Ca-rich minerals is not as clear for clinopyroxenes as it is for garnets. Nevertheless the clinopyroxene co-existing with group 3 garnets is distinctly less calcic than that co-existing with Ca-rich garnets. This is not the case for the Ca-rich clinopyroxene in sample 229 however, which coexists with a low-Ca group 9 garnet. Most of the clinopyroxenes of this study plot at the Ca and Mg-rich end of the compcsitional range shown by the eclogitic clinopyroxenes of the central Cape Province kimberlites (Robey, 1981, Fig. 4.12).

On the AFM diagram (Fig. 4.13) it is evident that the Abrahamskraal eclogitic clinopyroxenes show large ranges in Al content. These appear to be correlated with the Mg/Mg+Fe ratio of coexisting garnet rather than their Al content. The Al_2O_3 contents of the clinopyroxenes range from 5.07 to 9.90 wt%. Their Na content is high (2.58 to 6.08 wt% Na_2O), in accordance with eclogitic pyroxenes worldwide (White, 1964), and is indicative of their high-pressure origin. On a plot of Na vs Al+Cr two groups can be distinguished (Fig. 4.15). Clinopyroxenes coexisting with Ca- and Al-poor garnet show an approximate 1:1 ratio of Na/Al+Cr, while those coexisting with Ca- and Al-rich garnet have Na/Al+Cr ratios significantly less than 1. The latter indicates excess Al over that incorporated in the jadeite molecule ($(Na,Al)_2SiO_6$), and reflects Al-tschermak substitution ((Ca,Mg,Fe)Si = AlAl) in clinopyroxene.

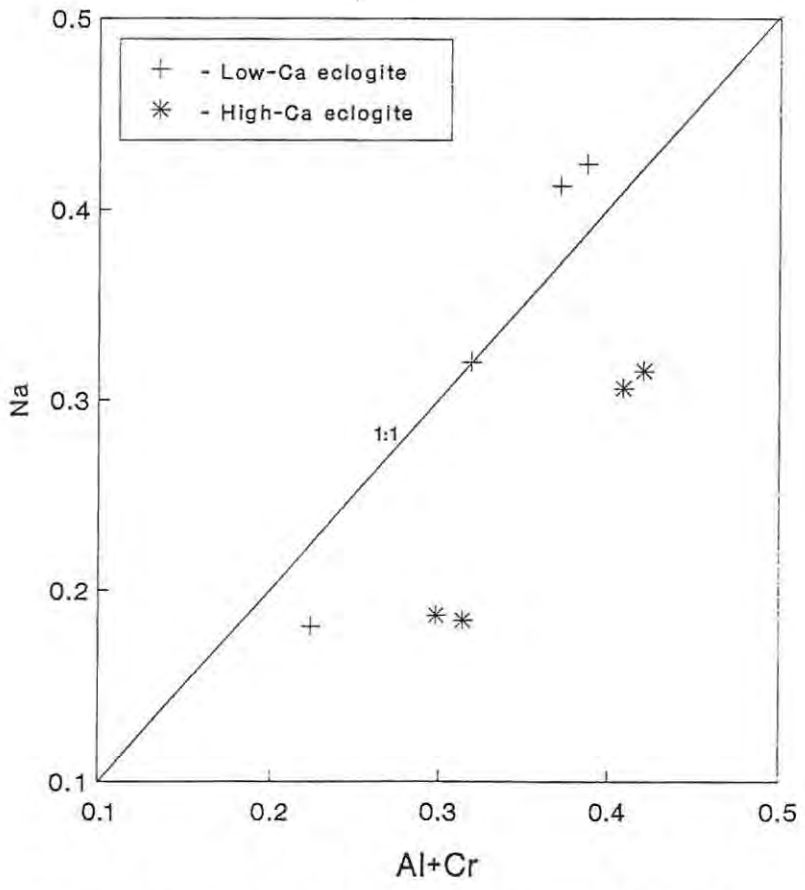

Fig. 4.15: Plot of Na vs Al+Cr in clinopyroxene from the Abrahamskraal eclogite xenoliths. In the low-Ca eclogites clinopyroxene coexists with Ca- and Al-poor garnet, whereas in the high-Ca eclogites the garnet is relatively Ca- and Al-rich.

4.4.3. Zoning

Apart from one sample (229) in which the garnet was zoned to more Fe-rich and Mg-poor rims, no zoning was observed in the eclogites. However, in many samples the primary Na-rich clinopyroxene is rimmed by a narrow band of Na-poor clinopyroxene, which is usually in optical continuity with the former (Table 4.3). As mentioned in section 3.5. this is probably due to the beakdown of the primary clinopyroxene as it decompresses in the rising kimberlite magma.

	CLINOPYROXENE	
	Primary	Secondary
SiO_2	54.86	50.26
TiO_2	0.20	0.28
Al_2O_3	8.94	7.40
Cr_2O_3	0.29	0.32
FeO	4.23	6.67
MnO	0.07	0.14
NiO	0.01	0.02
MgO	10.90	15.11
CaO	13.97	16.97
Na_2O	6.08	2.26
Total	99.56	99.43

Table 4.3: Composition of primary and secondary (rims) clinopyroxene in an eclogite (268).

5. THERMOBAROMETRY

5.1. Introduction

The application of thermobarometry to mantle xenoliths has been the subject of much research and debate over the last two decades. Since the pioneering work of Boyd (1973) who applied experimental calibrations of pyroxene equilibria (Davis and Boyd, 1966; MacGregor, 1974) to xenoliths from the northern Lesotho kimberlites, a plethora of mineralogical thermometers and barometers, based on a number of different mineral equilibria, have been published. The large number of thermometers and barometers available, the large errors associated with most of the calibrations, and disagreement amongst researchers as to which are the most reliable methods, makes the choice of a suitable thermobarometer a difficult task. Certain authors have attempted to resolve this problem by making comparative reviews of a large number of available thermometers and barometers (Carswell and Griffin, 1981; Carswell and Gibb, 1980, 1987a and b; Finnerty and Boyd, 1984, 1987; Finnerty, 1989). Unfortunately, the results of these comparisons depend on the criteria used for judging the thermobarometers.

Finnerty and Boyd (1984, 1987) have assessed thermobarometer pairs on the basis of their ability to yield temperature and pressure estimates (for xenoliths from the northern Lesotho kimberlites) in agreement with the diamond-graphite transition as determined by Kennedy and Kennedy (1976), and the phlogopite breakdown curve (Eggler and Wendlandt, 1979). This approach suffers from the problem that very few xenoliths actually contain graphite or diamond. In the northern Lesotho xenolith suite only one graphite- and one diamond-bearing garnet occur. The method is also very susceptible to small errors in the calibration of the diamond-graphite transition and the phlogopite breakdown curve. An additional problem is that thermometers and barometers cannot be tested independantly (all barometers are temperature dependant and most thermometers are pressure dependant), and hence it is difficult to determine sources of error.

Carswell and Gibb (1987a) have *independantly* tested 12 different barometer, and 20 different thermometer formulations against experimentally calibrated mineral composition data for "natural" multi-component garnet

lherzolite assemblages. The accuracy of results obtained using this approach is subject to uncertainties in the experimental data, although these have been minimised by carefull choice of test data. Nevertheless, it would appear to be a more rigorous means of testing individual thermometers and barometers than that used by Finnerty and Boyd (1984, 1987). Choice of thermobarometers for application to the xenoliths of this study is therefore based primarily on the recommendations of Carswell and Gibb (1987a). The thermometers and barometers used for this study are briefly described in Table 5.1, and the relevant equations are given in Appendix 4.

REFERENCE	DESCRIPTION
Wells, 1977	Semi-empirical formulation of the two-pyroxene solvus thermometer. No pressure correction term.
Finnerty and Boyd, 1987	Empirical fit to the diopside-enstatite miscibility gap. Incorporates pressure correction term.
Harley, 1984	Thermometer based on Fe-Mg exchange between garnet and orthopyroxene. Formulation based on experimental data in FMAS (FeO-MgO-Al_2O_3-SiO_2) and CFMAS (FMAS + CaO) systems.
O'Neill and Wood, 1979, 1980	Thermometer based on Fe-Mg exchange between garnet and olivine. Based on experimental data for the FMAS and CFMAS systems.
Ellis and Green, 1979	Thermometer based on Fe-Mg exchange between garnet and clinopyroxene. Based on experiments in the CFMAS system.
Nickel and Green, 1985	Empirical calibration of the barometer based on the Al content of orthopyroxene in equilibrium with garnet. Formulation based on experimental data for CMAS and SMACCr (includes Cr_2O_3), with Fe correction based on thermodynamic modelling.
Finnerty and Boyd, 1984	Formulation of orthopyroxene barometer based on the experimental data of MacGregor (1974) in the MAS system.

Table 5.1.: Brief descriptions of thermometers and barometers applied to the Abrahamskraal xenoliths. The equations used for calculating pressure and temperature are given in Appendix 4.

5.2. Barometry

Most barometer formulations applicable to mantle xenoliths are based on the Al-content of orthopyroxene coexisting with garnet. Others include: the barometer of O'Neill (1981), which is based on the equilibrium between spinel lherzolite and garnet lherzolite; formulations based on the Ca content of olivines (e.g. Finnerty and Boyd, 1978; Adams and Bishop, 1982); and those based on the Cr content of orthopyroxene coexisting with garnet (e.g. Nickel, 1989). The latter two barometers are still in a relatively crude state of calibration, and therefore cannot be expected to yield reliable pressure estimates. The O'Neill (1981) barometer may provide a reliable independant method for pressure estimation, but is only applicable to the rare five-phase assemblage garnet-spinel-olivine-orthopyroxene-clinopyroxene. Of the available formulations of the Al-in-orthopyroxene barometer, those of Nickel and Green (1985; recommended by Carswell and Gibb, 1987a) and Finnerty and Boyd (1984) have been applied to the Abrahamskraal xenoliths (see Table 5.1 and Appendix 4 for details).

All mineralogical mantle barometers (with the exception of O'Neill, 1981) are to a large extent temperature dependant. Therefore in order to calculate pressures, they need to be combined with a thermometer (either by simultaneous solution or by iterative procedures). For the purposes of comparison, the chosen barometers were combined with a garnet-orthopyroxene thermometer (Harley, 1984) as this is applicable to the widest range of rock types. Pressures and temperatures calculated using the two combinations are given in Table 5.2. It is evident that the Finnerty and Boyd (1984) formulation yields pressure estimates which are generally between 1 and 4 kb greater than those calculated using Nickel and Green (1985). Apart from a slight relative shift in pressures, the P-T arrays calculated using the two barometers (Fig. 5.1a and b) are very similar. In the light of these similarities, as well as uncertainties associated with each barometer, it is not possible to gauge which is the more accurate of the two barometers. For the purposes of evaluation of thermometers (see next section), and the construction of a geotherm for Abrahamskraal, the formulation of Nickel and Green has been used.

	PRESSURE(kb)		TEMPERATURE(^{o}C)	
SAMPLE	NG85	FB84	NG85	FB84
Peridotites				
142*	34.9	39.4	950.8	977.1
156	32.2	33.9	852.2	862.2
143	34.4	34.9	880.7	883.5
144	36.5	42.2	984.0	1018.6
145	40.8	42.9	997.8	1010.6
149	41.3	44.0	992.5	1008.7
154	37.5	39.6	951.6	963.8
217	31.9	31.8	851.2	850.6
Pyroxenites				
72	11.6	13.8	686.6	698.4
197	17.2	21.3	708.9	730.1
256*	14.4	16.5	673.0	683.9
257*	12.8	16.3	683.3	701.8
259	21.5	24.7	732.0	748.7
264	11.8	13.9	701.6	712.8
274	30.6	30.9	819.1	820.8
280*	12.4	14.8	650.9	663.1
283	13.4	15.8	708.7	721.4
147	20.6	26.1	711.1	739.4
187	21.1	25.0	707.6	726.9
262	18.8	20.3	711.4	718.7

Table 5.2: Pressures and temperatures for the Abrahamskraal xenoliths calculated using the two chosen barometers combined with the Harley (1984) thermometer. NG85 - Nickel and Green (1985); FB84 - Finnerty and Boyd (1984). Asterisks next to sample numbers indicate that inhomogeneities were observed in these samples (i.e. compositional variations between cores of different grains exceed analytical error).

5.3. Thermometry

In contrast to barometry methods, there are a relatively large number of mineral equilibria suitable for calibration as thermometers applicable to mantle xenoliths. However application of these thermometers to the Abrahamskraal xenolith suite is unfortunately limited by the lack of suitable mineral assemblages in many of the rocks.

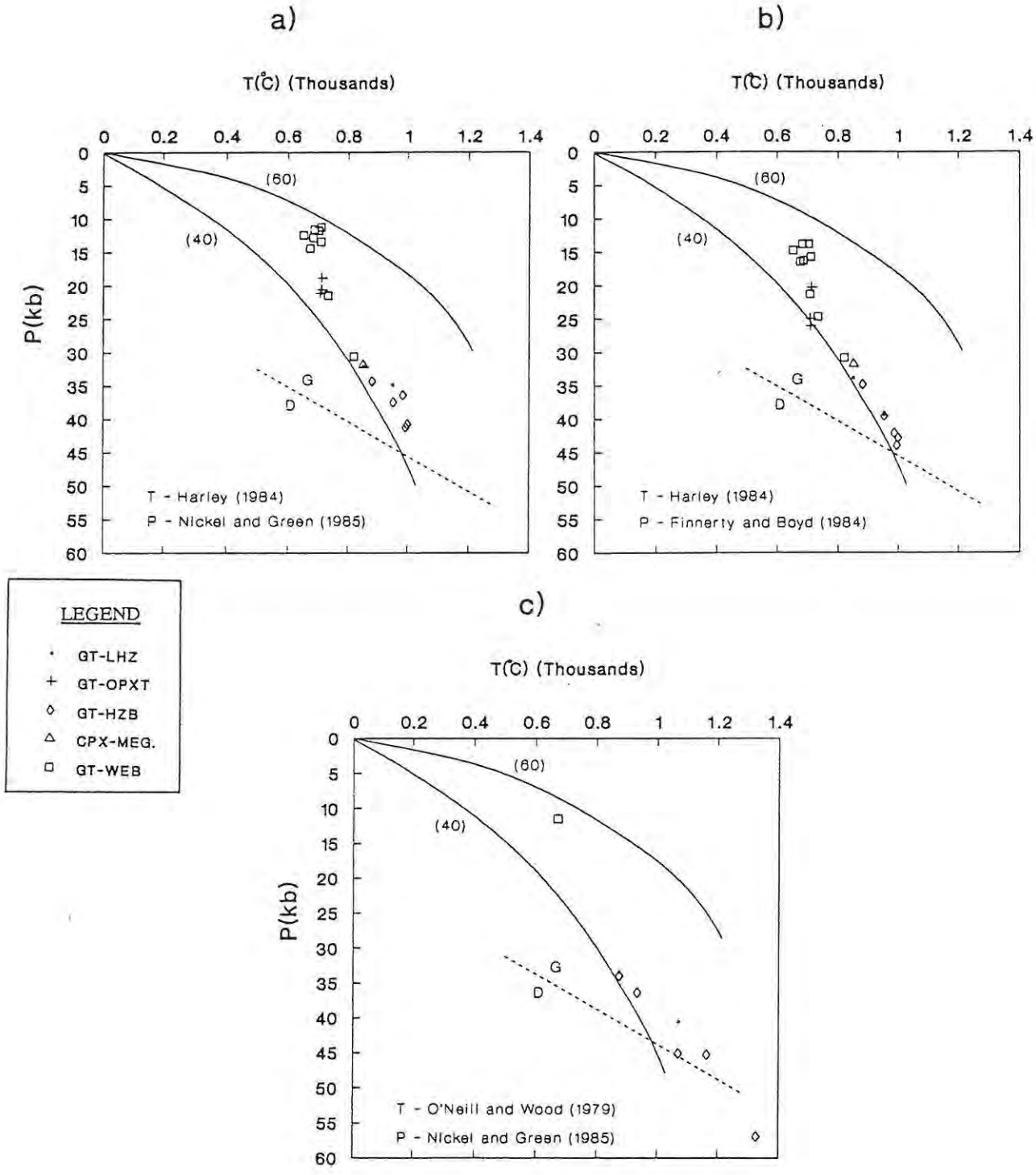

Fig. 5.1: Pressure-temperature (P-T) arrays for the Abrahamskraal xenoliths. P-T points were calculated using different thermobarometer combinations (see Table 5.1. for brief descriptions of thermometers and barometers). Thermometers (T) and barometers (P) used for each array are given in the bottom left corner of each plot. Also shown: calculated continental geotherms (——) for surface heat flows of 40 and 60 mWm^{-2} respectively (Pollack and Chapman, 1977); diamond-graphite transition (----- ; Kennedy and Kennedy, 1976). D - diamond; G - graphite.

Two-pyroxene thermometry, that most commonly used for mantle peridotites, is unsuitable for application to the Abrahamskraal suite for three reasons:

1) Only two clinopyroxene-bearing peridotites (garnet lherzolites) occur in the xenolith suite, making it impossible to construct a well-constrained geotherm, and very difficult to evaluate the accuracy of the calculated pressures and temperatures.

2) It is not entirely clear whether the clinopyroxene in the garnet lherzolites is of primary or metasomatic origin (see sections 3.2 and 4.2). Hence there is uncertainty about the significance of pressures and temperatures calculated using clinopyroxene compositions.

3) Carswell and Griffin (1981) in their study of garnet granulite and garnet websterite xenoliths from northern Lesotho, concluded that at the relatively low temperatures of equilibration of these xenoliths (<800°C), two-pyroxene thermometers are insensitive and unreliable. Application of two recommended two-pyroxene thermometers (Wells, 1977; Finnerty and Boyd, 1987; see Table 5.1 and Appendix 4) indicates that this is also the case for the Abrahamskraal garnet websterites. This is probably due to the very low (in some cases zero) solubility of enstatite in clinopyroxene from these rocks, which results in unrealistic and in some cases meaningless calculated temperature values.

Application of thermometers based on Fe-Mg exchange between garnet and clinopyroxene is subject to the same problems as outlined in 1) and 2) above. In addition, successful application of these thermometers is dependant on accurate estimations of the Fe^{2+} content of garnet and clinopyroxene (Carswell and Griffin, 1981). Therefore, if significant amounts of Fe^{3+} are present, the use of microprobe data which does not distinguish FeO and Fe_2O_3, can result in large errors. Methods of calculation of Fe^{3+} from microprobe data (e.g. Ryburn *et.al.* , 1975; Droop, 1987) are susceptable to relatively small analytical errors (particularly for SiO_2), and did not give realistic results when applied to clinopyroxenes from the Abrahamskraal xenolith suite. Unfortunately, garnet-clinopyroxene thermometers provide the only means for estimation of

temperatures for eclogite xenoliths. Hence despite the problems outlined above, the Ellis and Green (1979) garnet-clinopyroxene thermometer was applied to the Abrahamskraal eclogites (see section 6.3).

As mentioned in the previous section, thermometers based on Fe-Mg exchange between garnet and orthopyroxene are particularly suitable for application to the Abrahamskraal xenoliths, due to the wide range of rock-types to which they can be applied. Application of one such thermometer (Harley, 1984) results in temperature and pressure estimates for the peridotites which appear to lie along a realistic geothermal gradient (they would be expected to lie along a conductive geothermal gradient), and which do not contradict current understanding of phase relations and conditions in the subcontinental upper mantle.

Apart from the garnet-orthopyroxene thermometer, the only other method which can be applied to all of the peridotite xenoliths is that based on Fe-Mg exchange between garnet and olivine. Results obtained using the O'Neill and Wood (1979, 1980) garnet-olivine thermometer are given in Table 5.3. Temperatures calculated using this method are significantly higher

	PRESSURES(kb)		TEMPERATURES(^{o}C)	
	HA84	OW80	HA84	OW80
Peridotites				
142*	34.9	40.6	950.8	1069.6
156	32.2	33.4	852.2	875.3
143	34.4	34.0	880.7	873.4
144	36.5	45.3	984.0	1161.6
145	40.8	57.0	997.8	1325.3
149	41.3	45.1	992.5	1068.4
154	37.5	36.5	951.6	932.3
Websterite				
283	13.5	11.7	708.7	670.0

Table 5.3.: Temperatures and pressures for the Abrahamskraal xenoliths calculated using two different thermometers combined with the Nickel and Green (1985) barometer. HA84 - Harley (1984): OW80 - O'Neill and Wood (1979, 1980). Asterisks next to sample numbers indicate that inhomogeneities were observed in these samples. (i.e. compositional variations between cores of different grains exceed analytical error).

(for all but one of the xenoliths) than those obtained using the garnet-orthopyroxene thermometer of Harley (1984). In addition the P-T array produced using the O'Neill and Wood thermometer (Fig. 5.1c) shows a much wider spread of points, with one xenolith plotting within the diamond stability field. It is considered unlikely that the peridotites were sampled over such a large depth range, and particularly from the great depth indicated by the high-pressure xenolith. Thus it is suggested that the O'Neill and Wood (1979,1980) thermometer overestimates temperatures (resulting in overestimated pressures) for the Abrahamskraal xenolith suite.

6. THE ABRAHAMSKRAAL GEOTHERM

Discussion on the Abrahamskraal geotherm is based on the P-T array obtained using the Harley (1984) thermometer combined with the Nickel and Green (1985) barometer, as outlined in the previous section (Fig. 6.1). A brief outline of the principles of geotherm construction is given in section 1.2. The array is clearly separable into two portions defined primarily by the peridotites and pyroxenites respectively. These are discussed below under the headings peridotite "geotherm" and pyroxenite "geotherm".

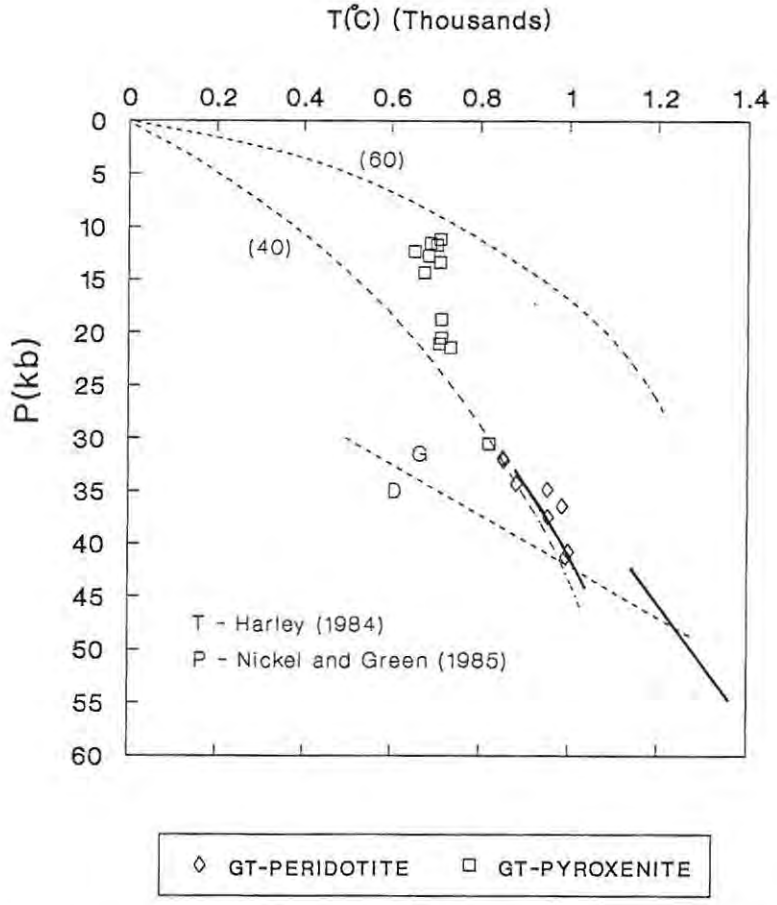

Fig. 6.1: Comparison of the Abrahamskraal P-T array with a cratonic geotherm for northern Lesotho (——; Carswell and Gibb, 1987b). The low- and high-temperature portions of the Lesotho geotherm are defined by coarse and porphyroclastic xenoliths respectively. Reference curves as for Fig. 5.1.

6.1. The Peridotite "Geotherm"

The garnet peridotite xenoliths define the lower portion of the P-T array shown in Fig. 6.1. Only two other xenoliths, a garnet websterite and the clinopyroxene megacryst, lie along the same trend, the rest of the pyroxenites plotting at significantly lower pressures.

Although zoning effects have been observed in most of the peridotite xenoliths, these are believed to be the result of late stage alteration of the grain rims rather than variations in the P-T conditions. This is supported by:

1) The erratic nature of the zoning. Large variations in zoning effects occur from one point to another along the margins of individual grains. In orthopyroxene grains these variations are often strongly related to the proximity of late-stage Al-spinel found in kelyphite rims around garnet. This suggests that formation of the zoning post-dates entrainment of the xenolith in the kimberlite, and is probably related to the alteration processes which formed the kelyphite and secondary spinel.

2) Pressures and temperatures calculated using rim compositions (Fig. 6.2) show no systematic relationship to core pressures and temperatures. Thus zoning is clearly not the result of rim reequilibration due to changing P-T conditions prior to kimberlite eruption.

With the possible exception of sample 142, the cores of mineral grains in the peridotites are homogenous (no significant intergrain variations) and are therefore believed to have been in equilibrium at the ambient P-T conditions prior to kimberlite eruption (Boyd and Finger, 1975). Thus the lower portion of the P-T array can be taken to represent the geothermal gradient (geotherm) at approximately 81 Ma.

In order to make comparisons between geotherms for different areas, it is necessary that the same thermobarometer combination be used for all pressure-temperature calculations. In this way, possible errors in the absolute position of each geotherm will not affect the *relative* positions of the geotherms, which can therefore be taken to reflect real *differences* in the ambient conditions at which the xenoliths equilibrated.

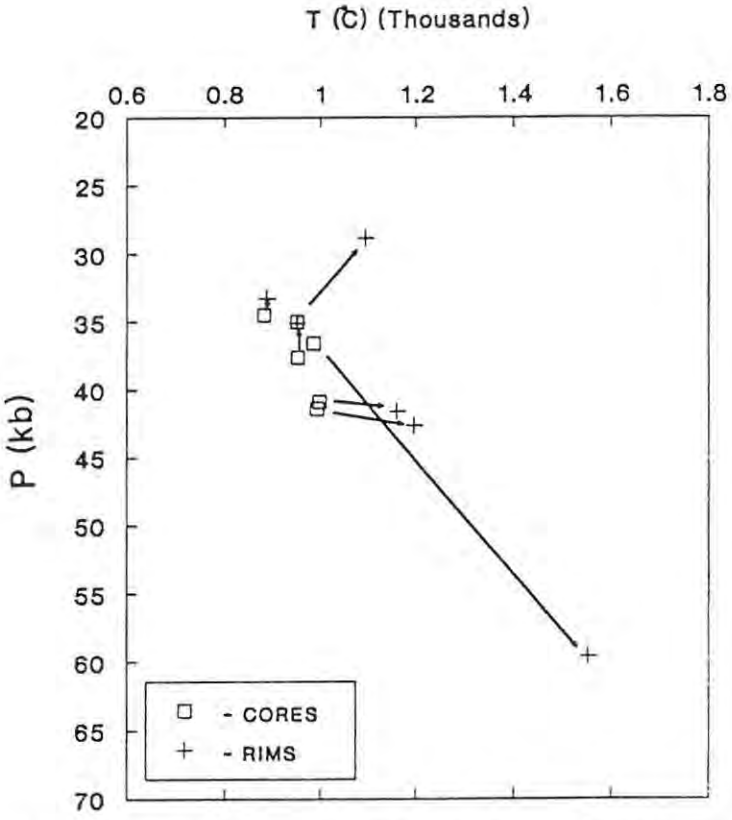

Fig. 6.2: Apparent pressure-temperature points for core and rim compositions in the peridotite xenoliths. Arrows point in the direction of the rims.

In Fig. 6.1 the Abrahamskraal P-T array is shown together with the geotherm for northern Lesotho (Carswell and Gibb, 1987b), traditionally regarded as the typical cool cratonic geotherm. The low-pressure portion of the Lesotho geotherm is defined by coarse garnet peridotites, while the high-pressure and temperature "inflected" portion is defined by porphyroclastic xenoliths. Calculated continental geotherms based on surface heat flows of 40 and 60 mWm^{-2} respectively (Pollack and Chapman, 1977), are also shown. There is a large degree of overlap between the Abrahamskraal geotherm (defined by the peridotites) and that defined by the northern Lesotho coarse peridotites, the latter extending to slightly greater depths (~45kb) than the former (41kb). Both geotherms display temperatures which are slightly elevated with respect to the calculated shield geotherm ($40mWm^{-2}$) of Pollack and Chapman (1977). Unlike the northern Lesotho geotherm however, the Abrahamskraal P-T array does not show an "inflection" to higher temperatures at its high-pressure end.

P-T arrays for the off-craton Namibian kimberlites (Hanaus and Louwrencia; Mitchell, 1984) are shown in Fig. 6.2, together with curves fitted (by eye) to the Abrahamskraal array. The Namibian P-T points do not fall on a well defined geotherm and it is clear that several of the xenoliths reflect temperatures significantly higher than those on the shield geotherm. Nonetheless, the majority of coarse xenoliths plot in the region of the shield geotherm, and although they extend down to greater depths than the

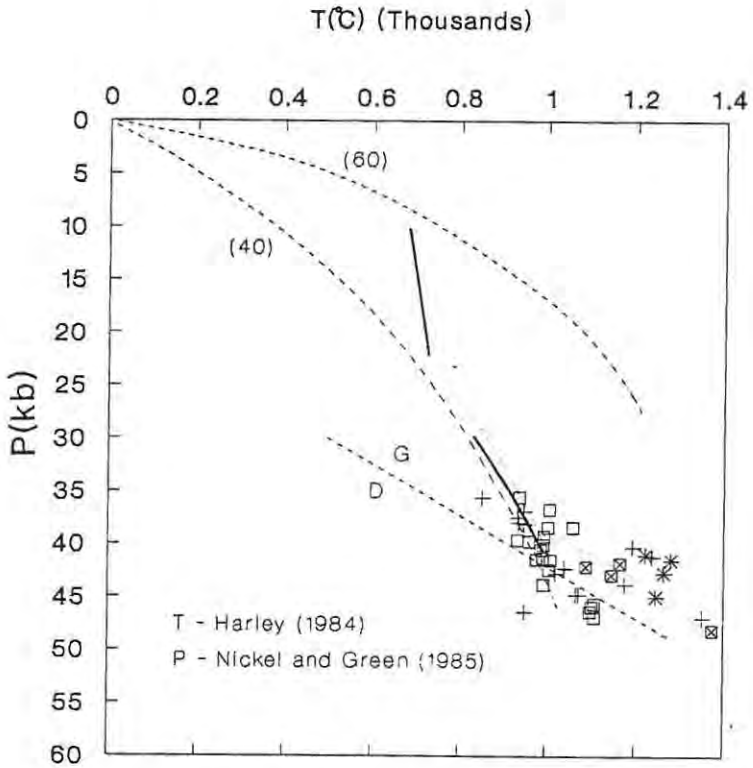

Fig. 6.3: Comparison of the Abrahamskraal geotherm with P-T arrays for the Namibian kimberlites (Hanaus and Louwrencia; Mitchell, 1984). Key: + - Hanaus coarse xenolith; ✳ - Hanaus sheared xenolith; ⊠ - Louwrencia coarse xenolith; □ - Louwrencia sheared xenolith; heavy solid lines - curves fitted by eye to the Abrahamskraal P-T array; light dotted line - Finnerty and Boyd's (1987) geotherm for East Griqualand, thermometer - Finnerty and Boyd (1987), barometer - Finnerty and Boyd (1984); reference curves as for Fig. 5.1.

Abrahamskraal xenoliths, there is a significant overlap between the P-T arrays. The main difference between the Abrahamskraal and Namibian P-T arrays is the absence at Abrahamskraal of high temperature xenoliths. Also shown on Fig.6.2 is the geotherm constructed by Finnerty and Boyd (1987)

for the off-craton East Griqualand kimberlites. Unfortunately the original data was not available, and therefore presssures and temperatures could not be calculated using the chosen thermobarometer of this study. Despite the fact that a different thermobarometer was used, the East Griqualand geotherm shows certain similarities with those from northern Lesotho and Namibia, i.e. it is made up of an upper cooler portion lying relatively close to the shield geotherm and overlapping with the Abrahamskraal array, and a lower portion which is inflected to higher temperatures. The geotherm differs from that of northern Lesotho in that its inflection occurs at lower pressures.

6.2. The Pyroxenite "Geotherm"

The garnet websterite and garnet orthopyroxenite xenoliths define a steep, essentially isothermal trend in P-T space (Fig. 6.1). This trend is not believed to be representative of the ambient conditions at the time of kimberlite eruption. There are three reasons for this:

1) A steepening of the geothermal gradient between 10 and 25 kb implies that a major heat source was present at these depths immediately prior to kimberlite eruption. This is considered highly unlikely as the cool nature of the peridotite geotherm precludes any additional heat flux from depths greater than about 70 km, and there is no petrological (xenoliths) or geophysical evidence suggesting the presence of a highly radiogenic rock mass in the lower crust or uppermost mantle.

2) Most of the pyroxenite xenoliths show zoning effects, and in some cases significant intergrain variations were observed. In contrast to the peridotites, zoning in the pyroxenites shows consistent patterns (see section 4.3.) and does not appear to be related to secondary processes. Apparent pressure-temperature points calculated for core and rim compositions are shown in Fig. 6.4. In all cases the rim compositions reflect higher apparent pressures than the corresponding cores (temperatures are approximately equal), indicating a consistent relationship between zoning and the calculated P-T conditions.

3) The temperatures calculated for the pyroxenites are all below 740°C (excluding the high pressure sample - 274). At these temperatures diffusion rates are extremely slow (Harte *et.al.*, 1981) and it is unlikely that the minerals were able to equilibrate fully.

The above evidence suggests that the pyroxenite "geotherm" is artificial, and results from the application of a mineralogical thermobarometer to disequilibrium mineral compositions. A consideration of the probable thermal history of the pyroxenite xenoliths together with the relative positions (in P-T space) of the isopleths upon which pressure and temperature calculations are based, facilitates modelling of the possible processes which resulted in the pyroxenite P-T array.

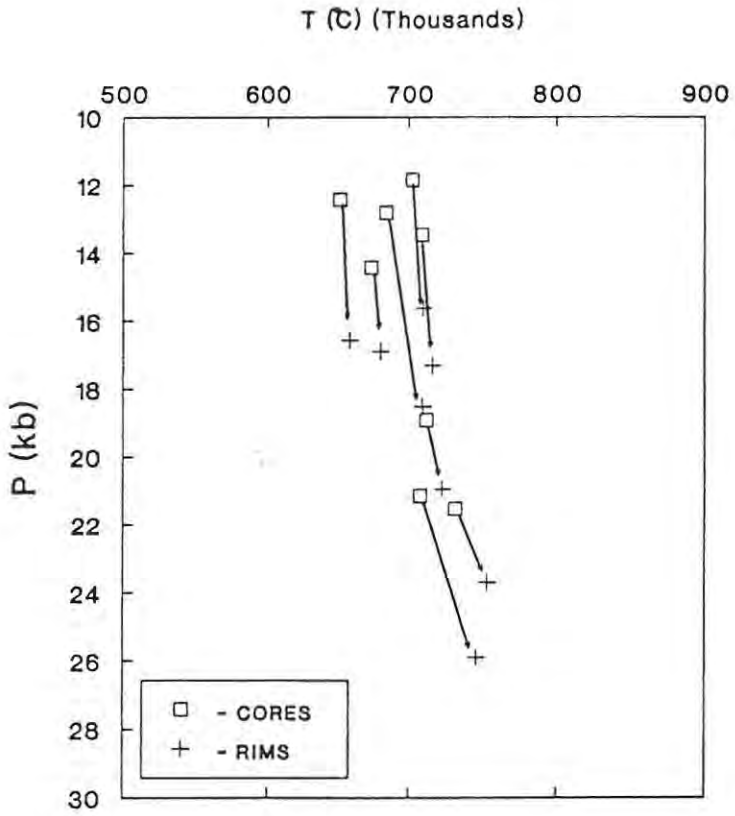

Fig. 6.4: Apparent pressure-temperature points for core and rim compositions in the pyroxenite xenoliths. Arrows point in the direction of the rims.

Textures in the pyroxenite xenoliths provide strong evidence for garnet (± clinopyroxene) exsolution from orthopyroxene (see section 3.4.). This occurs by the reaction:

$$\underbrace{(Mg,Fe)_2Si_2O_6 + (Mg,Fe)Al_2SiO_6}_{\text{orthopyroxene solid solution}} = \underbrace{(Mg,Fe)_3Al_2Si_3O_{12}}_{\text{garnet}} \qquad [1],$$

which has a positive slope in pressure-temperature space. Al_2O_3 isopleths for orthopyroxene involved in reaction [1] are illustrated schematically in Fig. 6.5, together with several possible P-T paths for a rock starting off at some high temperature point X. Theoretically, any P-T path on the high-pressure, low-temperature side of paths X-A and X-D could result in exsolution of garnet from an aluminous orthopyroxene. However significant

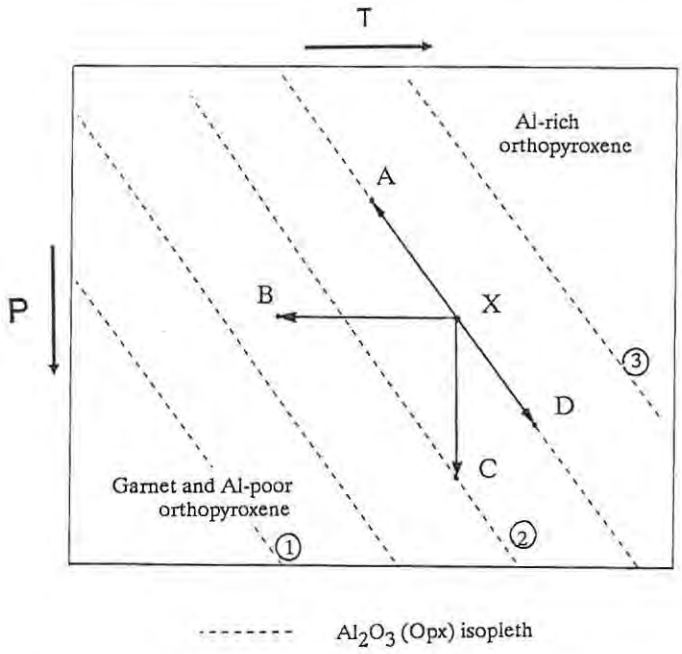

Fig. 6.5: Schematic diagram illustrating possible cooling paths for the pyroxenite xenoliths. The dashed lines are schematic Al_2O_3 isopleths for orthopyroxene involved in the reaction: Al-rich orthopyroxene = garnet + Al-poor orthopyroxene (see reaction [1] in text). Heavy lines, X-A to X-D, are some of the possible P-T paths from a high temperature point "X". Only paths between X-B and X-C are likely to result in significant exsolution of garnet from aluminous orthopyroxene. Ringed numbers indicate approximate Al_2O_3 values in wt%.

exsolution is not likely to occur for paths which are subparallel to the Al_2O_3 isopleths. P-T paths for the pyroxenite xenoliths are therefore likely to lie between X-B and X-C, as large amounts of garnet have been exsolved from orthopyroxene in these rocks. A P-T history involving significant increases in pressure would imply that either deep burial or tectonic thickening took place after emplacement of the pyroxenites (see below and section 7 for possible age of the pyroxenites). In view of the long-term stability of the Namaqua and Kaapvaal crust, this is considered highly unlikely. Thus isobaric (or near-isobaric) cooling (X-B) is believed to be the most likely path followed by the pyroxenites after their emplacement at high temperatures into the upper mantle or lower crust.

Kd_{Gt-Opx} isopleths (lines of constant Kd_{Gt-Opx} in P-T space) for the garnet-orthopyroxene Fe-Mg exchange reaction (Harley, 1984), and Al_2O_3 isopleths for orthopyroxene coexisting with garnet (MacGregor, 1974), are plotted on Fig. 6.6, along with the Abrahamskraal P-T array. Although there are other parameters involved, these "isopleths" are the main criteria upon which the garnet-orthopyroxene thermometer and Al-in-orthopyroxene barometer are based. Thus in a crude way one can establish pressures and temperatures by finding the intersection of two isopleths representing the Kd_{Gt-Opx} and Al_2O_3 content (in orthopyroxene) of coexisting garnet and orthopyroxene. If equilibrium is maintained with respect to all elements in both phases, then the pressures and temperatures obtained from the isopleth intersections should reflect the conditions of equilibration of the xenoliths. However, with decreasing temperatures diffusion slows down and eventually stops, resulting in a "freezing in" of compositions which may not reflect the later parts of the xenoliths cooling history. Diffusion rates differ for the variuos elements. Therefore one would not expect Fe-Mg exchange between garnet and orthopyroxene to cease at the same temperature as the reaction controlling the Al_2O_3 content of orthopyroxene (reaction [1] above). The pyroxenite P-T array obtained using the chosen thermobarometer will depend on the original depth and temperature of emplacement, the ambient conditions in the surrounding mantle or crust, and the relative blocking temperatures (temperature at which diffusion ceases) for Fe, Mg and Al diffusion.

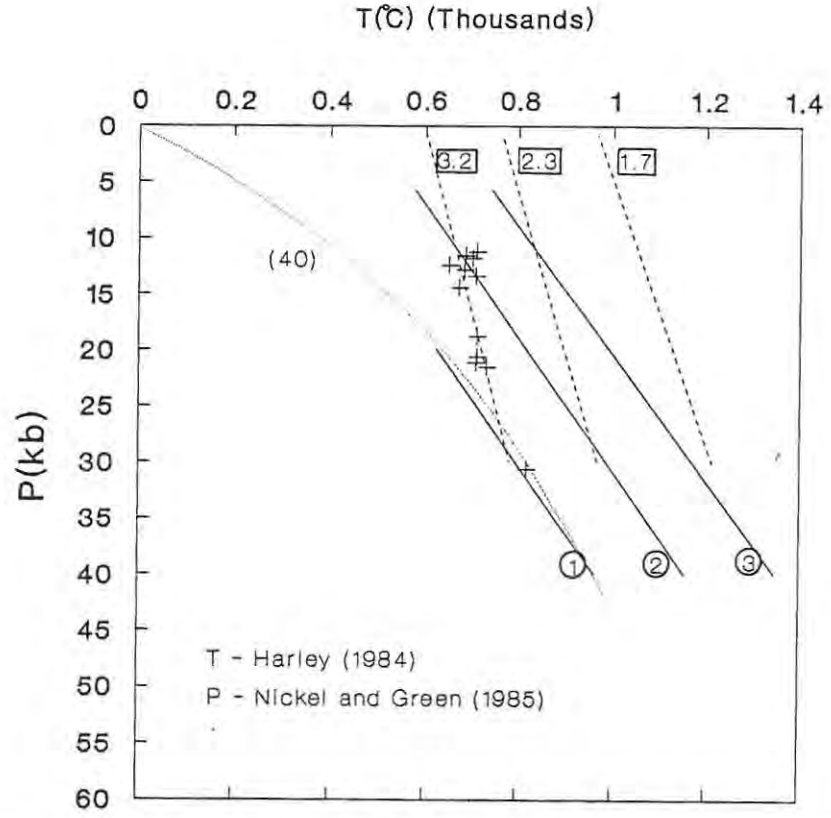

Fig. 6.6:Pressure-temperature diagram showing the pyroxenite P-T array together with Kd_{Gt-Opx} isopleths (dashed lines; Harley, 1984), and orthopyroxene Al_2O_3 isopleths (solid lines; MacGregor, 1974). Also shown is the shield geotherm (dotted line) of Pollack and Chapman (1977). Encircled numbers are Al_2O_3 wt% values, and numbers in boxes are Kd_{Gt-Opx} values.

Assuming an isobaric cooling history, the P-T array defined by the pyroxenites can be generated in a number of ways, which are to a large extent dependant on the original depths of emplacement of the pyroxenites. Two models for pyroxenite emplacement are described below.

1) The pyroxenites were emplaced over a range of pressures (Fig. 6.7):

Isobaric cooling and reequilibration would increase the Kd_{Gt-Opx} and decrease the Al_2O_3 content of orthopyroxene. This would continue until either the ambient geotherm is intersected (e.g. high-pressure xenolith, Fig. 6.6), or diffusion of Fe-Mg and/or Al is blocked. From this point three apparent P-T paths are possible.

a) If Al diffusion is blocked at higher temperatures than Fe and Mg diffusion, further cooling and Fe-Mg reequilibration would drive the

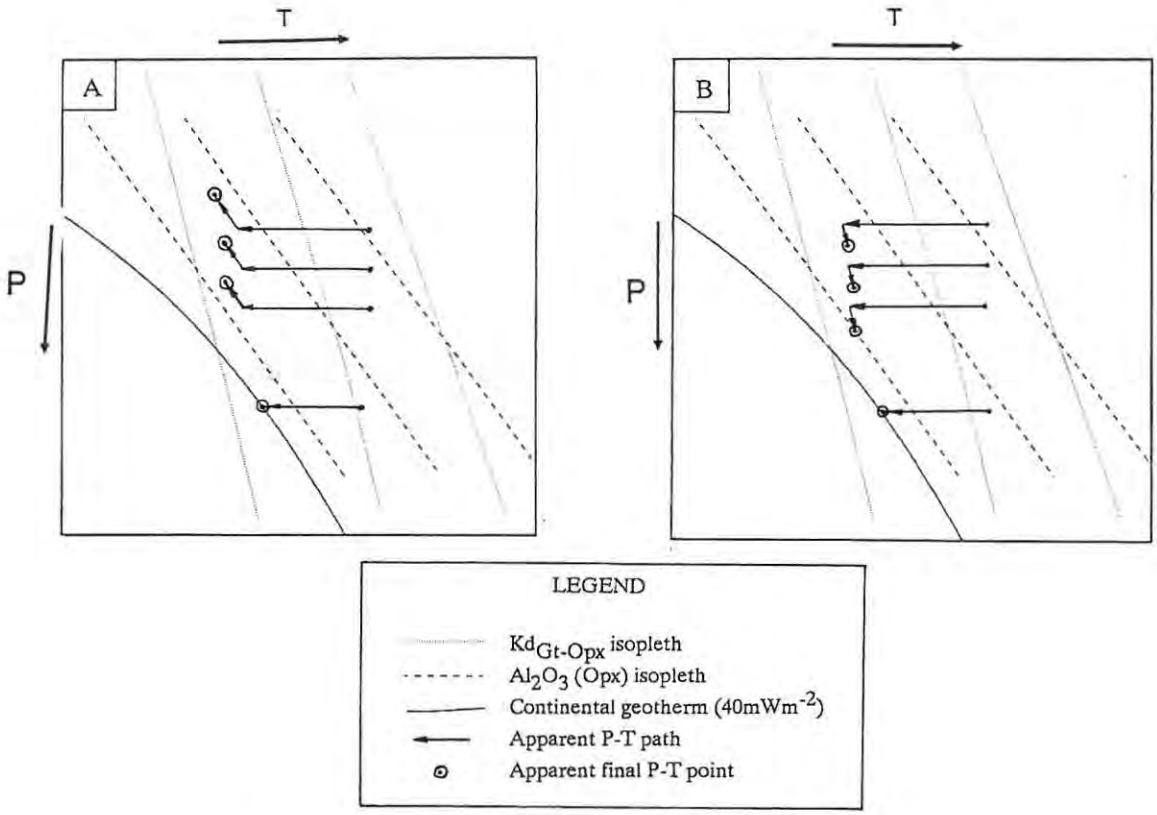

Fig. 6.7: Schematic diagram illustrating possible apparent P-T paths for pyroxenites emplaced over a wide range of pressures. In both a) and b) isobaric cooling causes increased Kd_{Gt-Opx} and decreased Al_2O_3 values in coexisting garnet and orthopyroxene. In a) Al diffusion is blocked at higher temperatures than Fe and Mg diffusion. Further cooling drives apparent P-T points along Al_2O_3 isopleths. In b) Fe and Mg diffusion is blocked at higher temperatures than Al diffusion. Further cooling drives apparent P-T points along Kd_{Gt-Opx} isopleths. In both cases the final P-T array is represented by the ringed points.

apparent pressure-temperature points along Al_2O_3 isopleths to higher Kd_{Gt-Opx} values, i.e. to lower apparent pressures (Fig. 6.7a). b) If on the other hand Fe or Mg diffusion is blocked at higher temperatures, further cooling drives apparent P-T points along Kd_{Gt-Opx} isopleths to lower Al_2O_3 values, i.e. to higher apparent pressures (Fig. 6.7b).

c) If Fe, Mg and Al diffusion are blocked at the same temperature, an isothermal P-T array will be generated. This array will reflect true pressures of emplacement and the blocking temperature for diffusion.

A consideration of the zoning patterns in the pyroxenites enables one to determine which of the above paths is more realistic. It can be seen from Fig. 6.8 that path a) should result in rim compositions which plot at higher pressures than their cores, while path b) results in the opposite. For path c) rim compositions would reflect the true cooling path of the pyroxenites, i.e. they would give lower temperatures than the cores, but pressures would be essentially the same. Thus the zoning in the pyroxenites

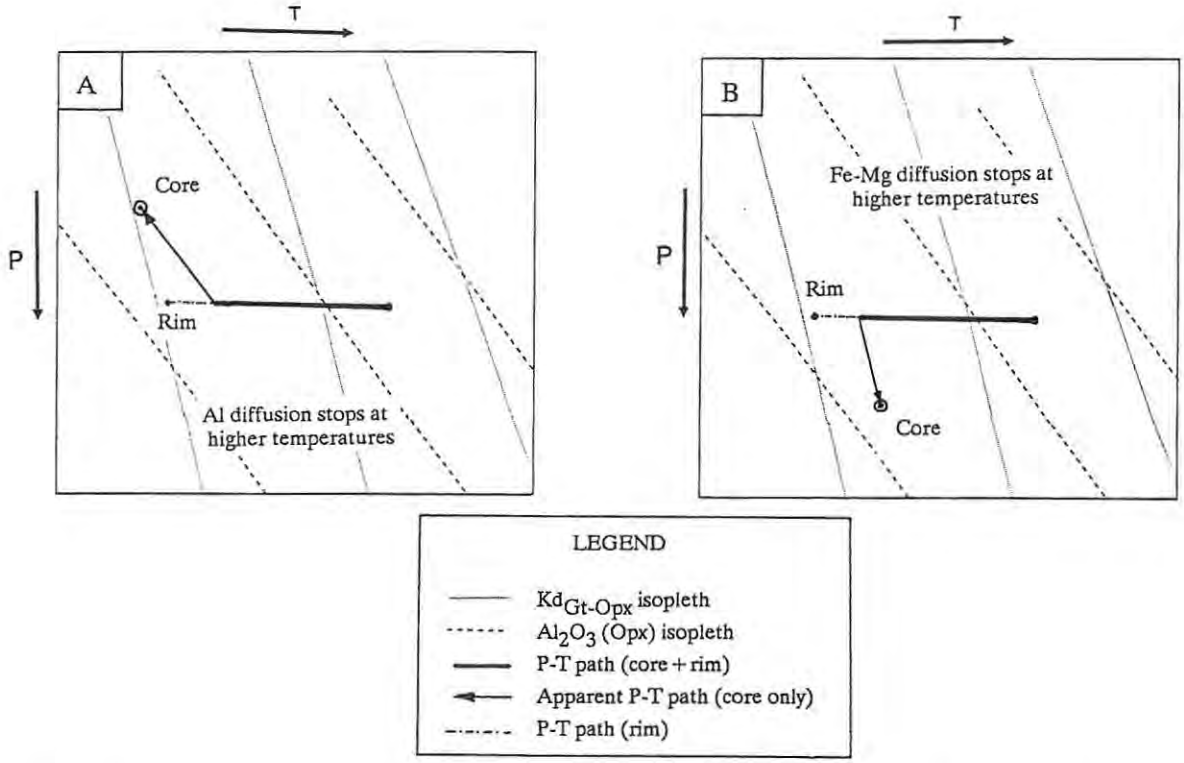

Fig. 6.8: Schematic diagram illustrating the relationship between calculated pressures and temperatures for cores and rims. Rims are likely to reequilibrate to lower temperatures than the cores due to smaller distances of diffusion, and therefore will reflect pressures and temperatures closer to the real ambient conditions. Diagrams a) and b) correspond to cases a) and b) in Fig. 6.7.

(see Fig.6.4.) supports model a), and indicates that Al diffusion was blocked at higher temperatures than Fe and Mg diffusion. The zoning also

implies that apparent presssures calculated from core compositions are significantly lower than the true pressures at which the original rocks were emplaced, and rim compositions provide minimum pressure estimates.

2) The pyroxenites were all emplaced at approximately the same depth (Fig.6.9):

As for the models described above, initial isobaric cooling would result in decreasing Al_2O_3 in orthopyroxene and increasing $Kd_{Gt\text{-}Opx}$. If for some reason Al diffusion in orthopyroxene was blocked over a range of temperatures (Fig 6.9), further cooling would drive the xenoliths along *different* Al_2O_3 isopleths, resulting in a range in apparent pressures. If one excludes the high-pressure pyroxenite xenolith from this model, blocking of Al diffusion would have to have taken place over a temperature range of approximately 150°C (Fig. 6.6 and 6.9). If the high pressure xenolith is included, the range would be extended to approximately 250°C. The final P-T array and zoning patterns resulting from these proceses would be very similar to that described for case a) above.

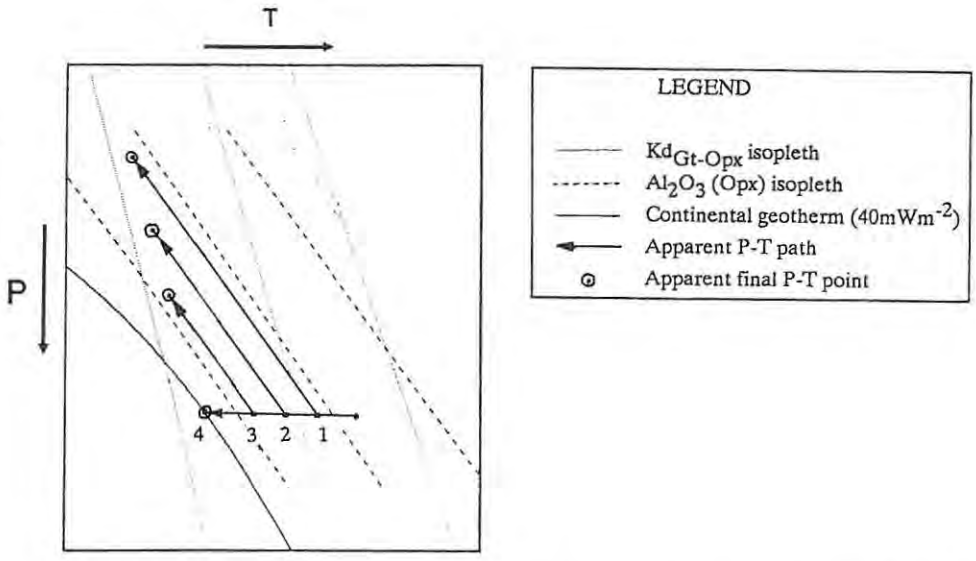

Fig. 6.9: Schematic diagram illustrating the possible apparent P-T paths for pyroxenites emplaced at approximately the same pressure. In order to generate the P-T array displayed by the Abrahamskraal pyroxenites, Al diffusion in the various samples would have to be blocked at different temperatures, represented by points 1 to 3 on the diagram. As for the model illustrated in Fig. 6.6a, further cooling drives the apparent P-T points along Al_2O_3 isopleths to lower pressures, and results in an apparent range in pressures.

To summarise, it would appear that only two of the above models for generating the pyroxenite P-T array (1a and 2) are capable of accounting for the zoning patterns observed in these rocks. In model 1a) it is assumed that the range of calculated pressures displayed by the pyroxenites reflects real differences in depths of emplacement, and the apparent P-T array deviates only slightly from the true array due to the blocking of Al diffusion at relatively high temperatures. In model 2 it is proposed that the pressure range is primarily the result of variable blocking temperatures for Al diffusion, and that the pyroxenites were not emplaced over a wide range of depths. No petrographic (varying states of textural reequilibration) or chemical evidence supporting variable diffusion rates has been found. If diffusion rates in the pyroxenites were variable, differences between core and rim compositions should also vary (larger differences for slower diffusion rates), and according to model 2 this variation should correlate with calculated pressures. The zoning observed in the pyroxenites (Fig. 6.4) does not conform to these patterns. Although the pyroxenites do show varying degrees of recrystallisation (see section 3.4), these do not show any consistent relationship to calculated pressures. It is therefore unlikely that the conditions at which the pyroxenites equilibrated were sufficiently different to result in the large variations in Al blocking temperature (between 150 and 250°C) required to generate the observed range in calculated pressure. In order to account for the possibility that apparent pressure variations displayed by the pyroxenites are a function of some bulk compositional parameter, calculated pressures were compared to whole-rock compositional data (calculated from mineral compositions and modes). No correlation between pressures and any bulk compositional parameters was observed.

The above discussion indicates that the mineral equilibria in the pyroxenites are frozen-in relics, reflecting earlier high-temperature conditions. Similar pressure-temperature conditions have been calculated for the lower-crustal and shallow upper-mantle granulite and pyroxenite xenoliths from the northern Lesotho kimberlites (Griffin *et.al.*, 1979). Harte *et.al.* (1981) have shown that these pressures and temperatures are based on frozen-in mineral equilibria which yield ages of 714 to 1000 Ma, suggesting that the P-T array reflects high temperature conditions possibly associated with the Namaqua event. A similar age for mineral equilibria in the Abrahamskraal pyroxenites is feasible (see section 7.2).

6.3. Temperatures and Pressures for the Eclogites and Garnet Dunite

There are no barometers applicable to the eclogite and garnet dunite assemblages. However temperatures can be calculated (using Ellis and Green, 1979, and O'Neill and Wood, 1979, 1980, respectively) for a range of estimated pressures, and comparison with the geotherm defined by the other xenoliths allows speculation as to the depth of origin of the eclogites and the garnet dunite (Fig. 6.10 and 6.11).

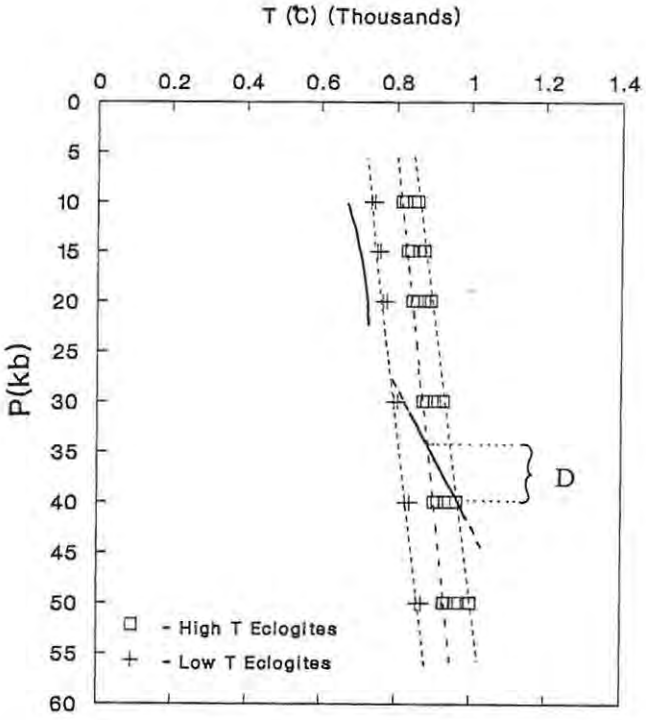

Fig. 6.10.: Pressure-temperature (P-T) plot showing possible conditions of equilibration for the eclogite xenoliths. P-T points were calculated for a range of estimated pressures using the Ellis and Green (1979) garnet-clinopyroxene Fe-Mg exchange thermometer (see section 5.2). Dashed lines are lines of equal composition (i.e. approximately constant Kd_{Gt-Cpx}). Heavy solid line is the Abrahamskraal geotherm. Assuming that the Kd_{Gt-Cpx} values reflect ambient conditions of equilibration of the eclogites, projection of the P-T points along lines of equal composition onto the Abrahamskraal geotherm will yield the true depth range for the xenoliths. Kd_{Gt-Cpx} values for the low-temperature eclogites may reflect "frozen-in" equilibria, and projection of these points onto the geotherm will yield maximum pressure estimates. "D" - likely true depth range for the high-temperature eclogites.

Temperatures calculated for the eclogites (based on Kd_{Gt-Cpx}) cover a range of approximately 150°C, and a significant temperature difference between the coarse- and fine-grained varieties is evident (Fig. 6.10). Blocking temperatures for Fe-Mg diffusion are unlikely to differ significantly from sample to sample, particularly in view of the textural uniformity of the coarse-grained eclogites. Thus the Kd_{Gt-Cpx} of the coarse-grained high-temperature eclogites are likely to reflect the ambient conditions at which

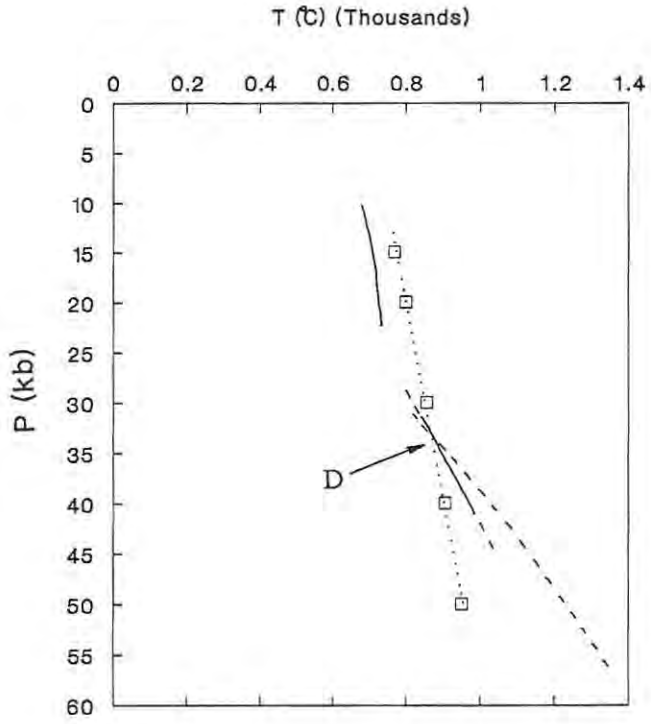

Fig. 6.11: Pressure-temperature plot showing possible equilibration conditions for the garnet dunite sample (258). P-T points were calculated for a range of estimated pressures using the O'Neill and Wood (1979,1980) garnet-olivine Fe-Mg exchange thermometer (see section 5.2). Solid curve - Abrahamskraal geotherm calculated using the Harley (1984) thermometer combined with the Nickel and Green (1985) barometer. Dashed curve - Abrahamskraal geotherm calculated using the O'Neill and Wood (1979,1980) thermometer combined with the Nickel and Green (1985) barometer. Assuming that the Kd_{Gt-Ol} value reflects the ambient conditions of equilibration of the garnet dunite xenolith, projection of the P-T points along lines of equal composition (dotted line on plot) onto the Abrahamskraal geotherm will yield an approximate true depth of origin (D).

the xenoliths equilibrated, and projection along lines of equal composition (Fig. 6.10) onto the geotherm should yield pressure estimates which reflect the true depth of origin of these xenoliths. Pressures obtained in this way (34 to 40 kb) indicate that the coarse-grained eclogites equilibrated in the upper mantle at similar depths to those of the garnet peridotites.

The Kd_{Gt-Cpx} of the low-temperature eclogites may represent frozen-in equilibria, and can be taken to reflect the maximum possible temperatures of equilibration for these xenoliths. Thus projection onto the geotherm (along lines of equal composition) will yield maximum pressure estimates (~27 kb). This implies that depths of origin significantly shallower than those of the high-temperature eclogites are possible, as the xenoliths may not have equilibrated to the ambient conditions defined by the geotherm (Fig. 6.10).

Estimates (based on Fe-Mg exchange between garnet and olivine), of the equilibration temperatures for the garnet dunite sample (258), are shown in Fig. 6.11. If these temperatures reflect the ambient conditions at the time of kimberlite eruption, then a pressure estimate of approximately 33kb is indicated.

7. ORIGIN OF THE XENOLITHS

7.1. Peridotites and Dunites

Textural and compositional data on the peridotite xenoliths (see sections 3.2. and 4.2.) indicates that they belong to the coarse, magnesium-rich, low-temperature variety of mantle xenoliths (type I; Harte and Hawkesworth, 1989) which generally dominate kimberlite xenolith suites, and which are believed to constitute a large proportion of the sub-continental lithosphere (e.g. Nixon *et.al.*, 1973; Boyd and Gurney, 1986; see section 1.1). Thus, despite the small number of samples and the limited data obtained therefrom, certain broad inferences can be made with regard to the origin of the Abrahamkraal peridotites. As discussed in section 1.1, type I xenoliths are believed to represent residues after large scale extraction of basaltic and/or komatiitic magmas from "fertile" mantle peridotite (e.g. Cox *et.al.*, 1987; Boyd and Mertzman, 1987). The depleted nature of the Abrahamskraaal peridotites (see section 4.2), and the absence of chemical variations suggestive of differentiation trends, are in agreement with such an origin.

Coarse aggregates of clinopyroxene, phlogopite and Cr-spinel in the Abrahamskraal harzburgites indicate that these rocks have been subject to metasomatism at depth (Harte, 1983, 1987). Textural evidence (section 3.2.) suggests that metasomatism has resulted in the replacement of garnet in these rocks. Although the cause and timing of metasomatism is not certain, evidence from elsewhere suggests that it may have been related to Karoo magmatism (Hawkesworth *et.al.*, 1983; Erlank *et.al.*, 1987).

Two varieties of dunite, i.e. coarse- and finer-grained, are distinguishable on the basis of petrographic and mineral composition data (see sections 3.3 and 4.2). Olivine in the coarse-grained dunites is very magnesium-rich and shows a restricted range of compositions (Fo91-Fo93). It is therefore compositionally very similar to olivine from the peridotite xenoliths. Although the dunite assemblages are generally not amenable to the application of thermobarometric methods, an approximate pressure and temperature can be obtained for the single garnet dunite sample (258) by projecting possible temperatures (obtained using the garnet-olivine

thermometer) onto the Abrahamskraal geotherm (section 6.3.). According to this method, sample 258 plots at the low pressure end of the peridotite P-T array for Abrahamskraal (Fig. 6.11). The similarities in olivine composition and conditions of equilibration for the coarse-grained dunites and the peridotites, suggest that the coarse-grained dunites may also represent solid residues after partial melting.

Olivine from the finer-grained dunites displays variable compositions which extend to significantly more Fe-rich values than those found in the coarse-grained dunites and peridotites. These features would not be expected in residual rocks, and may indicate that the finer-grained dunites are ultramafic cumulates formed by igneous fractionation proceses (Harte, 1983).

The metasomatic features of the dunites provide further evidence regarding the distinction between the coarse- and finer-grained varieties. Potassic-richterite is believed to form only in the depth range of 70 - 100 km (on a typical conductive shield geotherm, Erlank *et.al*, 1987). Thus its presence in the finer-grained dunites suggests that these rocks equilibrated at relatively shallow depths. The coarse-grained garnet dunite sample and most of the garnet peridotites appear to have equilibrated at depths greater than 100km (~31 kb; Fig. 6.1 and 6.11). Despite evidence for significant metasomatism in some of the coarse-grained dunites (abundant coarse phlogopite), none of them contain potassic-richterite, suggesting that they may also have originated from depths greater than those at which the finer-grained dunites equilibrated.

7.2. Pyroxenites and Eclogites

Several features of the garnet pyroxenite xenoliths are suggestive of an igneous origin for these rocks. As discussed in section 6.2., exsolution textures in the garnet websterites indicate that the rocks have undergone isobaric cooling from high temperatures, and thus they may represent the reequilibrated crystallisation products of mafic magmas. Large variations in mineral composition (particularly Fe/Mg ratio) reflect bulk compositional variations which are likely to have arisen by igneous fractionation processes. At certain other kimberlite and alkali basalt

localities (e.g. eastern Australia, Griffin *et.al.*, 1984), pyroxenites showing textural and compositional similarities to the Abrahamskraal garnet pyroxenites, display cross-cutting relationships with the presumed mantle wall-rock, indicating an intrusive origin. Thus a similar origin may be inferred for the Abrahamskraal rocks.

The depth range over which the garnet websterites have been intruded, and the absence of peridotitic xenoliths from this depth range is somewhat enigmatic (in view of the currently accepted belief that the lithospheric mantle is dominated by residual peridotitic material, section 1.1). If one excludes the possibility that the pressure range is an artefact of the thermobarometric methods (section 6.2.), two interpretations are possible:

1) The upper mantle above approximately 85km and possibly the lowermost portion of the crust is dominated by garnet pyroxenites. It is also possible that some of the eclogites and dunites (the finer-grained varieties, see previous section) originated from these depths.
2) The pyroxenites represent a zone of mafic dykes rather than horizontal bodies. This may have been a zone of weakness which was exploited and sampled by the kimberlite intrusion.

A model similar to 1, has been proposed by Griffen *et.al* (1979) to account for the depths of origin of garnet websterite xenoliths from the northern Lesotho kimberlites. They envisage a 40-50km thick zone of garnet websterite and eclogite immediately underlying the subcontinental Moho (~37km, Hales and Sacks, 1959). These rocks are believed to have been produced by the underplating of rising mafic magmas which pond at the Moho due to density contrasts. The suite of mafic lower-crustal and shallow upper-mantle xenoliths, appear to be restricted to kimberlites intruded at or near to the boundary between the Kaapvaal craton and the Namaqua-Natal mobile belt (Griffin *et.al* , 1979; Rogers and Hawkesworth, 1982; see Fig. 7.1). Sm-Nd whole-rock ages of 1400 ±100 Ma have been obtained for lower-crustal garnet granulite xenoliths from northern Lesotho (Rogers and Hawkesworth, 1982), which are believed to have formed by similar processes to those that formed the garnet websterites and shallow eclogites (Griffin, *et.al* , 1979). Although no garnet granulite xenoliths have been found at Abrahamskraal, they are common in many of the other kimberlites of the

central Cape Province (Fig. 7.1), suggesting the presence of a mafic lower crust of similar origin to that inferred for northern Lesotho (Grütter and Robey, 1988). The dates obtained for the granulites suggest that the suite of mafic lower-crustal and possibly the upper-most mantle xenoliths represent a major magmatic episode associated with the evolution of the Namaqua-Natal mobile belt (Rogers and Hawkesworth, 1982; Grütter and Robey, 1988). A similar origin for the Abrahamskraal garnet pyroxenites is suggested by the probable Namaqua age of "frozen-in" mineral equilibria in these rocks (section 6.2.).

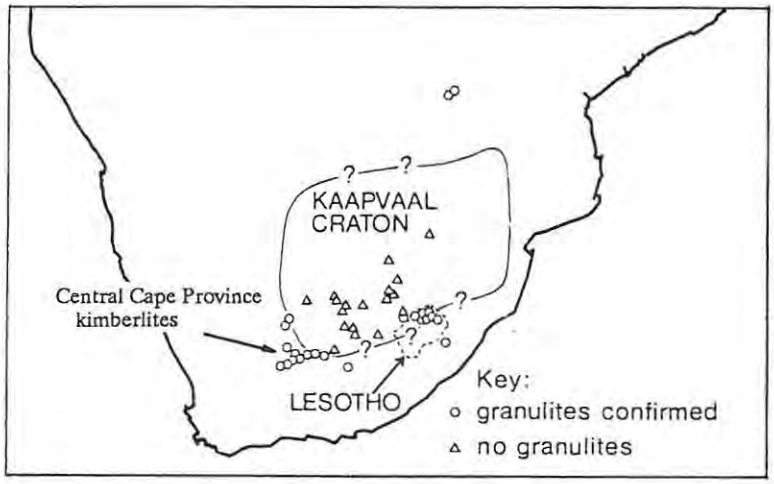

Fig. 7.1: Distribution of kimberlite hosted granulite xenoliths in relation to the boundary of the Kaapvaal Craton (modified after Griffin et.al., 1979).

Model 2 is not entirely inconsistent with the origin outlined above. It implies that the mantle above approximately 85km is not necessarily dominated by pyroxenitic material, but it does not preclude the possibility of significant underplating of mafic magmas at the crust-mantle boundary. A similar origin has been suggested for garnet websterite xenoliths from the Colarado-Wyoming kimberlites in the U.S.A., which are believed to represent a network of dykes intruded into the shallow upper-mantle (Eggler *et.al.*, 1987). In this case however, a relatively large number of enriched garnet- and spinel-bearing peridotite xenoliths appear to have originated from the same depth range as the garnet websterites. These rocks are thought to represent the mantle wall-rock through which the garnet websterite dykes have intruded (Eggler *et.al*, 1987).

Due to the lack of barometers applicable to the garnet-clinopyroxene mineral assemblage, one cannot accurately determine the equilibration conditions of the eclogite xenoliths, and in the absence of whole-rock compositions and isotopic data it is difficult to constrain the origin of these rocks. The P-T data obtained for the eclogites in section 6.3. indicates that they did not originate from depths greater than 35 - 40 kb. The evidence also suggests that two groups of eclogite are distinguishable on the basis of equilibration conditions. The higher-temperature group probably originated from greater depths than the lower-temperature eclogites, and may have equilibrated at similar depths to the garnet peridotites. This is supported by the textural characteristics of the high-temperature eclogites (section 3.5.). These are very similar to those in some of the group I eclogites from Roberts Victor which are presumed to be of mantle origin (MacGregor and Carter, 1970; Hatton and Gurney, 1987). Unfortunately the textures in the low-temperature eclogites are obscured by late-stage alteration. Nonetheless their fine grain-size and granuloblastic textures suggest that they may be of similar origin to the lower-crustal or shallow upper-mantle eclogites described from northern Lesotho (Griffin *et.al.*, 1979) and the central Cape Province (Robey, 1981).

Mineral compositions in the eclogites do not show any correlation with their textural characteristics or temperatures of equilibration (see section 4.4). Variations in mineral composition are believed to reflect variations in the compositions of the magmas from which the eclogites crystallised. Thus the lack of correlation between mineral compositions and conditions of formation is surprising, as one would expect to find compositional differences between magmas intruded at different depths and possibly during different events.

An origin for mantle eclogites involving the subduction and metamorphism of oceanic crust, has been proposed by several authors (Helmstaedt and Doig, 1975; Ater *et.al.*, 1984, MacGregor and Manton, 1986), primarily on the basis of isotopic and whole-rock compositonal features. In the absence of whole-rock compositions and isotopic data for the Abrahamskraal eclogites, it is dificult to assess the applicability of a subduction model. However the possible association of the eclogites, particularly the low-temperature variety, with the garnet-pyroxenites, would suggest an igneous, rather than metamorphic origin for these rocks.

8. DISCUSSION: VARIATIONS IN THE THICKNESS AND GEOTHERMAL GRADIENTS OF THE KAAPVAAL AND NAMAQUA LITHOSPHERE

8.1. Evidence from Geotherms and Diamond Distribution

The apparent confinement of diamondiferous kimberlites to the geographical area of the Kaapvaal craton, and the nature of xenolith-derived geotherms constructed for the craton and surrounding mobile belts, has led to the generally held belief that the Kaapvaal craton is underlain by a lithospheric root which is significantly thicker than that underlying the mobile belts (e.g. Nixon *et.al.*, 1973; Boyd and Nixon, 1975, 1978, 1979; Boyd and Gurney, 1986). This is partly based on current understanding of the stability of diamond in the mantle, and of the origin of kimberlitic magmas. In continental lithosphere with a typical conductive geothermal gradient, diamonds are only stable below approximately 130km (Kennedy and Kennedy, 1976). Kimberlites are generated at the base of the lithosphere (Wyllie, 1980, 1989; Eggler, 1989), thus only those which intrude cratons with thick cool lithospheric keels (≥130km) are capable of sampling diamond-bearing lithosphere.

The presence and positions of temperature discontinuities or "inflections" at the high-pressure ends of xenolith-derived mobile belt and cratonic geotherms, is believed to provide explicit evidence for a thinning of the lithosphere across the craton margin (Boyd and Nixon, 1979; Boyd and Gurney, 1986). However as pointed out by Mitchell (1984), this is dependent on how the temperature discontinuities are interpreted. Although there is still much debate regarding the exact origins of the high-temperature xenoliths which define the discontinuities, it is generally believed that they originated at the lithosphere/asthenosphere boundary due to the interaction of hot convecting asthenospheric material (or magmas derived therefrom) with the cooler and more rigid lower lithosphere (Nixon and Boyd, 1973a; Boyd, 1973; Harte and Gurney, 1980; Harte, 1983; Harte and Hawkesworth, 1989). Thus the position of the high-temperature discontinuity is believed to reflect the depth of the lithosphere/asthenosphere boundary at the time of kimberlite eruption. Geotherms constructed by Boyd and Gurney (1986) for two on-craton and two off-craton kimberlites are shown in Fig. 8.1. The temperature discontinuity on the two off-craton geotherms

appears to occur at significantly shallower depths than that of the on-craton geotherms. This is taken to reflect a thinning of the lithosphere from craton to mobile belt, as illustrated in Fig. 8.2. However, comparison of the geotherms in Fig. 8.1. with those constructed for the same xenolith suites using the chosen thermobarometer of this study (Fig. 8.3), indicates that the position of the discontinuity is strongly dependant on the choice of thermometer and barometer. Thus one should not attach too much significance to the absolute position of the discontinuity obtained for any particular xenolith suite.

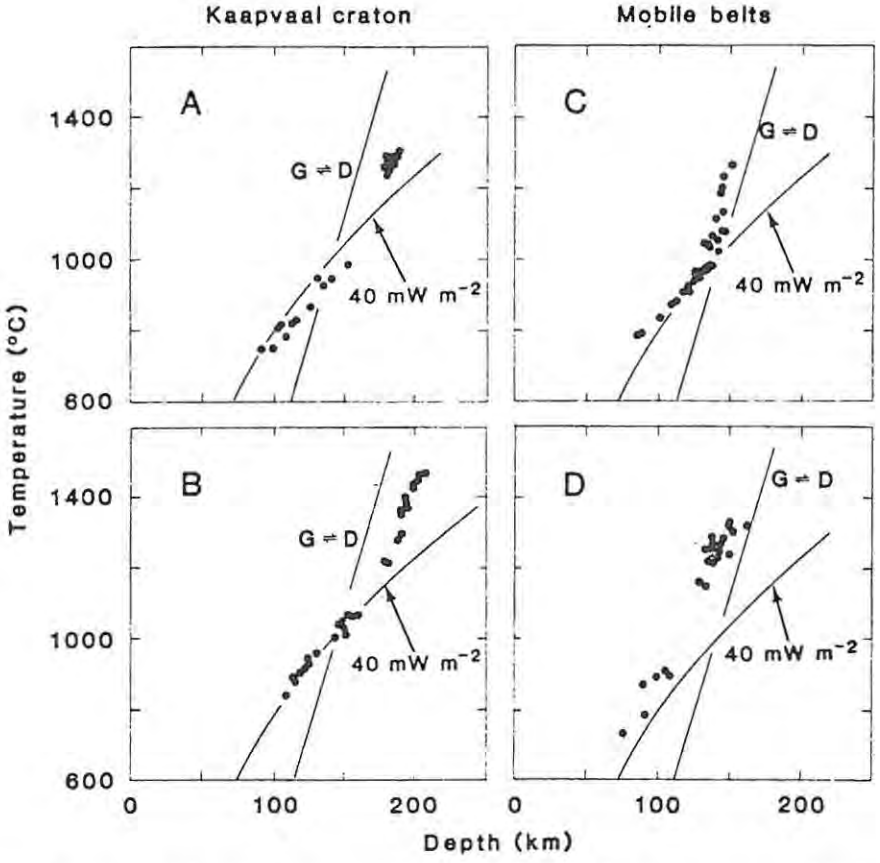

Fig. 8.1: Pressure(depth)-temperature arrays for four xenolith suites from southern Africa (after Boyd and Gurney, 1986). Geotherms were calculated using pyroxene thermobarometry (Finnerty and Boyd, 1984).The Frank Smith (A) and northern Lesotho (B) suites are from the craton, whereas Louwrencia (C) is west of the craton and East Griqualand (D) to the southeast. The diamond-graphite boundary (Kennedy and Kennedy, 1976) and a typical shield geotherm (Pollack and Chapman, 1977) are also shown.

The model outlined above implies a long-lived variation in lithospheric thickeness between craton and mobile belt. An alternative hypotheses involving the fluctuation of lithospheric thickness in accordance with

changes in heat flux from the underlying mantle, has been proposed by Nickel and Green (1985). These authors assume that the base of the lithosphere is defined by the intersection of the continental geotherm with the mantle solidus. At this point small amounts of partial melt are generated, resulting in the low velocity zone at the base of the lithosphere. Thus a cool shield geotherm *produces* a thick lithosphere. Estimates of the time taken for continental lithosphere to cool to an equilibrium geotherm after a major tectonothermal event, range from 150 to 500 Ma (Crough and Thompson, 1976; Sass and Lachenbruch, 1979; Vitorello and Pollack, 1980). Therefore, according to the above model, in the absence of additional heat flux from the mantle, continental lithosphere greater

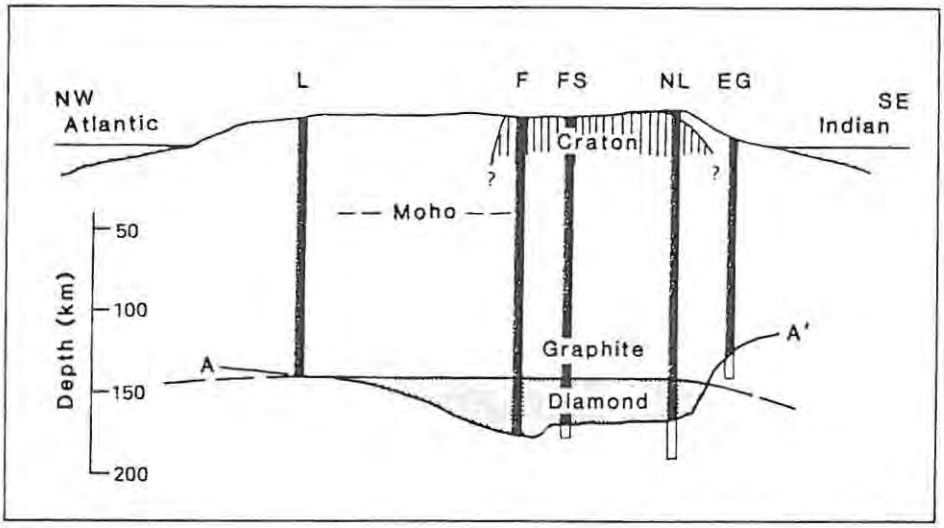

Fig. 8.2: Model for the lithosphere beneath southern Africa based primarily on the P-T arrrays shown in Fig. 8.1 (after Boyd and Gurney, 1986). Ratio of depth scale to horizontal scale is 4:1; the topography shown is greatly exaggerated. Vertical bars represent xenolith suites, and the maximum depths shown are for clusters of xenoliths of deepest origin in each suite. The line A - A' is approximately the locus of points of inflection or breaks between high and low-temperature clusters in the xenolith geotherms (Fig. 8.1). Xenolith suites: L - Louwrencia; F - Finsch; FS - Frank Smith; NL - northern Lesotho; EG - East Griqualand. The diamond graphite transition is represented by a line drawn through the points of intersection of individual geotherms with the equilibrium boundary of Kennedy and Kennedy (1976).

than 500 Ma should have attained maximum thickness, and hence there should be no significant difference in thickness between Archaean and Proterozoic lithosphere. According to Nickel and Green's model, overriding of a heat

source by the continent will result in a thinning of the lithosphere by "thermal erosion", and the formation of a temperature discontinuity at the base of the lithosphere. However they do acknowledge that in order to preserve diamonds believed to have formed prior to 3 Ga (Richardson *et.al.*, 1984), the Kaapvaal craton has to have retained a thickness greater than ~120 km since the Archaean. Possible long-lived differences in lithospheric thickness between the craton and adjacent mobile belt are not accounted for by the above model.

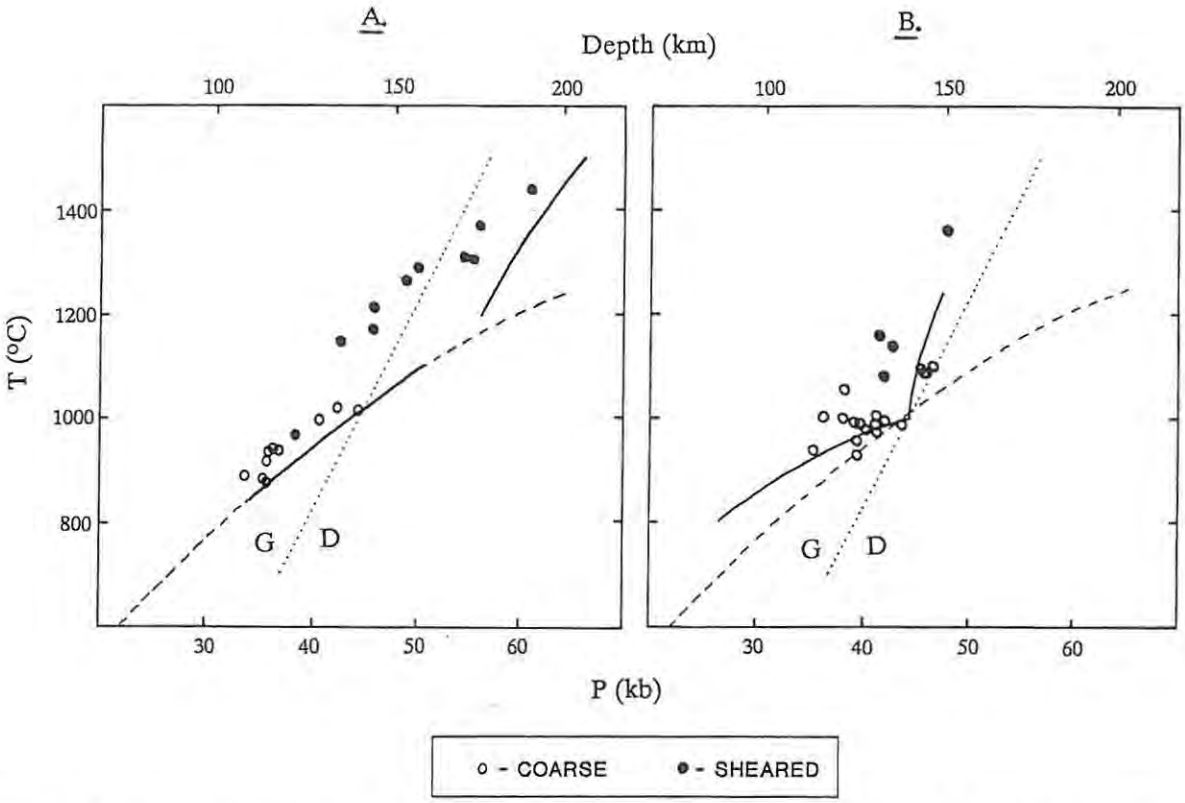

Fig. 8.3: Pressure-temperature arrays for xenolith suites B and C in Fig. 7.1. calculated using the chosen thermobarometer of this study. Reference curves as for Fig. 8.1. Solid curves are geotherms for the same xenolith suites taken from Fig. 8.1

The assumption that on- and off-craton kimberlites are generated at different depths, and hence that the lithosphere thins from craton to mobile belt,has been challenged by Mitchell (1984). Differences between geotherms, and the presence or absence of diamonds in the kimberlite, are ascribed by Mitchell (1984) to variations in the magma generation and segregation processes. He proposes that emplacement of the Namibian and

East Griqualand kimberlites involved larger volumes of magma and longer transport times than those intruded into the Kaapvaal craton. This would have allowed for greater interaction between the kimberlitic magma and the xenoliths, accounting for the shallower temperature discontinuity, and would have enhanced the possibilty of diamond resorbtion. However there is no independant evidence supporting different magma generation and segregation processes for on- and off-craton, or for diamondiferous and non-diamondiferous kimberlites. It is therefore difficult to reconcile the above model with the observed confinement of diamondiferous kimberlites to the Kaapvaal craton.

8.2. Evolution of the Continental Crust and Lithosphere

A number of authors have pointed out the probable close correlation between the formation of the continental crust and the developement of the underlying lithosphere (Jordan, 1978; Davies, 1979; Pollack, 1986). Davies (1979) proposes that formation of a deep lithospheric root to continents is not only a likely consequence of crust formation, it is in fact essential for the preservation of thick Archean continental crust. His argument is based on the probable high heat flows which pertained during the Archaean. It is generally believed that the heat flow out of the earth's surface during the Archaean was between two and three times greater than present day values (Jessop and Lewis, 1978; Davies, 1979; Campbell and Jarvis, 1984). Without the buffering effect of thick rigid lithospheric roots, this elevated heat flux would melt the base of the continental crust (Davies, 1979). The effect of the lithospheric root is to divert heat away from the continental lithosphere towards surrounding oceanic regions, through which most of the earth's heat flux is directed (Burke and Kidd, 1978). Archaean geotherms based on diamond inclusion studies (Boyd *et.al.*, 1985; Boyd and Gurney, 1986), and the probable Archaean ages of diamonds from the Kaapvaal craton (Richardson *et.al.*, 1984), provide evidence supporting the presence of thick, cool sub-continental lithosphere during the Archaean.

In order to retain its thickness under conditions of high heat flow, the lithosphere has to be compositionally and mechanically distinct from the underlying asthenosphere. It has been demonstrated that the developement and stabilisation of such a lithosphere is an integral part of continental

crust formation, and cannot be accounted for by thermal arguments alone (Jordan, 1978; Pollack, 1986). The basic principle involved is that magmatic events associated with crust formation, particularly the extraction of basaltic and komatiitic partial melts, results in the depletion and devolatilisation of the subcontinental mantle. Jordan (1978) argues that the lower density of this depleted peridotite will compensate for density increases associated with cooling of the lithosphere after a major tectonothermal event. Thus the lithosphere will maintain approximate neutral buoyancy and will not sink into the underlying mantle. The resistance of the lithosphere to thermal erosion from below results from its refractory and volatile-poor nature which raises the solidus to significantly higher temperatures, and inhibits partial melting (Jordan, 1978; Pollack, 1986). In addition, the low volatile content of the depleted material significantly enhances its viscosity (Pollack, 1986). Thus at any given temperature, the lithosphere will be more rigid than the underlying asthenosphere, and therefore will resist incorporation into mantle convection.

Two important implications of the models discussed above should be noted. Firstly, the arguments presented above indicate that the thickness of the sub-continental lithosphere cannot be defined simply in terms of geothermal gradients and the peridotite solidus. The establishment of a relatively cool conductive geothermal gradient appears to be consequent upon the stabilisation of a thick rigid lithosphere, rather than the other way around. The second important aspect of the above theories is that crust formation, and hence developement of the cratonic lithosphere, was likely to have been far more efficient during the earth's early history than it was during later periods (McLennan and Taylor, 1982; Pollack, 1986). Higher Archaean heat flow is believed to have increased the fractional extent and depth range of partial melting, thereby enhancing the efficiency of the devolatilisation and cratonisation process (Pollack, 1986). Thus according to the above model, one would expect the Archaean Kaapvaaal lithosphere to be thicker than that of the surrounding Proterozoic mobile belts.

8.3. Heat Flow Arguments

Modelling of present-day heat flow differences between the Kaapvaal craton and the Namaqua mobile belt, supports the concept of a relatively thick Archaean lithospheric keel which diverts heat away from its base towards thinner lithosphere underlying the surrounding mobile belts (Jones, 1987; Ballard and Pollack, 1987). Heat flow measurements in southern Africa (Jones, 1984) indicate a difference in surface heat flow of some 25mWm^{-2} between the centre of the Kaapvaal craton and that of the surrounding mobile belts (Fig. 8.4.). Ballard and Pollack (1987) propose two possible mechanisms to account for these heat flow variations: 1) differences in crustal heat productions; and 2) differences in lithospheric thickness which allow diversion of heat away from the base of the craton. They have constructed numerical heat flow models with these two parameters as variables (see Fig. 8.5.). By assuming that crustal heat production differences are unlikely to excede 0.35 μWm^{-3}, Ballard and Pollack conclude that the differences in surface heat flow between craton and mobile belt

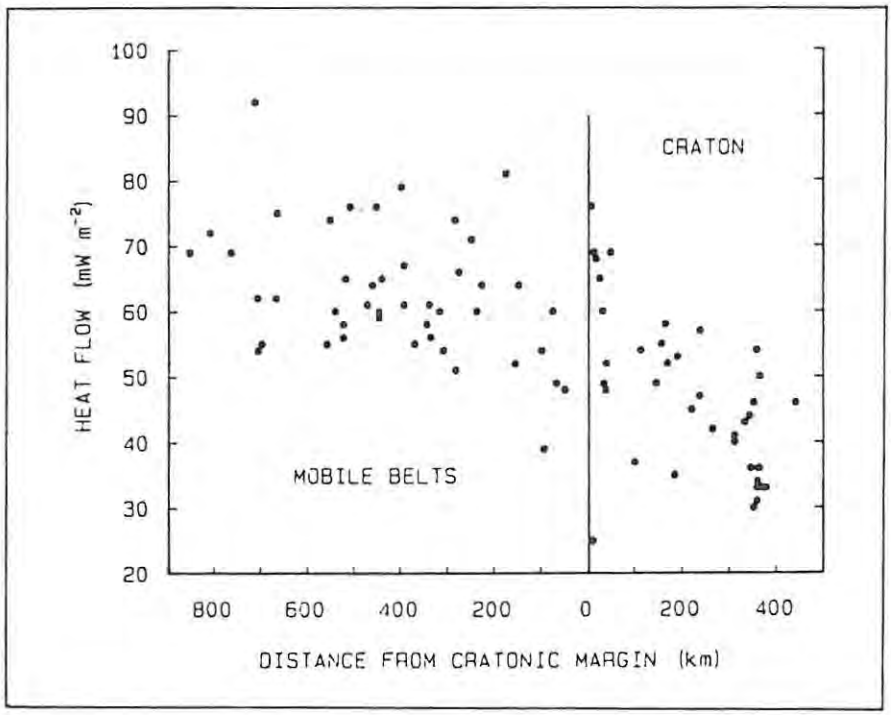

Fig. 8.4.: Heat flow vs. distance from the margin of the Kaapvaal-Limpopo-Zimbabwe Craton (after Ballard and Pollack, 1987).

cannot be accounted for by differences in crustal heat production alone, and suggest that a difference in lithospheric thickness of greater than 100 km is required. It is evident from Fig. 8.5. that the increased heat

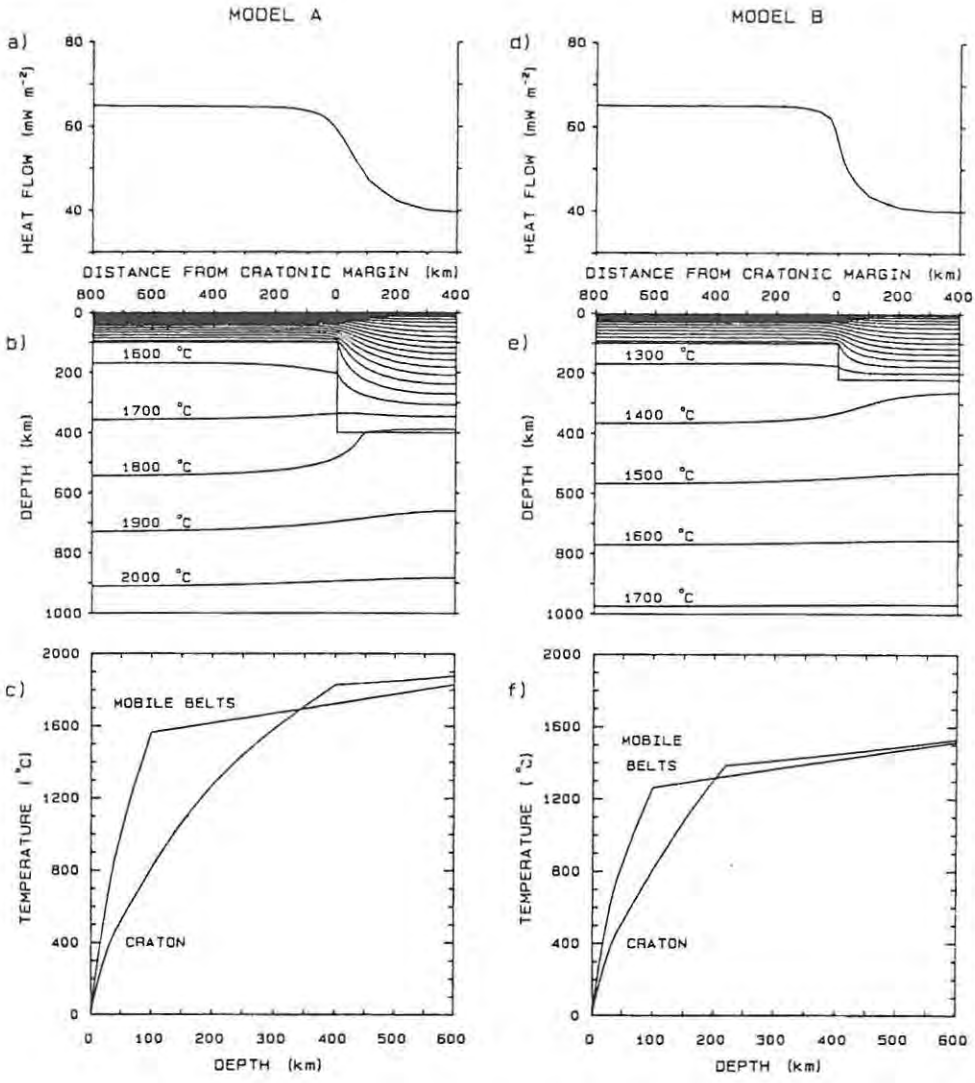

Fig. 8.5.: Models derived by Ballard and Pollack (1987) to account for heat flow differences between Archaean cratons and Proterozoic mobile belts in southern Africa. The two models show the effects of using different values of lithospheric thickness (T) and difference in crustal heat production (H). In model A, T = 400km and H = 0.25μWm^{-3}. In model B, T = 220km and H = 0.35μWm^{-3}. (a) and (d) - surface heat flows; (b) and (e) - temperature fields; (c) and (f) - geotherms for the craton and mobile belts.

flow through the thinner lithosphere of the mobile belt results in a geothermal gradient which is significantly steeper than that of the craton.

8.4. Implications of the Abrahamskraal Geotherm

The evidence discussed in sections 8.1 to 8.3 suggests that the Kaapvaal lithosphere is thicker and cooler than that of the surrounding mobile belts. Thus the craton boundary should be marked by a shallowing of the lithosphere and a steepening of the geothermal gradient. As discussed in section 6.1., the peridotite geotherm for Abrahamskraal shows neither of these features. The Abrahamskraal peridotites appear to be derived from only marginally shallower depths than equivalent on-craton xenoliths, and their P-T points lie on a typical cool shield geotherm, implying no additional heat flux from the mantle. If one assumes that the mineral equilibria in the cool coarse xenoliths reflect ambient conditions in the lower lithosphere at the time of kimberlite emplacement (see section 6.1.), and that the temperature discontinuity (in the northern Lesotho geotherm) reflects the position of the lithosphere/asthenosphere boundary, then the above features suggest that there is no significant change in lithospheric thickness at the geophysically defined boundary of the Kaapvaal craton.

The absence of evidence indicating a shelving of the lithosphere across the craton boundary can be accounted for in a number of ways (Fig. 8.6):

a)The position of the geophysically defined boundary of the craton (i.e. its boundary in the shallow upper crust) does not coincide with the boundary between the lower Kaapvaal and Namaqua lithosphere. If the craton boundary dips towards the Namaqua mobile belt, a wedge of thick cratonic lithosphere may underly significant portions of the Namaqua crust (Fig. 8.6a)

b) Thinning of the lithosphere from craton to mobile belt is gradational (as implied by the model of Boyd and Gurney, 1986; Fig 8.2; see Fig. 8.6b). Because the Abrahamskraal kimberlite occurs close to the craton margin, thickness variations are likely to be too small to be detected by the relatively insensitive thermobarometry techniques available.

c) The Namaqua lithosphere is not significantly thinner than that of the

Kaapvaal craton (Fig. 8.6c). This would imply that the formation of the Namaqua mobile belt was a major crust-forming event which affected large portions of the underlying mantle, resulting in the development of a thick lithospheric keel similar to that occurring beneath cratonic regions. It also implies that heat production in the upper parts of the Namaqua crust is significantly higher than that of the Kaapvaal crust, and can account for the observed surface heat flow variation.

d) Tectono-magmatic processes related to the accretion of the Namaqua mobile belt to the Kaapvaal craton may have resulted in a localised thickening of the Namaqua lithosphere adjacent to the craton margin (Fig. 8.6d). The significant difference between this model and a), is that the lithosphere underlying the craton margin is of Namaqua age (~1000-1400 Ma), whereas in a) the craton margin is underlain by ancient Kaapvaal lithosphere (Archaean to early Proterozoic).

8.5. Diamond Genesis and Distribution in Southern Africa

In conjunction with the Abrahamskraal geotherm, the age and distribution of diamonds in southern Africa places further constraints on models for the Namaqua/Kaapvaal boundary. Evidence provided by the Abrahmskraal geotherm (as discussed above), suggests that the boundary between the Kaapvaal craton and the Namaqua mobile belt as observed at crustal levels, is not reflected by an associated variation in lithospheric thickness at depth (although thinning may occur at greater distances from the craton margin). However, as discussed in section 8.2, diamond-bearing kimberlites appear to be confined to the geographical region of the Kaapvaal craton (as defined at shallow-crustal levels). In view of the Archaean or early-Proterozoic ages proposed for the majority of dated diamonds from southern African kimberlites (Richardson *et.al*, 1984; Gurney, 1989), it is suggested that in terms of diamond distribution, the age of the Namaqua lithosphere is of greater significance than its thickness. This implies that diamond genesis in the Kaapvaal lithosphere may have been associated with processes which occurred primarily during the Archaean and early Proterozoic, or with conditions (e.g. redox state ?) which were prevalent at these times only, and that diamonds could not form in significant quantities within younger lithosphere.

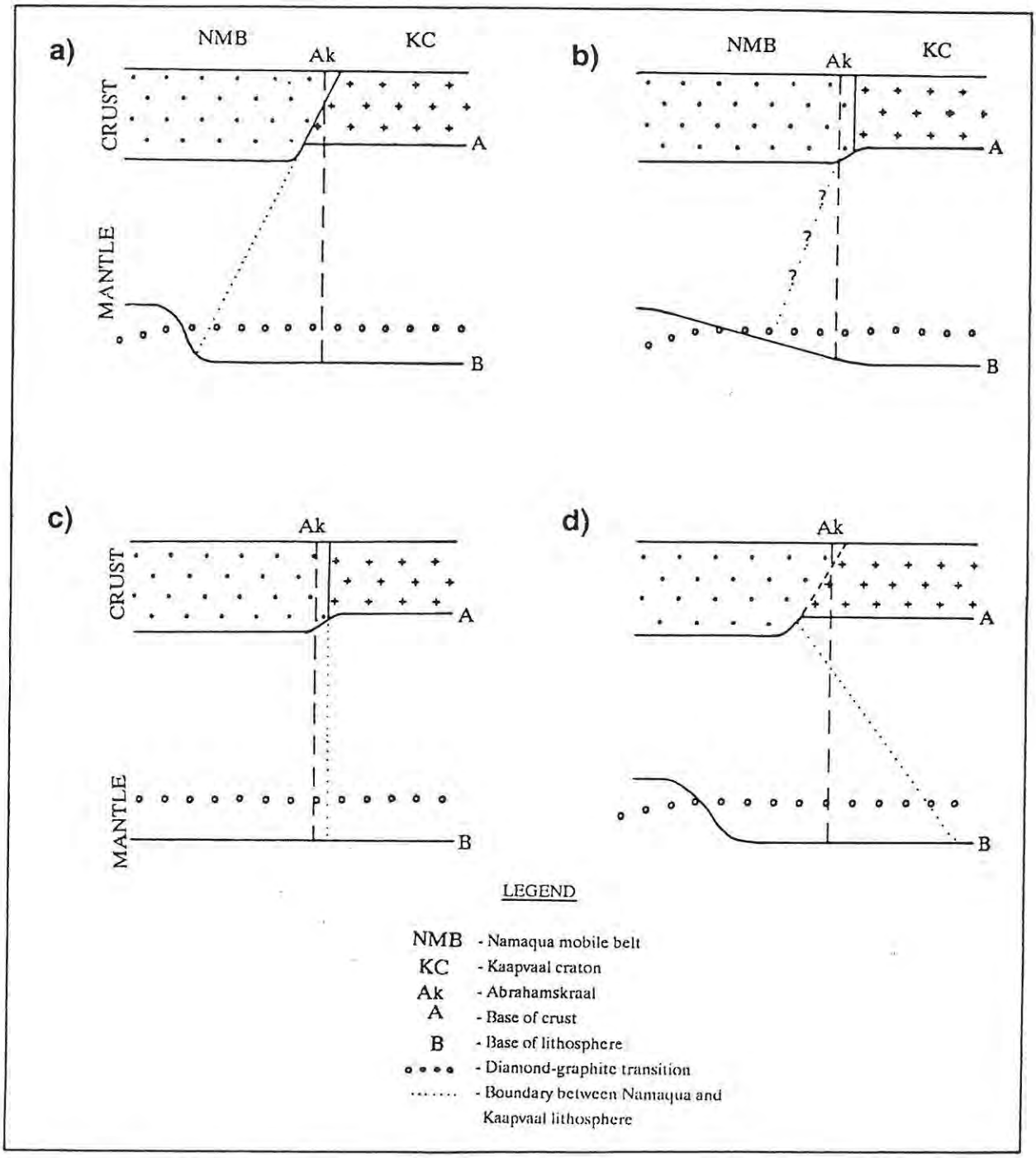

Fig. 8.6: Schematic models of the margin between the Kapvaal craton and the Namaqua mobile belt. In all of the models, the thickness of the lithosphere at the craton margin is not significantly less than that beneath the craton (in accordance with the constraint provided by the Abrahamskraal geotherm). In a), b), and d) the Namaqua lithosphere away from the vicinity of the craton margin is thinner than that of the craton. Relatively thick lithosphere at the margin can be accounted for by a dipping craton/mobile belt boundary (a), a shallow dipping shelf (b), or a local thickening of the Namaqua lithosphere (d). In model c), the Namaqua lithosphere is not significantly thinner than that beneath the Kaapvaal craton.

Of the four models outlined in the previous section, model 1 and possibly 2 do not satisfy the constraint of diamond distribution. In these models, old, thick, potentially diamondiferous lithosphere underlies portions of the Namaqua crust, and one would expect some of the "off-craton" kimberlites intruding this region to be diamond-bearing. In models 3 and 4, the lithosphere sampled by the Abrahamskraal kimberlite is not significantly thinner, but is younger than that of the Kaapvaal craton, and therefore is unlikely to contain diamonds in significant amounts. Thus the latter two models appear to be more viable than the former.

9. SUMMARY AND CONCLUSIONS

Xenoliths of deep-seated origin occurring within the Abrahamskraal kimberlite can be grouped into four major categories, i.e. peridotites, dunites, eclogites, and garnet pyroxenites. Rocks belonging to these categories are distinguishable in terms of their petrographic features, mineral compositions, and conditions of equilibration, and yield information regarding different portions of the lithosphere sampled by the kimberlite.

The peridotites are coarse-textured (Harte, 1977), magnesium-rich rocks, and are typical examples of the common type I peridotites which generally dominate mantle xenolith suites in kimberlites. By analogy with type I peridotites found elsewhere, the Abrahamskraal peridotites are believed to represent depleted residues after large scale extraction of basaltic and/or komatiitic magmas from "fertile" mantle peridotite.

The garnet peridotite xenoliths yield pressure and temperature estimates which are believed to represent the ambient conditions in the lower lithosphere at the time of kimberlite emlacement (~81 Ma). The xenoliths define a geotherm which lies along a typical theoretical conductive geothermal gradient for shield areas (Pollack and Chapman, 1977), and which extends to a maximum pressure of 41 kb (~130 km). Comparison of the Abrahamskraal geotherm with that constructed for the northern Lesotho xenolith suite (calculated using the same thermobarometric couple), suggests that the lithosphere at the Namaqua/Kaapvaal boundary is not significantly thinner or hotter than that underlying the craton. Modelling of the craton boundary under the constraints provided by the Abrahamskraal geotherm, and by the distribution of diamond bearing kimberlites in southern Africa, suggests that the Abrahamskraal kimberlite has sampled relatively thick, cool, lithospheric mantle of probable Namaqua age. It is inferred that lithosphere with these characteristics underlies the region close to the craton-mobile belt boundary defined at crustal levels. In view of the lack of evidence indicating significant thinning of the lithosphere across the craton margin, it is suggested that, in terms of diamond distribution, the age and magmatic history of the Namaqua lithosphere is possibly of greater significance than its thickness.

Two varieties of dunite occur at Abrahamskraal. Coarse-textured dunites with Mg-rich olivine compositions similar to those of the peridotitic olivines, probably originated by similar (but perhaps more extreme) processes to those which formed the peridotites. A finer-grained and relatively Fe-rich variety of dunite may represent ultramafic cumulates formed by fractionation of basic or ultrabasic magmas within the mantle.

Eclogite xenoliths are not amenable to the application of geobarometry methods, and are therefore of limited use for the determination of the thermal nature and thickness of the lithosphere sampled by the Abrahamskraal kimberlite. Nevertheless a number of these xenoliths have been studied and two varieties have been distinguished. Coarse-grained eclogites, which yield relatively high temperature estimates, are believed to have originated from depths similar to those determined for the garnet peridotites, i.e. from the lower lithosphere. Two examples of a distinctly finer-grained variety of eclogite, yield significantly lower temperatures which may be based on frozen-in equilibria. A maximum depth of approximately 87 km (~27 kb) has been estimated for these xenoliths, but they may have originated from significantly shallower (possibly lower-crustal) levels.

The garnet pyroxenite xenoliths are generally orthopyroxene-rich rocks which contain varying amounts of garnet (8 to 33 %) and clinopyroxene (0 to 64 %). Textural features indicate that the garnet and possibly some of the clinopyroxene have exsolved from an originally Al-rich orthopyroxene. The rocks are significantly more Fe-rich than the peridotite xenoliths, and their constituent minerals show a wide range of Mg/Mg+Fe ratios. These features suggest an origin involving crystalisation and subsequent subsolidus cooling of mafic magmas intruded into the mantle or lower crust.

The pressure-temperature array defined by the garnet pyroxenites is approximately isothermal, and spans a depth range from approximately 30 to 95 km. It deviates strongly (to higher temperatures) from the ambient geothermal gradient at the time of kimberlite emplacement, as inferred from the garnet peridotite xenoliths. The pressures and temperatures calculated for the garnet pyroxenites are based on mineral equilibria which are

believed to have been frozen-in during cooling from an intial high-temperature (probably molten) state. Qualitative modelling of possible cooling paths in pressure-temperature-composition space, indicates that the apparent depth range displayed by the garnet pyroxenites approximates the true depth range over which these rocks were emplaced. However, the apparent pressures calculated from core compositions are significantly lower than the true pressures at which the original rocks formed.

The garnet pyroxenite xenoliths appear to represent a major magmatic event involving the emplacement of large amounts of mafic magma over a significant depth range in the shallow upper mantle. By analogy with more extensively studied lower-crustal and shallow upper-mantle xenolith suites found elsewhere in southern Africa, a Namaqua age (~1000-1400 Ma) is tentatively suggested for this event.

ACKNOWLEDGEMENTS

Funding for this project was generously provided by DeBeers Consolidated and the FRD.

I am indebted to a number of people who provided useful advice, criticism and support during the past twelve months. Thanks to Herman Grütter for suggesting the project, and for providing invaluable advice and guidance. Goonie Marsh and Clyde Mallinson provided constructive criticism of endless rough drafts of the thesis. John Bristow, Jock Robey and Fanus Viljoen at Anglo American Research Laboratories willingly assisted with technical and financial problems encountered during my research. Finally thanks to my wife Anouchka, for endless moral support and many hours spent typing parts of this thesis.

REFERENCES

Adams, G.E. and Bishop, F.C., 1982: Experimental investigation of Ca-Mg exchange betweeen olivine, orthopyroxene and clinopyroxene: potential for geobarometry. Earth Plan. Sci. Lett., v.57, p.241-250.

Ater, P.C., Eggler, D.H. and McCallum, M.E., 1984: Petrology and geochemistry of mantle eclogite xenoliths from the Colarado-Wyoming kimberlites. In: Kornprobst, J. (ed.), Kimberlites: II, The Mantle and Crust-Mantle Relationships. Dev's in Petrology, vIIB, Elsevier, Amsterdam, p.309-318.

Ballard, S. and Pollack, H.N., 1987: Diversion of heat by Archean cratons: a model for southern Africa. Earth Planet. Sci. Lett., v.85, p.253-264.

Boyd, F.R., 1973: A pyroxene geotherm. Geochim. Cosmochim. Acta, v.37, p.2533-2546.

Boyd, F.R., 1974: Ultramafic nodules from the Frank Smith kimberlite pipe, South Africa. Carnegie Inst. Wash. Yearbk., v.73, p.285-293.

Boyd, F.R. and Finger, L.W. 1975: Homogeneity of minerals in mantle rocks from Lesotho. Carnegie Inst. Wash. yearbook, v.75, p.362-373.

Boyd, F.R. and Nixon, P.H., 1975: Origins of the ultramafic nodules from some kimberlites of northern Lesotho and the Monastry Mine, South Africa. Phys. Chem. Earth, v.9, p.431-454.

Boyd, F.R. and Nixon, P.H., 1978: Ultramafic nodules from the Kimberly pipes, South Africa. Geochim. Cosmochim. Acta, v.42, p.1367-1382.

Boyd, F.R. and Nixon, P.H., 1979: Garnet lherzolite xenoliths from the kimberlites of East Griqualand, South Africa. Carnegie Inst. Wash. Yearbook, v.78, p.488-492.

Boyd, F.R. and Gurney, J.J., 1986: Diamonds and the African lithosphere. Science, v.232, p.472-477.

Boyd, F.R. and Mertzman, S.A., 1987: Composition and structure of the Kaapvaal lithosphere. In: Mysen, B.O. (ed.), Magmatic Processes: Physicochemical Principles. Spec. Publ. 1, Geochem. Soc., p.13-24.

Boyd, F.R., Gurney, J.J. and Richardson, S.H., 1985: Evidence for a 150-200 km thick Archaean lithosphere from diamond inclusion thermobarometry. Nature, v.315, p.387-389.

Burke, K. and Kidd, W.S.F., 1978: Were Archean continental geothermal gradients much steeper than those of today ? Nature, v.272, p.240-241.

Callow, S., 1988: A petrographic study of the Abrahamskraal kimberlite and associated xenoliths. Unpubl. Honours thesis, Univ. of Natal.

Campbell, I.H. and Jarvis, G.T., 1984: Mantle convection and early crustal evolution. Precambr. Res., v.26, p.15-56.

Carswell, D.A. and Griffin, W.L., 1981: Calculation of equilibration conditions for garnet granulite and garnet websterite nodules in African Kimberlite pipes. Tschermaks Mineral. Petrogr. Mitt., v.28, p.229-244.

Carswell, D.A. and Gibb, F.G.F., 1980: Geothermometry of garnet lherzolite nodules with special reference to those from the kimberlites of northern Lesotho. Contr. Min. Petr., v.74, p.403-416.

Carswell, D.A. and Gibb, F.G.F., 1987(a): Evaluation of mineral thermometers and barometers applicable to garnet lherzolite assemblages. Contr. Min. Petr., v.95, p.499-511.

Carswell, D.A. and Gibb, F.G.F., 1987(b): Garnet lherzolite xenoliths in the kimberlites of northern Lesotho: revised P-T equilibration conditions and upper mantle paleogeotherm. Contr. Min. Petr., v.97, p.473-487.

Clarke, T.C., Smith, C.B., Bristow, J.W. and Skinner, E.M.W., 1988: Isotopic characteristics of kimberlites in a craton-margin setting from the northern Cape Province, South Africa, 22nd Earth Sciences Congress of the Geol. Soc. S.Afr., Extended Abstracts, p.97-100.

Cox, K.G., Gurney, J.J and Harte, B. 1973: Xenoliths from the Matsoku pipe. In: Nixon, P.H., (ed), Lesotho Kimberlites. Lesotho National Development Corporation, Maseru, p.76-100.

Cox, K.G., Smith, M.R. and Beswetherick, S., 1987: Textural studies of garnet lherzolites: evidence of exsolution origin from high temperature harzburgites. In: Nixon, P.H., (ed.), Mantle Xenoliths, John Wiley & Sons, Chichister-New York-Brisbane-Toronto-Singapore, p.537-550.

Crough, S.T. and Thompson, G.A., 1976: Thermal model of the continental lithosphere. Journ. Geophys. Res., v.81, p.4857-4862.

Danchin, R.V., 1979: Mineral and bulk chemistry of garnet lherzolite and garnet harzburgite xenoliths from Premier Mine. South Africa. In: Boyd, F.R. and Meyer, H.O.A. (ed's), The mantle Sample: Inclusions in Kimberlites and Other Volcanics, AGU, Washington, p.104-126.

Davies, G.E., 1979: Thickness and thermal history of continental crust and root zones. Earth and Planet. Sci. Lett., v.44, p.231-238.

Davis, B.T.C. and Boyd, F.R., 1966: The join $Mg_2Si_2O_6$-$CaMgSi_2O_6$ at 30kb pressure and its application to pyroxenes from kimberlite. Journ. Geophys. Res., v.71, p.3567-3576.

Dawson, J.B., 1980: Kimberlites and Their Xenoliths. Springer-Verlag. 252p.

Dawson, J.B., 1987a: The MARID suite of xenoliths in kimberlite: relationship to veined and metasomatised peridotite xenoliths. In: Nixon, P.H., (ed.), Mantle Xenoliths, John Wiley & Sons, Chichister-New York-Brisbane-Toronto-Singapore, p.465-473.

Dawson, J.B., 1987b: Metasomatized harzburgites in kimberlite and alkaline magmas: Enriched restites and "flushed" lherzolites. In: Menzies, M.A. and Hawkesworth, C.J. (ed's), Mantle Metasomatism, Academic Press, London, p.125-144.

Dawson, J.B. and Stephens, W.E., 1975: Statistical analysis of garnets from kimberlites and associated xenoliths. Journ. Geol., V.83, p. 589-601.

Dawson, J.B. and Smith, J.V., 1977: The MARID (mica-amphibole-rutile-ilmenite-diopside) suite of xenoliths in kimberlite. Geochim. Cosmochim. Acta, v. 41, p.309-323.

DeBeer, J.H. and Meyer, R., 1984: Geophysical characteristics of the Namaqua-Natal belt and its boundaries, South Africa. Journ. Geodynamics, v.1, p.473-494.

Droop, G.T.R., 1987: A general equation for estimating Fe^{2+} concentrations in ferromagnesian silicates and oxides from microprobe analyses, using stochiometric criteria. Min. Mag., v.51, p.431-435.

Eggler, D.H., 1989: Kimberlites: How do they form ? In: Kimberlites and Related Rocks, vol. I, Geol. Soc. Aust. Spec. Publ. No. 14, Blackwell Scientific Publications, p.489-504.

Eggler, D.H and Wendlandt, R.F., 1979: Experimental studies on the relationship between Kimberlite magmas and partial melting of peridotites. In: Boyd, F.R. and Meyer, H.O.A. (ed's), Kimberlites, Diatremes and Diamonds; Their Geology, Petrology and Chemistry. AGU, Washington, D.C., p.330-338.

Eggler, D.H., Dudas, F.O., McCallum, M.E., McGee, E.S., Meyer, H.O.A. and Schulze, D.J., 1987: Lithosphere of the continental United States: Xenoliths in Kimberlites and other alkaline magmas. In: Nixon, P.H., (ed.), Mantle Xenoliths, John Wiley & Sons, Chichister-New York-Brisbane-Toronto-Singapore, p.41-57.

Ellis, D.J. and Green, D.H., 1979: An experimental study of the effect of Ca on garnet-clinopyroxene Fe-Mg exchange equilibria. Contr. Min. Petr., v.71, p.13-22.

Erlank, A.J., Waters, F.G., Hawkesworth, C.J., Haggerty, S.E., Allsopp, H.L., Rickard, R.S. and Menzies, M. 1987: Evidence for mantle metasomatism in peridotite nodules from the Kimberly pipes, South Africa. In: Menzies, M.A. and Hawkesworth, C.J., (ed's), Mantle metasomatism, Academic Press, London, p.221-311.

Finnerty, A.A., 1989: Inflected mantle geotherms are real: Evidence from olivine barometry. In: Kimberlites and Related Rocks, vol.II, Geol. Soc. Aust Spec. Publ. No. 14, Blackwell Scientific Publications, p.883-900.

Finnerty, A.A and Boyd, F.R., 1978: Pressure-dependent solubility of calcium in forsterite coexisting with diopside and enstatite. Carnegie Inst. Wash. Yearbk, v.77, p.713-717.

Finnerty, A.A and Boyd,F.R., 1984: Evaluation of thermobarometers for garnet peridotites. Geochim. Cosmochim. Aeta, v.48, p.15-27

Finnerty, A.A. and Boyd, F.R., 1987: Thermobarometry for garnet peridotites: basis for the determination of thermal and compositional structure of the upper mantle. In: Nixon, P.H., (ed), Mantle Xenoliths, John Wiley & Sons, Chichister-New York-Brisbane-Toronto-Singapore, p.381-402.

Garvie, O.G. and Robinson, D.N., 1982: The mineralogy structure and mode of formation of kelyphite and associated sub-kelyphitic surfaces on pyrope from kimberlite. Terra Cognita, v.2, p.229-230.

Griffin, W.L. and O'Reilly, S.Y., 1987: The composition of the lower crust and the nature of the continental Moho - xenolith evidence. In: Nixon, P.H., (ed.), Mantle Xenoliths, John Wiley & Sons, Chichister-New York-Brisbane-Toronto-Singapore, p.413-430.

Griffin, W.L., Carswell, C.A. and Nixon, P.H., 1979: Lower-crustal granulites and eclogites from northern Lesotho, southern Africa. In. Boyd, F.R. and Meyer, H.O.H. (ed's), Inclusions in Kimberlites and Other Volcanics, AGU, Washington, p.59-86.

Griffin, W.L., Wass, S.Y. and Hollis, J.D., 1984: Ultramafic xenoliths from Bullenmerri and Gnotuk Maars, Australia: Petrology of a subcontinent crust-mantle transition. Journ. of Petrol. v.25, p.53-87.

Grütter, H.S., 1987a: Summary report of the Philipstown Hanover kimberlite province, R.S.A. Internal report, DeBeers Consol. Mines Ltd., Kimberlite Petrology Unit.

Grütter, H.S., 1987b: Petrography of the Abrahamskraal kimberlite, R.S.A.. Internal report, DeBeers Consol. Mines Ltd., Kimberlite Petrology Unit.

Grütter, H.S. and Robey, J., 1988: Lower-crustal xenoliths and garnets from the Cape Province kimberlites. Geobulletin, v.31, No.1, p.34.

Gurney, J.J., 1989: Diamonds. In: Kimberlites and Related Rocks, vol. II, Geol. Soc. Aust. Spec. Publ. No. 14, Blackwell Scientific Publications, p.935-965.

Gurney, J.J. and Harte, B., 1980: chemical variations in uppermantle nodules from southern African kimberlites. Phil. Trans. Roy. Soc. London, v.a297, p.273-293.

Gurney, J.J, Dawson, J.B., Harte, B. and Lawless, P.J., 1975: The bulk chemical composition of peridotite facies rocks from the matsoku and Bultfontein pipes. Kimb. Symp. Cambridge 1975, Ext. Abstr., p.3-5.

Hales, A.L. and Sacks, I.S., 1959: Evidence for an intermediate layer from crustal seismic studies in the Eastern Transvaal, Geophys. Journ. Roy. Astr. Soc., v.2, p.15-33.

Harley, S.L., 1984: an experimental study of the partioning of Fe and Mg between garnet and orthopyroxene. Contr. Min. Petr., v.86, p. 359-373.

Harte, B., 1977: Rock nomenclature with particular reference to deformation and recrystallization textures in olivine bearing xenoliths. Journ. Geol., v.85, p.279-288.

Harte, B., 1983: Mantle peridotites and processes - the kimberlite sample. In: Hawkesworth, C.J. and Norry, M., (ed's), Continental Basalts and Mantle Xenoliths, Shiva, Nantwich, p.46-91.

Harte, B., 1987: Metasomatic events recorded in the mantle: an overview. In: Nixon, P.H., (ed.), Mantle Xenoliths, John Wiley & Sons, Chichister-New York-Brisbane-Toronto-Singapore, p. 625-640.

Harte, B and Gurney, J.J., 1982: Compositional and textural features of peridotite nodules from the Jagersfontein kimberlite pipe, South Africa. Terra Cognita, v.2, p.256-257.

Harte, B. and Hawkesworth, C.J., 1989: Mantle domains and mantle xenoliths. In: Kimberlites and Related Rocks, vol. II, Geol. Soc. Aust. Spec. Publ. No. 14, Blackwell Scientific Publications, p.649-686.

Harte, B., Jackson, P.M. and Macintyre, R.M., 1981: Age of mineral equilibria in granulite facies nodules from kimberlites. Nature, v.291, p.147-148.

Harte, B., Winterburn, P.A. and Gurney, J.J., 1987: Metasomatic and enrichment phenomena in garnet peridotite facies xenoliths from the Matsoku kimberlite pipe, Lesotho. In: Menzies, M.A. and Hawkesworth, C.J., (ed's), Mantle Metasomatism, Academic Press, p.145-220.

Hatton, C.J. and Gurney, J.J., 1977: Igneous fractionation trends in Roberts Victor eclogites. 2nd Int. Kimb. Conf., Santa Fe, Ext. Abstr.

Hatton, C.J. and Gurney, J.J., 1987: Roberts Victor eclogites and their relation to the mantle. In: Nixon, P.H., (ed.), Mantle Xenoliths, John Wiley & Sons, Chichister-New York-Brisbane-Toronto-Singapore, p.453-463.

Hawkesworth, C.J., Erlank, A.J., Marsh, J.S., Menzies, M.A. and Van Calsteren, P., 1983: Evolution of the continental lithosphere: Evidence from volcanics and xenoliths in southern Africa. In: Hawkesworth, C.J. and Norry, M., (ed's), Continental Basalts and Mantle Xenoliths, Shiva, Nantwich, p.111-138.

Helmstaedt, H. and Doig., R., 1975: Eclogite nodules from kimberlites of the Colarado Plateau - samples of subducted Franciscan-type oceanic lithosphere. Phys. Chem. Earth, v.9, p.95-111.

Jessop, A.M. and Lewis, T., 1978: Heat flow and heat generation in the Superior province of the Canadian shield. Tectonophysics, v.38, p.119-136.

Jones, M.Q.W., 1984: Heat flow and heat production studies in the Namaqua mobile belt and the Kaapvaal craton. PhD thesis, Univ. of the Witwatersrand, 319p.

Jones, M.Q.W., 1987: Heat flow and heat production in the Namaqua mobile belt, South Africa. Journ. Geophys. Res., v.92, p.6273-6289.

Jordan, T.H., 1978: Composition and development of the continental lithosphere. Nature, v.274, p.544-548.

Kennedy, C.S. and Kennedy, G.C., 1976: The equilibrium boundary between graphite and diamond. Journ Geophys Res., v.81, p.2467-2470.

Klinkert, P.S., 1982: Preliminary aeromagnetic interpretation of the Colesburg and Middelburg areas. Anglo American Corporation, Geophysical Unit report.

MacGregor, I.D., 1974: The system MgO - Al_2O_3 - SiO_2: Solubility of Al_2O_3 in enstatite for spinel and garnet peridotite compositions. Amer. Min., v.59, p.110-119.

MacGregor, I.D. and Carter, J.L., 1970: The chemistry of clinopyroxenes and garnets of eclogites and peridotite xenoliths from the Roberts Victor mine, South Africa. Phys. Earth Planet. Inter., v.3, p.391-397.

MacGregor, I.D. and Manton, W.I., 1986: Roberts Victor eclogites: ancient oceanic crust. Journ. Geophys. Res., v.91, p.14063-14079.

McLennan, S.M. and Taylor, S.R., 1982: Geochemical constraints on the growth of the continental crust. Journ. Geol., v.90, p.342-361.

Menzies, M.A., 1983: Mantle ultramafic xenoliths in alkaline magmas: Evidence for mantle heterogeneity modified by magmatic activity. In: Hawkesworth, C.J. and Norry, M.J. (ed's), Continental Basalts and Mantle Xenoliths, Shiva, Nantwich, Cheshire, p.111-138.

Mitchel, R.H., 1984: Garnet lherzolite from the Hanaus-1 and Louwrencia Kimberlites of Namibia. Contr. Min. Petr., v.86, p.178-188.

Nickel, K.G., 1989: Garnet-pyroxene equilibria in the system SMACCR (SiO_2-MgO-Al_2O_3-CaO Cr_2O_3) the Cr-geobarometer. In: Kimberlites and Related Rocks, vol. II, Geol. Soc. Aust. Spec. Publ. No. 14, Blackwell Scientific Publications, p.901-912.

Nickel, K.G. and Green, D.H., 1985: Empirical geothermobarometry for garnet peridotites and implications for the nature of the lithosphere, kimberlites and diamonds. Earth Planet. Sci. Lett., v.73, p.158-170.

Nixon, P.H. and Boyd, F.R., 1973a: Petrogenesis of granular and sheared ultrabasic nodule suite in kimberlites. In: Nixon, P.H., (ed), Lesotho Kimberlites, Lesotho National development Corporation, Maseru, p.48-56.

Nixon, P.H. and Boyd, F.R., 1973b: Deep seated nodules. In: Nixon, P.H., (ed), Lesotho Kimberlites, Lesotho National Development Corporation, Maseru, p.106-109.

Nixon, P.H., Boyd, F.R. and Boullier, A.M., 1973: The evidence of kimberlite and its inclusions on the constitution of the outer part of the Earth. In: Nixon, P.H., (ed.), Mantle Xenoliths, John Wiley & Sons, Chichister-New York-Brisbane-Toronto-Singapore, p.312-318.

Nixon, P.H., 1987: Kimberlite xenoliths and their cratonic setting. In: Nixon, P.H., (ed.), Mantle Xenoliths, John Wiley & Sons, Chichister-New York-Brisbane-Toronto-Singapore, p.215-239.

O'Neill, H.St.C., 1981: The transition between spinel lherzolite and garnet lherzolite, and its use as a geobarometer. Contr. Min. Petr., v.77, p.185-194

O'Neill, H.St.C. and Wood, B.J., 1979: An experimental study of Fe-Mg partitioning between garnet and olivine and its calibration as a geothermometer. Contr. Min. Petr., v.70, p.59-70.

O'Neill, H.St.C. and Wood, B.J., 1980: An experimental study of Fe-Mg partitioning between garnet and olivine and its calibration as a geothermometer: Corrections. Contr. Min. Petr., v.72, p. 337.

Pollack, H.N. and Chapman, D.S., 1977: On the regional variation of heat flow, geotherms, and lithospheric thickness. Tectonophysics, v.38, p.279-298.

Pollack, H.N., 1986: Cratonisation and thermal evolution of the mantle. Earth and Planet. Sci. Lett., v.80, p.172-182.

Reid, A.M. and Dawson, J.B., 1972: Olivine-garnet reaction in peridotites from Tanzania. Lithos, v.5, p.115-124.

Richardson, S.H., Gurney, J.J., Erlank, A.J. and Harris, J.W., 1984: Origin of diamonds in old enriched mantle. Nature, v.310, p.198-202.

Robey, J.vA., 1981: Kimberlites of the central Cape Province, R.S.A. Unpubl. PhD thesis, Univ. Cape Town.

Rogers, N.W. and Hawkesworth, C.J., 1982: Proterozoic age and cumulate origin for granulite xenoliths, Lesotho. Nature, v.299, p.409-413.

Ryburn, R.J., Raheim, A. and Green, D.H., 1975: Determination of the P, T paths of natural eclogites during metamorphism - record of subduction. Lithos., v.9, p.161-164.

Sass, J.H. and Lachenbruch, A.H., 1979: Thermal regime of the Australian continental crust. In: McElhinny, M.W. (ed.), The Earth, It's Origin, Structure and Evolution. Academic Press, London, p.301-351.

Shee, S.R., 1978: The mineral chemistry of xenoliths from the Orapa kimberlite, Botswana. Unpubl. PhD thesis, Univ. of Cape Town, 148p.

Skinner, C.P., 1989: The petrology of peridotite xenoliths from the Finsch mine South Africa. Journ. Geol. Soc. S.Afr., v.92, p.197-206.

Sobolev, N.V., Laurent'ev, Yu G., Pokhilenko, N.P. and Usova, L.V., 1973: Chrome-rich garnets from the kimberlites of Yakutia and their parageneses. Contr. Min. Petr. v.40, p.39-52.

Switzer, G. and Melson, W.G., 1969: Partially melted kyanite eclogite from Roberts Victor mine, South Africa. Smithsonian Contr. to Earth Sci., v.1, p.1-9.

Vitorello, I. and Pollack, H.N., 1980: On the variation of continental heat flow with age and the thermal evolution of continents. Journ. Geophys. Res., v.85, p.983-995.

Wells, P.R.A., 1977: Pyroxene thermometry in simple and complex systems. Contr. Min. Petr., v.62, p.129-139.

White, A.J.R., 1964: Clinopyroxenes from eclogites and basic granulites. Amer. Min., v.49, p.883-886.

Wood, B.J. and Banno, S., 1973: Garnet-orthopyroxene and orthopyroxene-clinopyroxene relationships in simple and complex systems. Contr. Min. Petr., v.42, p. 109-124.

Wyllie, P.J., 1980: The origin of kimberlite. Journ. Geophys. Res., v.85, p.6902-6910.

Wyllie, P.J., 1989: The genesis of kimberlites and some low-SiO_2 high-alkali magmas. In:Kimberlites and Related Rocks, vol. I, Geol. Soc. Aust. Spec. Publ. No. 14, Blackwell Scientific Publications, p.603-615.

ABBREVIATIONS USED IN THE FOLLOWING APPENDICES

MINERALS

Ab - Albite
Am - Amphibole
Ca - Carbonate
Cht - Chromite
Co - Corundum
Cpx - Clinopyroxene
Gt - Garnet
KR - K-Richterite
Ky - Kyanite
Opx - Orthopyroxene
Ol - Olivine
Ru - Rutile
Ph^1 - Phlogopite - coarse grained (primary metasomatic)
Ph^2 - Phlogopite - fine grained (secondary)
Sp - Spinel
Su - Sulphide
TiM - Titanomagnetite/Magnetite

ROCK TYPES

AGP - Altered garnet pyroxenite
CP - Clinopyroxenite
CPX - Clinopyroxene megacryst
D - Dunite
E - Eclogite
GD - Garnet dunite
GH - Garnet harzburgite
GL - Garnet lherzolite
GOP - Garnet orthopyroxenite
GW - Garnet websterite
H - Harzburgite
KE - Kyanite eclogite

avg. - average

APPENDIX 1: MINERAL ASSEMBLAGES

SAMPLE	ROCK TYPE	PRIMARY MINERALS	SECONDARY MINERALS*	TEXTURE**
18	GD	Ol, Cht, (Gt)	KR, Ph^1	fine grained
19A	D	Ol, Cht	Ph^1	fine grained
19B	D	Ol, Cht	KR, Ph^1	fine grained
19C	D	Ol, Cht	Ph^1, Cpx	fine grained
70	GW	Opx, Gt, Cpx, (Ru)	-	well equilibrated
71	D	Ol, Cht	-	coarse grained
72	GW	Opx, Gt, Cpx, TiM	-	poorly equilibrated
73	H	Ol, Opx, Cht	(Am), (Sp), (Ph^2)	coarse
99	D	Ol, Cht	Ph^1	fine grained
107	D	Ol, Cht	Ph^1, Cpx	coarse grained
142	GL	Ol, Opx, Gt, Cpx	(Ph^2)	coarse
143	GH	Opx, Ol, Gt, (Cht)	(Ph^2), (Cpx)	coarse
144	GH	Ol, Opx, Gt	Cpx, (Ph^2), (Sp)	coarse
145	GH	Opx, Gt, Ol	(Ph^2)	coarse
147	GOP	Opx, Gt, (TiM), (Ru)	-	well equilibrated
148	H	Ol, Opx	Ph^1, Cpx, Cht	coarse
149	GH	Ol, Opx, Gt	(Ph^2)	coarse
154	GH	Opx, Ol, Gt	(Ph^2), (Am)	coarse
156	GL	Ol, Opx, Gt, Cht, (Cpx)	-	coarse
158	H	Ol, Opx	Ph^1, Cpx, Cht	coarse
160	AGP	Cpx, Gt	Ph^2, (Sp), (Ca)	well equilibrated
167	E	Cpx, Gt, (Ru)	Ph^2, (Am), (Sp)	coarse grained
178	E	Gt, Cpx, (Ru), (Co)	Ab, (Su), (Sp)	coarse grained
187	GOP	Opx, Gt, TiM, (Ru), (Su)	-	well equilibrated
197	GW	Opx, Gt, Cpx, TiM	(Ph^1)	intermediate equil.
217	CPX	Cpx, (Gt), (Opx)	-	-
229	E	Gt, Cpx, (Ru), (Su)	(Sp), (Ca)	fine grained
255	KE	Gt, Ky, Ru	-	-
256	GW	Opx, Cpx, Gt, (Ru)	-	poorly equilibrated
257	GW	Opx, Cpx, Gt, TiM, (Ru),(Su)	(Ph^2)	intermediate equil.
258	GD	Ol, Cht, (Gt)	-	coarse grained
259	GW	Opx, Gt, Cpx, (Ru), (Su)	-	poorly equilibrated
260	AGP	Cpx, Gt, (Cht), (Su)	(Ph^2), (Ca)	well equilibrated
261	H	Ol, Opx	Ph^1, Cpx, Cht	
262	GOP	Opx, Gt, (Ru)	-	well equilibrated
263	D	Ol, Cht	Ph^1, Cpx	fine grained
264	GW	Opx, TiM, Gt, Cpx	Am, (Ph^2)	poorly equilibrated
265	D	Ol, (Cpx), (Su)	-	coarse grained
266	CP	Cpx, Cht	Am	well equilibrated
267	D	Ol, Cht	Ph^1, Cpx	coarse grained
268	E	Cpx, Gt, (Cht)	Ph^1, Am, (Cpx)	coarse grained
269	E	Cpx, Gt	(Ca)	coarse grained
270	E	Gt, Cpx	Ph^1, Am, (Ca)	coarse grained

Notes: * - "secondary minerals" exclude kelyphite and other fine grained alteration products.
** - for explanation of textural terms see section 3.
- minerals in brackets occur in trace amounts.

APPENDIX 1 CONTINUED:

SAMPLE	ROCK TYPE	PRIMARY MINERALS	SECONDARY MINERALS*	TEXTURE**
271	E	Cpx, Gt, (Ru)	(Ph^2), (Sp), (Cpx)	coarse grained
272	E	Cpx, GT, Ru	(Ph^2), (Sp)	coarse grained
273	AGP	Cpx, Gt, (Ru)	Ph^1, (Ph^2)	coarse grained
274	GW	Cpx, Opx, Gt, Cht	(Ph^2)	well equilibrated
275	E	Cpx, Gt	Am, (Ph^2)	coarse grained
280	GW	Opx, Cpx, Gt, (Ru)	Ph^1, Am	well equilibrated
283	GW	Opx, Gt, TiM, Ol, Cpx, (Ru)	Am	intermediate equil.
284	E	Gt, Cpx, (Ru), (TiM)	-	fine grained

Notes: * - "secondary minerals" exclude kelyphite and other fine grained alteration products.
** - for explanation of textural terms see section 3.
- minerals in brackets occur in trace amounts.

APPENDIX 2: MODAL COMPOSITIONS

SAMPLE	PRIMARY MINERALS								SECONDARY MINERALS					
	Gt	Opx	Cpx	Ol	Cht	TiM	Ru	Su	Ph[1]	Ph[2]	Am	Sp	Cpx	Ca
Garnet Lherzolites														
142	5	43	1	51						Tr				
156	2	13	Tr	84	1									
Garnet Harzburgites														
143	4	52		43	Tr					Tr	Tr	Tr	Tr	
144	6	35		58						Tr		Tr	1	
145	(5)	(90)		(5)						Tr				
149	3	20		77						Tr				
154	(1)	(50)		(49)	Tr					Tr	Tr			
Harzburgites														
73		2		94	4					Tr	Tr	Tr		
148		33		60	1				3			1	3	
158		Tr		50					Tr			Tr	Tr	
261		11		82					5			Tr	2	
Garnet Pyroxenites														
70	(10)	(80)	(10)											
72	8	77	7			8								
160	15	-	75							Tr		Tr		Tr
197	33	59	7			1			Tr					
256	13	60	23											
257	10	50	34			4				Tr				
259	16	70	9			2	(1)	Tr						
260	(10)	-	(80)							Tr				Tr
264	(5)	(80)	(5)			(10)				Tr	Tr			
273	(33)		(62)				Tr		Tr	Tr				
274	11	19	64		1					Tr				
280	18	56	19					Tr	4		2			
283	23	63	2	4		6					1			
Garnet Orthopyroxenites														
147	19	72												
187	14	85				1								
262	26	74												

Notes: - modes given in brackets are visual estimates.
- all other modes were estimated by point counting (800 to 1100 points).
- kelyphite counted as garnet.
- serpentine after olivine counted as olivine.
- where values do not sum to 100 %, balance is made up by other fine-grained alteration products.

APPENDIX 2 CONTINUED:

SAMPLE	PRIMARY MINERALS								SECONDARY MINERALS					
	Gt	Opx	Cpx	Ol	Cht	TiM	Ru	Su	Ph^1	Ph^2	Am	Sp	Cpx	Ca
Eclogites														
167	41		57				Tr			Tr	Tr	Tr		
229	(48)		(47)				Tr	Tr				Tr		Tr
268	(25)		(5)		Tr				Tr		Tr		Tr	
269	44		45											Tr
270	59		34						Tr		Tr			Tr
271	(30)		(65)				Tr		Tr	Tr		Tr	Tr	
272	(24)		(70)				1			Tr		Tr		
275	(30)		(60)							Tr	Tr			

Notes: - modes given in brackets are visual estimates.
- all other modes were estimated by point counting (800 to 1100 points).
- kelyphite counted as garnet.
- serpentine after olivine counted as olivine.
- where values do not sum to 100 %, balance is made up by other fine-grained alteration products.

APPENDIX 3: MINERAL COMPOSITION DATA

APPENDIX 3A: GARNET COMPOSITIONS

SAMPLE	(142)		(156)	(143)		(144)		(145)		(149)	(154)	
ROCK TYPE	GL		GL	GH		GH		GH		GH	GH	
	Core	Rim^{opx}	Core	Core	Rim^{opx}	Core	Rim^{avg}	Core	Rim^{avg}	Core	Core	Rim^{opx}
n	9	7	10	9	3	10	13	14	17	16	7	6
SiO2	41.73	41.93	41.98	42.41	42.43	42.03	41.89	41.35	41.45	41.66	42.01	42.01
TiO2	0.02	0.04	0.00	0.00	0.00	0.08	0.09	0.01	0.03	0.02	0.01	0.01
Al2O3	20.16	19.67	22.25	22.13	22.14	20.87	20.86	19.96	19.92	20.19	21.95	21.81
Cr2O3	5.10	5.10	2.16	2.51	2.41	4.13	3.89	4.86	5.02	4.85	2.74	2.78
FeO	6.28	6.47	7.68	6.76	6.88	6.18	6.25	6.04	5.99	6.26	6.68	6.58
MnO	0.36	0.38	0.50	0.45	0.47	0.32	0.33	0.29	0.32	0.33	0.45	0.44
NiO	0.00	0.01	0.01	0.00	0.00	0.02	0.01	0.01	0.03	0.00	0.02	0.01
MgO	21.38	21.97	20.19	20.29	20.17	21.82	22.04	21.32	21.22	20.81	22.50	22.86
CaO	4.94	4.62	5.33	5.42	5.36	4.65	4.51	5.71	5.75	5.65	3.52	3.50
Na2O	0.04	0.03	0.02	0.01	0.01	0.04	0.05	0.01	0.01	0.02	0.04	0.03
TOTAL	100.01	100.22	100.12	99.99	99.85	100.14	99.91	99.56	99.74	99.79	99.91	100.02
Si	2.982	2.991	2.989	3.011	3.016	2.985	2.981	2.972	2.975	2.986	2.976	2.972
Ti	0.001	0.002	0.000	0.000	0.000	0.004	0.005	0.001	0.001	0.001	0.001	0.000
Al	1.698	1.654	1.867	1.852	1.855	1.747	1.750	1.690	1.685	1.706	1.832	1.818
Cr	0.288	0.288	0.121	0.141	0.135	0.232	0.219	0.276	0.285	0.275	0.154	0.155
Fe	0.375	0.386	0.457	0.401	0.409	0.367	0.372	0.363	0.360	0.375	0.395	0.389
Mn	0.022	0.023	0.030	0.027	0.028	0.020	0.020	0.018	0.019	0.020	0.027	0.026
Ni	0.000	0.001	0.001	0.000	0.000	0.001	0.001	0.001	0.002	0.000	0.001	0.000
Mg	2.277	2.336	2.143	2.148	2.137	2.310	2.338	2.285	2.270	2.224	2.375	2.411
Ca	0.378	0.353	0.406	0.412	0.408	0.354	0.344	0.439	0.442	0.434	0.267	0.265
Na	0.005	0.004	0.003	0.001	0.001	0.005	0.006	0.001	0.002	0.003	0.005	0.005
TOTAL	8.027	8.038	8.018	7.993	7.989	8.024	8.033	8.045	8.040	8.024	8.033	8.043
Ca/Ca+Mg+Fe	0.124	0.114	0.134	0.138	0.137	0.116	0.112	0.141	0.143	0.142	0.087	0.086
Mg/Ca+Mg+Fe	0.746	0.754	0.706	0.719	0.717	0.757	0.761	0.736	0.734	0.728	0.775	0.780
Fe/Ca+Mg+Fe	0.123	0.125	0.150	0.134	0.137	0.120	0.121	0.117	0.116	0.123	0.129	0.126

SAMPLE	(72)	(197)	(256)		(257)		(259)		(264)		(274)
ROCK TYPE	GW	GW	GW		GW		GW		GW		GW
	Core	Core	Core	Rim^{avg}	Core	Rim^{avg}	Core	Rim^{avg}	Core	Rim^{avg}	Core
n	8	13	13	10	14	10	9	13	19	7	10
SiO2	41.39	39.62	40.20	40.03	39.63	39.36	40.56	40.62	41.60	41.60	41.02
TiO2	0.04	0.05	0.02	0.02	0.06	0.05	0.02	0.01	0.04	0.04	0.03
Al2O3	22.64	21.63	21.77	21.86	21.61	21.63	22.26	22.34	22.67	22.84	21.78
Cr2O3	0.26	0.35	0.92	0.96	0.46	0.48	0.71	0.72	0.32	0.31	1.86
FeO	12.12	19.35	18.02	17.93	20.19	20.31	16.60	16.37	11.36	11.48	10.72
MnO	0.72	0.89	0.57	0.55	0.86	0.84	0.56	0.53	0.71	0.72	0.55
NiO	0.01	0.02	0.03	0.01	0.00	0.01	0.00	0.00	0.01	0.01	0.02
MgO	17.09	12.41	12.61	12.54	11.56	11.48	14.28	14.40	17.49	17.54	17.68
CaO	5.48	5.08	5.55	5.51	5.29	5.32	4.89	4.89	5.61	5.64	5.90
Na2O	0.02	0.04	0.00	0.01	0.01	0.02	0.01	0.01	0.01	0.00	0.01
TOTAL	99.76	99.45	99.69	99.42	99.67	99.49	99.91	99.91	99.82	100.10	99.57
Si	3.005	2.992	3.009	3.003	2.998	2.987	3.000	3.000	3.008	3.000	2.985
Ti	0.002	0.003	0.001	0.001	0.003	0.003	0.001	0.000	0.002	0.002	0.002
Al	1.937	1.925	1.921	1.933	1.927	1.934	1.940	1.954	1.933	1.941	1.867
Cr	0.015	0.021	0.054	0.057	0.028	0.029	0.042	0.042	0.018	0.018	0.107
Fe	0.736	1.222	1.128	1.125	1.277	1.289	1.026	1.011	0.687	0.692	0.652
Mn	0.044	0.057	0.036	0.035	0.055	0.054	0.035	0.033	0.043	0.044	0.034
Ni	0.000	0.001	0.002	0.001	0.000	0.001	0.000	0.000	0.001	0.001	0.001
Mg	1.850	1.397	1.407	1.402	1.304	1.299	1.574	1.586	1.886	1.886	1.918
Ca	0.426	0.411	0.445	0.443	0.429	0.433	0.388	0.387	0.435	0.436	0.460
Na	0.002	0.005	0.000	0.001	0.002	0.002	0.002	0.002	0.001	0.000	0.001
TOTAL	8.018	8.035	8.003	8.002	8.022	8.030	8.009	8.007	8.014	8.019	8.027
Ca/Ca+Mg+Fe	0.139	0.133	0.147	0.147	0.140	0.141	0.128	0.128	0.143	0.143	0.150
Mg/Ca+Mg+Fe	0.605	0.453	0.467	0.467	0.425	0.422	0.521	0.526	0.618	0.617	0.626
Fe/Ca+Mg+Fe	0.241	0.396	0.374	0.374	0.417	0.419	0.339	0.335	0.225	0.226	0.213

- Cations calculated on the basis of 12 oxygens.
- Superscripts on rim compositions denote the minerals adjacent to which the analyses were taken.

APPENDIX 3A CONTINUED: GARNET COMPOSITIONS

SAMPLE	(280)		(283)		(160)	(260)		(273)		(147)	(187)	
ROCK TYPE	GW		GW		AGP	AGP		AGP		GOP	GOP	
	Core	Rim^{opx}	Core	Rim^{opx}	Core	Core	Rim^{cpx}	Core	Rim^{cpx}	Core	Core	Rim^{op}
n	17	19	14	11	9	9	11	12	9	7	10	11
SiO2	39.74	39.96	41.02	41.09	40.73	41.08	41.15	40.73	40.88	39.33	39.03	39.19
TiO2	0.04	0.03	0.05	0.06	0.04	0.05	0.04	0.05	0.02	0.02	0.04	0.04
Al2O3	21.94	21.75	22.66	22.65	21.54	21.59	21.57	22.12	22.36	21.22	21.32	21.38
Cr2O3	0.67	0.66	0.24	0.24	1.41	1.92	1.89	0.48	0.43	0.40	0.64	0.65
FeO	19.41	19.16	11.68	11.67	12.16	12.34	12.39	13.93	13.79	22.97	22.07	22.08
MnO	0.58	0.59	0.69	0.70	0.46	0.56	0.57	0.39	0.40	0.69	0.76	0.75
NiO	0.01	0.00	0.01	0.01	0.00	0.01	0.02	0.00	0.00	0.00	0.01	0.02
MgO	12.74	12.59	18.07	17.84	17.14	15.96	15.77	14.84	14.88	9.98	10.36	10.27
CaO	4.97	4.95	5.53	5.54	5.69	6.33	6.13	7.04	7.01	5.06	5.54	5.60
Na2O	0.02	0.01	0.00	0.01	0.02	0.01	0.01	0.02	0.01	0.02	0.02	0.02
TOTAL	100.12	99.69	99.92	99.81	99.18	99.84	99.55	99.59	99.77	99.68	99.78	99.99
Si	2.977	3.001	2.971	2.979	2.990	3.005	3.02	3.001	3.00	3.011	2.982	2.987
Ti	0.002	0.001	0.003	0.003	0.002	0.003	0.00	0.003	0.00	0.001	0.002	0.002
Al	1.937	1.925	1.934	1.935	1.863	1.861	1.86	1.920	1.94	1.914	1.920	1.920
Cr	0.039	0.039	0.014	0.014	0.082	0.111	0.11	0.028	0.02	0.024	0.038	0.039
Fe	1.216	1.203	0.707	0.708	0.746	0.755	0.76	0.858	0.85	1.470	1.410	1.408
Mn	0.037	0.037	0.042	0.043	0.028	0.035	0.04	0.024	0.02	0.045	0.049	0.048
Ni	0.001	0.000	0.000	0.001	0.000	0.000	0.00	0.000	0.00	0.000	0.001	0.001
Mg	1.423	1.409	1.951	1.929	1.875	1.740	1.72	1.630	1.63	1.139	1.180	1.167
Ca	0.399	0.398	0.429	0.430	0.448	0.496	0.48	0.556	0.55	0.415	0.454	0.457
Na	0.003	0.002	0.000	0.002	0.003	0.001	0.00	0.002	0.00	0.003	0.002	0.003
TOTAL	8.034	8.017	8.052	8.044	8.037	8.007	8.00	8.023	8.02	8.021	8.038	8.032
Ca/Ca+Mg+Fe	0.130	0.131	0.137	0.138	0.145	0.164	0.16	0.181	0.18	0.135	0.147	0.148
Mg/Ca+Mg+Fe	0.463	0.462	0.623	0.620	0.605	0.575	0.57	0.531	0.53	0.371	0.381	0.379
Fe/Ca+Mg+Fe	0.395	0.395	0.226	0.228	0.241	0.250	0.25	0.280	0.28	0.479	0.456	0.457

SAMPLE	(262)		(178)		(229)		(268)		(269)		(270)	
ROCK TYPE	GOP		E		E		E		E		E	
	Core	Rim^{opx}	Core	Rim^{cpx}	Core	Rim^{cpx}	Core	Rim^{cpx}	Core	Rim^{cpx}	Core	Rim^{cp}
n	11	9	8	4	9	13	9	7	11	11	11	9
SiO2	40.05	40.38	40.17	40.08	41.60	41.28	40.54	40.52	41.05	41.29	41.37	41.36
TiO2	0.06	0.05	0.07	0.06	0.01	0.00	0.02	0.01	0.05	0.04	0.03	0.04
Al2O3	21.41	21.38	22.36	22.25	23.25	23.22	22.61	22.61	23.17	23.00	23.15	23.12
Cr2O3	1.30	1.43	0.11	0.05	0.19	0.19	0.16	0.13	0.04	0.05	0.06	0.05
FeO	19.24	18.88	13.95	13.87	11.90	12.95	17.71	17.72	9.65	9.61	8.61	8.58
MnO	0.86	0.86	0.29	0.29	0.29	0.37	0.45	0.48	0.26	0.27	0.23	0.23
NiO	0.02	0.03	0.00	0.01	0.01	0.01	0.00	0.01	0.02	0.00	0.01	0.01
MgO	12.44	12.29	10.72	10.82	17.60	16.91	15.09	15.08	14.28	14.24	15.07	15.16
CaO	4.80	4.92	11.61	11.82	4.93	4.97	3.18	3.17	11.64	11.48	11.06	10.88
Na2O	0.01	0.01	0.03	0.02	0.01	0.03	0.04	0.03	0.01	0.02	0.01	0.01
TOTAL	100.21	100.23	99.32	99.28	99.79	99.94	99.79	99.75	100.18	100.01	99.59	99.44
Si	3.002	3.020	3.004	3.00	3.002	2.99	2.996	3.00	2.981	3.00	2.999	3.00
Ti	0.003	0.003	0.004	0.00	0.000	0.00	0.001	0.00	0.003	0.00	0.002	0.00
Al	1.891	1.884	1.970	1.96	1.978	1.98	1.969	1.97	1.982	1.97	1.978	1.98
Cr	0.077	0.085	0.007	0.00	0.011	0.01	0.009	0.01	0.002	0.00	0.003	0.00
Fe	1.206	1.180	0.872	0.87	0.718	0.79	1.094	1.10	0.586	0.58	0.522	0.52
Mn	0.055	0.054	0.019	0.02	0.018	0.02	0.028	0.03	0.016	0.02	0.014	0.01
Ni	0.001	0.002	0.000	0.00	0.001	0.00	0.000	0.00	0.001	0.00	0.000	0.00
Mg	1.390	1.370	1.195	1.21	1.893	1.83	1.662	1.66	1.546	1.54	1.629	1.64
Ca	0.385	0.394	0.930	0.95	0.381	0.39	0.252	0.25	0.906	0.89	0.859	0.85
Na	0.002	0.002	0.004	0.00	0.001	0.00	0.006	0.00	0.002	0.00	0.001	0.00
TOTAL	8.012	7.994	8.006	8.02	8.004	8.01	8.017	8.02	8.025	8.01	8.009	8.01
Ca/Ca+Mg+Fe	0.127	0.131	0.308	0.31	0.127	0.13	0.083	0.08	0.297	0.29	0.284	0.28
Mg/Ca+Mg+Fe	0.458	0.457	0.396	0.40	0.629	0.60	0.548	0.55	0.506	0.51	0.539	0.54
Fe/Ca+Mg+Fe	0.397	0.394	0.289	0.29	0.239	0.26	0.360	0.36	0.192	0.19	0.173	0.17

- Cations calculated on the basis of 12 oxygens.
- Superscripts on rim compositions denote the minerals adjacent to which the analyses were taken.

APPENDIX 3A CONTINUED: GARNET COMPOSITIONS

SAMPLE	(271)		(272)		(275)		(284)		(217)	(258)	
ROCK TYPE	E		E		E		E		CPX	GD	
	Core	Rim^{cpx}	Core	Rim^{cpx}	Core	Rim^{cpx}	Core	Rim^{cpx}	Core	Core	Rim^{cpx}
n	9	10	8	5	11	6	23	16	6	12	11
SiO2	40.30	40.30	40.00	40.04	40.21	39.92	40.74	40.78	42.32	42.08	42.12
TiO2	0.05	0.04	0.07	0.06	0.03	0.04	0.04	0.01	0.07	0.01	0.01
Al2O3	22.48	22.60	22.37	22.36	22.43	22.51	21.84	22.08	22.14	20.99	21.15
Cr2O3	0.07	0.08	0.07	0.07	0.08	0.08	0.16	0.14	1.82	3.74	3.64
FeO	13.49	13.60	13.80	13.55	19.56	19.30	17.91	17.60	6.70	7.52	7.45
MnO	0.28	0.28	0.31	0.29	0.50	0.49	0.47	0.48	0.37	0.50	0.50
NiO	0.01	0.01	0.01	0.01	0.01	0.02	0.01	0.01	0.01	0.00	0.01
MgO	10.77	10.75	10.86	10.88	13.74	13.68	14.57	14.58	21.07	19.10	19.16
CaO	11.97	12.08	11.79	11.80	3.33	3.38	3.92	3.92	4.99	6.23	6.15
Na2O	0.03	0.02	0.02	0.03	0.04	0.03	0.02	0.02	0.01	0.00	0.01
TOTAL	99.44	99.75	99.30	99.08	99.93	99.46	99.69	99.55	99.49	100.18	100.19
Si	3.005	3.00	2.993	3.00	2.995	2.99	3.024	3.03	3.010	3.013	3.013
Ti	0.003	0.00	0.004	0.00	0.002	0.00	0.002	0.00	0.004	0.000	0.000
Al	1.976	1.98	1.972	1.97	1.969	1.98	1.911	1.93	1.856	1.772	1.783
Cr	0.004	0.00	0.004	0.00	0.005	0.00	0.009	0.01	0.102	0.212	0.206
Fe	0.841	0.85	0.863	0.85	1.219	1.21	1.112	1.09	0.399	0.450	0.445
Mn	0.018	0.02	0.020	0.02	0.032	0.03	0.030	0.03	0.022	0.030	0.030
Ni	0.000	0.00	0.001	0.00	0.001	0.00	0.001	0.00	0.001	0.000	0.000
Mg	1.197	1.19	1.212	1.22	1.526	1.53	1.612	1.61	2.234	2.039	2.043
Ca	0.956	0.96	0.945	0.95	0.266	0.27	0.312	0.31	0.380	0.478	0.471
Na	0.004	0.00	0.003	0.00	0.006	0.00	0.003	0.00	0.002	0.001	0.001
TOTAL	8.004	8.01	8.017	8.01	8.019	8.02	8.015	8.01	8.009	7.995	7.993
Ca/Ca+Mg+Fe	0.317	0.32	0.311	0.31	0.087	0.09	0.102	0.10	0.125	0.159	0.158
Mg/Ca+Mg+Fe	0.397	0.39	0.399	0.40	0.502	0.50	0.526	0.53	0.736	0.680	0.683
Fe/Ca+Mg+Fe	0.279	0.28	0.284	0.28	0.401	0.40	0.363	0.36	0.131	0.150	0.149

SAMPLE	(255)	
ROCK TYPE	KE	
	Core	Rim^{cpx}
n	9	4
SiO2	39.72	39.68
TiO2	0.01	0.01
Al2O3	22.35	22.39
Cr2O3	0.03	0.02
FeO	25.66	25.63
MnO	0.43	0.43
NiO	0.00	0.00
MgO	11.21	11.28
CaO	0.73	0.73
Na2O	0.01	0.01
TOTAL	100.15	100.18
Si	3.011	3.006
Ti	0.000	0.000
Al	1.996	1.999
Cr	0.002	0.001
Fe	1.626	1.624
Mn	0.028	0.027
Ni	0.000	0.000
Mg	1.267	1.274
Ca	0.059	0.059
Na	0.002	0.002
TOTAL	7.991	7.994
Ca/Ca+Mg+Fe	0.020	0.020
Mg/Ca+Mg+Fe	0.425	0.427
Fe/Ca+Mg+Fe	0.546	0.544

- Cations calculated on the basis of 12 oxygens.
- Superscripts on rim compositions denote the minerals adjacent to which the analyses were taken.

APPENDIX 3B CONTINUED: ORTHOPYROXENE COMPOSITIONS

SAMPLE	(259)		(264)		(274)		(280)		(283)		(147)
ROCK TYPE	GW		GW		GW		GW		GW		GOP
	Core	Rim	Core	Rim	Core	Rim^{avg}	Core	Rim	Core	Rim	Core
n	9	10	14	5	8	9	17	11	13	14	4
SiO2	55.87	56.01	55.99	56.73	56.94	56.75	54.62	55.32	55.59	56.02	54.08
TiO2	0.01	0.01	0.04	0.03	0.05	0.05	0.02	0.02	0.04	0.02	0.02
Al2O3	1.06	0.84	2.47	1.78	0.91	0.90	1.71	1.28	2.14	1.56	0.88
Cr2O3	0.12	0.08	0.09	0.07	0.16	0.17	0.15	0.12	0.06	0.05	0.04
FeO	10.73	10.65	6.77	6.71	6.66	6.54	12.58	12.52	6.83	6.79	17.25
MnO	0.11	0.11	0.13	0.15	0.12	0.14	0.14	0.12	0.13	0.12	0.17
NiO	0.05	0.03	0.15	0.16	0.07	0.04	0.13	0.12	0.16	0.18	0.09
MgO	31.37	31.34	34.11	34.33	34.92	34.85	30.43	30.78	34.62	35.24	26.49
CaO	0.20	0.18	0.26	0.17	0.21	0.22	0.19	0.14	0.23	0.17	0.20
Na2O	0.03	0.03	0.01	0.00	0.01	0.00	0.03	0.03	0.01	0.01	0.04
TOTAL	99.56	99.28	100.03	100.14	100.04	99.66	100.00	100.44	99.82	100.17	99.25
Si	1.973	1.982	1.936	1.957	1.966	1.966	1.941	1.955	1.929	1.937	1.977
Ti	0.000	0.000	0.001	0.001	0.001	0.001	0.000	0.000	0.001	0.001	0.001
Al	0.044	0.035	0.101	0.072	0.037	0.037	0.072	0.053	0.088	0.063	0.038
Cr	0.003	0.002	0.003	0.002	0.004	0.005	0.004	0.003	0.002	0.001	0.001
Fe	0.317	0.315	0.196	0.194	0.192	0.189	0.374	0.370	0.198	0.196	0.527
Mn	0.003	0.003	0.004	0.004	0.004	0.004	0.004	0.003	0.004	0.004	0.005
Ni	0.002	0.001	0.004	0.004	0.002	0.001	0.004	0.003	0.004	0.005	0.003
Mg	1.651	1.653	1.758	1.765	1.797	1.800	1.612	1.622	1.791	1.816	1.443
Ca	0.008	0.007	0.010	0.006	0.008	0.008	0.007	0.005	0.009	0.006	0.008
Na	0.002	0.002	0.000	0.000	0.001	0.000	0.002	0.002	0.001	0.000	0.003
TOTAL	4.004	4.000	4.012	4.005	4.012	4.012	4.021	4.018	4.026	4.031	4.005
Mg/Mg+Fe	0.839	0.840	0.900	0.901	0.903	0.905	0.812	0.814	0.900	0.903	0.732
Fe/Mg+Fe	0.161	0.160	0.100	0.099	0.097	0.095	0.188	0.186	0.100	0.097	0.268

SAMPLE	(187)		(262)		(217)
ROCK TYPE	GOP		GOP		CPX
	Core	Rim	Core	Rim	Core
n	10	6	9	9	6
SiO2	54.52	54.64	55.42	55.45	58.07
TiO2	0.03	0.02	0.02	0.01	0.07
Al2O3	0.91	0.74	1.37	1.17	0.99
Cr2O3	0.09	0.08	0.34	0.28	0.22
FeO	16.20	16.56	13.06	13.01	3.93
MnO	0.20	0.20	0.17	0.17	0.08
NiO	0.04	0.03	0.27	0.26	0.10
MgO	27.53	27.40	29.11	29.28	36.48
CaO	0.24	0.23	0.15	0.14	0.24
Na2O	0.02	0.02	0.03	0.04	0.03
TOTAL	99.78	99.92	99.94	99.80	100.21
Si	1.972	1.977	1.973	1.976	1.976
Ti	0.001	0.001	0.001	0.000	0.002
Al	0.039	0.031	0.057	0.049	0.040
Cr	0.003	0.002	0.010	0.008	0.006
Fe	0.490	0.501	0.389	0.388	0.112
Mn	0.006	0.006	0.005	0.005	0.002
Ni	0.001	0.001	0.008	0.007	0.003
Mg	1.484	1.477	1.544	1.555	1.850
Ca	0.009	0.009	0.006	0.005	0.009
Na	0.002	0.002	0.002	0.003	0.002
TOTAL	4.007	4.007	3.994	3.997	4.001
Mg/Mg+Fe	0.752	0.747	0.799	0.800	0.943
Fe/Mg+Fe	0.248	0.253	0.201	0.200	0.057

- Cations calculated on the basis of 6 oxygens.
- Unless otherwise indicated rims were analysed adjacent to garnet grains.

APPENDIX 3C CONTINUED: CLINOPYROXENE COMPOSITIONS

SAMPLE	(273)		(178)	(229)		(268)		(269)		(270)	
ROCK TYPE	AGP		E	E		E		E		E	
	Core	Rim	Core	Core	Rim	Core	Rim	Core	Rim	Core	Rim
n	8	9	9	15	12	9	9	9	9	7	9
SiO2	53.56	53.20	54.00	53.42	53.41	54.86	54.90	53.69	53.25	53.31	53.36
TiO2	0.06	0.08	0.19	0.10	0.09	0.20	0.21	0.16	0.17	0.12	0.15
Al2O3	1.34	1.60	9.56	5.07	5.11	8.94	9.14	6.98	7.44	7.36	7.64
Cr2O3	0.14	0.14	0.09	0.26	0.27	0.29	0.28	0.04	0.05	0.07	0.07
FeO	3.02	3.03	2.38	1.98	2.14	4.23	4.25	1.50	1.64	1.29	1.31
MnO	0.06	0.07	0.02	0.02	0.03	0.07	0.05	0.02	0.01	0.01	0.02
NiO	0.04	0.03	0.02	0.03	0.01	0.01	0.01	0.04	0.07	0.03	0.04
MgO	17.02	16.97	11.32	14.65	14.61	10.90	10.84	13.80	13.40	13.65	13.50
CaO	23.96	23.77	18.11	21.75	21.78	13.97	13.81	20.51	20.74	21.09	20.98
Na2O	0.73	0.80	4.30	2.58	2.54	6.08	6.22	2.68	2.74	2.63	2.70
TOTAL	99.93	99.69	99.99	99.86	99.98	99.56	99.70	99.43	99.51	99.56	99.76
Si	1.958	1.95	1.93	1.935	1.93	1.972	1.97	1.935	1.92	1.921	1.920
Ti	0.002	0.00	0.01	0.003	0.00	0.005	0.01	0.004	0.00	0.003	0.000
Al	0.058	0.07	0.40	0.220	0.22	0.379	0.39	0.297	0.32	0.313	0.320
Cr	0.004	0.00	0.00	0.010	0.01	0.008	0.01	0.001	0.00	0.002	0.000
Fe	0.092	0.09	0.07	0.060	0.06	0.127	0.13	0.045	0.05	0.039	0.040
Mn	0.002	0.00	0.00	0.001	0.00	0.002	0.00	0.001	0.00	0.000	0.000
Ni	0.001	0.00	0.00	0.001	0.00	0.000	0.00	0.001	0.00	0.001	0.000
Mg	0.928	0.93	0.60	0.791	0.79	0.584	0.58	0.741	0.72	0.733	0.720
Ca	0.939	0.93	0.69	0.844	0.85	0.538	0.53	0.792	0.80	0.814	0.810
Na	0.052	0.06	0.30	0.181	0.18	0.424	0.43	0.187	0.19	0.184	0.190
TOTAL	4.035	4.04	4.01	4.040	4.04	4.041	4.04	4.005	4.01	4.010	4.010
Mg/Mg+Fe	0.909	0.91	0.89	0.929	0.92	0.821	0.82	0.943	0.94	0.950	0.950
Fe/Mg+Fe	0.091	0.09	0.11	0.071	0.08	0.179	0.18	0.057	0.06	0.050	0.050
Ca/Ca+Mg+Fe	0.479	0.477	0.51	0.498	0.50	0.431	0.43	0.502	0.51	0.513	0.516

SAMPLE	(271)		(272)		(275)		(284)		(266)	(217)
ROCK TYPE	E		E		E		E		CP	CPX
	Core	Rim	Core	Rim	Core	Rim	Core	Rim	Core	Core
n	9	9	11	6	12	8	11	10	4	10
SiO2	53.59	53.29	53.57	53.65	54.74	54.83	54.41	54.58	54.47	54.06
TiO2	0.17	0.21	0.19	0.20	0.22	0.24	0.34	0.27	0.04	0.18
Al2O3	9.61	9.85	9.90	9.93	8.63	8.66	7.34	7.35	1.09	2.05
Cr2O3	0.07	0.08	0.06	0.06	0.14	0.13	0.26	0.27	0.44	1.04
FeO	2.37	2.32	2.17	2.18	4.96	4.96	3.31	3.28	1.94	1.31
MnO	0.02	0.02	0.02	0.03	0.06	0.07	0.03	0.04	0.10	0.06
NiO	0.03	0.03	0.02	0.01	0.00	0.00	0.01	0.01	0.04	0.06
MgO	11.29	11.26	11.18	11.17	10.71	10.63	12.06	11.97	17.96	17.06
CaO	18.04	18.04	17.83	17.86	14.06	14.09	17.25	17.36	24.47	22.94
Na2O	4.39	4.43	4.52	4.47	5.89	5.89	4.57	4.62	0.59	1.16
TOTAL	99.59	99.53	99.46	99.56	99.42	99.50	99.57	99.76	101.14	99.91
Si	1.926	1.92	1.925	1.93	1.977	1.98	1.963	1.97	1.960	1.959
Ti	0.005	0.01	0.005	0.01	0.006	0.01	0.009	0.01	0.001	0.005
Al	0.407	0.42	0.419	0.42	0.367	0.37	0.312	0.31	0.046	0.088
Cr	0.002	0.00	0.002	0.00	0.004	0.00	0.007	0.01	0.012	0.030
Fe	0.071	0.07	0.065	0.07	0.150	0.15	0.100	0.10	0.058	0.040
Mn	0.001	0.00	0.001	0.00	0.002	0.00	0.001	0.00	0.003	0.002
Ni	0.001	0.00	0.001	0.00	0.000	0.00	0.000	0.00	0.001	0.002
Mg	0.605	0.60	0.599	0.60	0.576	0.57	0.648	0.64	0.963	0.922
Ca	0.695	0.70	0.686	0.69	0.544	0.54	0.667	0.67	0.943	0.891
Na	0.306	0.31	0.315	0.31	0.413	0.41	0.320	0.32	0.041	0.082
TOTAL	4.018	4.02	4.017	4.01	4.038	4.04	4.028	4.03	4.030	4.018
Mg/Mg+Fe	0.895	0.90	0.902	0.90	0.794	0.79	0.867	0.87	0.943	0.959
Fe/Mg+Fe	0.105	0.10	0.098	0.10	0.206	0.21	0.133	0.13	0.057	0.041
Ca/Ca+Mg+Fe	0.507	0.51	0.508	0.51	0.428	0.43	0.471	0.48	0.480	0.481

- Cations calculated on the basis of 6 oxygens.
- Unless otherwise indicated rims were analysed adjacent to garnet grains.

APPENDIX 3C CONTINUED: COMPOSITIONS OF SECONDARY CLINOPYROXENE

SAMPLE	(19C)	(73)	(107)	(267)	(143)
ROCK TYPE	D	H	D	D	GH
	Core	Core	Core	Core	Core
n	4	2	4	4	2
SiO2	52.64	54.11	54.17	54.10	50.85
TiO2	1.04	0.04	0.35	0.05	0.79
Al2O3	1.00	1.17	0.41	0.60	6.41
Cr2O3	0.40	0.56	0.69	1.50	0.73
FeO	3.64	1.67	3.17	2.70	2.49
MnO	0.12	0.08	0.09	0.11	0.11
NiO	0.04	0.02	0.04	0.04	0.02
MgO	17.29	17.53	19.01	16.62	15.37
CaO	22.70	24.57	20.82	22.18	21.76
Na2O	0.66	0.64	0.88	1.43	1.28
TOTAL	99.53	100.39	99.64	99.32	99.80

APPENDIX 3D: OLIVINE COMPOSITIONS

SAMPLE	(142)		(156)	(143)		(144)		(145)		(149)	
ROCK TYPE	GL		GL	GH		GH		GH		GH	
	Core	Rim	Core	Core	Rim	Core	Rim	Core	Rim	Core	Rim
n	14	9	6	8	7	10	11	14	8	10	3
SiO2	41.56	41.21	40.95	41.48	41.02	41.19	40.79	40.61	40.38	41.04	40.45
FeO	7.03	7.80	7.56	6.69	9.45	7.21	9.87	7.80	9.51	7.04	8.97
MnO	0.08	0.10	0.09	0.07	0.13	0.07	0.09	0.06	0.09	0.09	0.14
NiO	0.39	0.40	0.42	0.41	0.28	0.41	0.35	0.38	0.39	0.40	0.28
MgO	51.19	50.52	50.38	51.83	49.63	50.96	49.36	51.22	49.79	51.47	49.75
CaO	0.00	0.02	0.00	0.01	0.02	0.01	0.01	0.02	0.01	0.01	0.07
TOTAL	100.25	100.50	99.41	100.49	100.52	99.85	100.46	100.10	100.19	100.05	99.78
Si	1.003	1.00	0.990	0.998	0.999	1.000	0.996	0.988	0.989	0.994	0.990
Fe	0.142	0.16	0.153	0.135	0.192	0.146	0.202	0.159	0.195	0.143	0.180
Mn	0.002	0.00	0.002	0.001	0.003	0.001	0.002	0.001	0.002	0.002	0.000
Ni	0.008	0.01	0.008	0.008	0.005	0.008	0.007	0.007	0.008	0.008	0.010
Mg	1.842	1.83	1.815	1.859	1.801	1.844	1.797	1.857	1.818	1.858	1.820
Ca	0.000	0.00	0.000	0.000	0.001	0.000	0.000	0.000	0.000	0.000	0.000
TOTAL	2.997	3.00	2.968	3.002	3.001	3.000	3.004	3.012	3.011	3.006	3.010
Mg/Mg+Fe	0.928	0.92	0.922	0.932	0.903	0.926	0.899	0.921	0.903	0.929	0.910
Fe/Mg+Fe	0.072	0.08	0.078	0.068	0.097	0.074	0.101	0.079	0.097	0.071	0.090

SAMPLE	(154)		(148)	(261)		(283)		(258)		(18)	(19A)
ROCK TYPE	GH		H	H		GW		GD		GD	D
	Core	Rim	Core	Core	Rim	Core	Rim	Core	Rim^{avg}	Core	Core
n	13	3	7	4	2	14	13	10	9	11	8
SiO2	41.27	41.15	40.77	40.11	40.10	40.35	40.33	40.70	40.80	39.64	40.54
FeO	6.79	7.89	7.60	7.85	7.89	10.39	10.56	7.69	7.69	12.59	11.17
MnO	0.05	0.06	0.09	0.11	0.12	0.08	0.08	0.09	0.08	0.20	0.18
NiO	0.42	0.35	0.43	0.36	0.35	1.00	0.97	0.38	0.38	0.28	0.36
MgO	51.88	50.35	50.64	50.46	50.56	48.14	48.04	50.92	50.70	46.71	47.92
CaO	0.01	0.00	0.00	0.00	0.00	0.00	0.00	0.01	0.01	0.01	0.00
TOTAL	100.43	99.80	99.54	98.88	99.02	99.96	99.99	99.79	99.65	99.42	100.17
Si	0.995	1.002	0.996	0.988	0.987	0.996	0.996	0.992	0.995	0.992	0.999
Fe	0.137	0.161	0.155	0.162	0.162	0.215	0.218	0.157	0.157	0.263	0.230
Mn	0.001	0.001	0.002	0.002	0.003	0.002	0.002	0.002	0.002	0.004	0.004
Ni	0.008	0.007	0.008	0.007	0.007	0.020	0.019	0.008	0.007	0.006	0.007
Mg	1.864	1.827	1.843	1.853	1.855	1.772	1.769	1.850	1.844	1.743	1.761
Ca	0.000	0.000	0.000	0.000	0.000	0.000	0.000	0.000	0.000	0.000	0.000
TOTAL	3.005	2.998	3.004	3.012	3.013	3.004	3.004	3.008	3.005	3.008	3.001
Mg/Mg+Fe	0.932	0.919	0.922	0.920	0.920	0.892	0.890	0.922	0.922	0.869	0.884
Fe/Mg+Fe	0.068	0.081	0.078	0.080	0.080	0.108	0.110	0.078	0.078	0.131	0.116

SAMPLE	(19B)	(19C)	(71)	(73)	(99)	(107)	(263)	(265)	(267)
ROCK TYPE	D	D	D	H	D	D	D	D	D
	Core	Core	Core	Core	Core	Core	Core	Core	Core
n	8	4	6	4	6	6	7	6	6
SiO2	39.54	40.68	40.58	40.76	40.25	40.55	39.40	40.48	40.61
FeO	13.79	10.11	7.68	9.07	8.80	9.09	13.88	8.10	9.60
MnO	0.23	0.18	0.11	0.12	0.11	0.16	0.20	0.11	0.13
NiO	0.25	0.36	0.35	0.25	0.35	0.37	0.27	0.36	0.37
MgO	46.18	49.07	50.46	49.26	49.96	50.32	45.72	50.55	48.73
CaO	0.00	0.01	0.00	0.01	0.00	0.00	0.00	0.00	0.00
TOTAL	99.99	100.41	99.18	99.47	99.47	100.49	99.47	99.60	99.44
Si	0.989	0.996	0.995	1.001	0.989	0.988	0.991	0.991	1.001
Fe	0.288	0.207	0.157	0.186	0.181	0.185	0.292	0.166	0.198
Mn	0.005	0.004	0.002	0.003	0.002	0.003	0.004	0.002	0.003
Ni	0.005	0.007	0.007	0.005	0.007	0.007	0.005	0.007	0.007
Mg	1.723	1.791	1.844	1.804	1.831	1.828	1.715	1.844	1.790
Ca	0.000	0.000	0.000	0.000	0.000	0.000	0.000	0.000	0.000
TOTAL	3.011	3.004	3.005	2.999	3.011	3.012	3.009	3.009	2.999
Mg/Mg+Fe	0.857	0.896	0.921	0.906	0.910	0.908	0.855	0.918	0.900
Fe/Mg+Fe	0.143	0.104	0.079	0.094	0.090	0.092	0.145	0.082	0.100

- Cations calculated on the basis of 4 oxygens.
- Unless otherwise indicated rims were analysed adjacent to garnet grains.

APPENDIX 3E: Cr/Al-SPINEL COMPOSITIONS

SAMPLE	(142)	(156)	(143a)	(143b)	(73)	(148)	(261a)	(261b)	(274)	(160)	(262)
ROCK TYPE	GL	GL	GH	GH	H	H	H	H	GW	AGP	GOP
n	2	9	12	2	4	1	2	2	9	3	3
TiO2	1.16	0.05	0.00	0.19	0.19	1.11	0.95	0.00	1.25	1.05	0.13
Al2O3	37.20	17.95	15.91	54.82	20.90	3.13	3.72	27.46	14.94	51.39	49.86
Cr2O3	26.70	49.66	51.64	9.79	42.97	59.91	55.52	35.12	42.05	4.62	6.52
Fe2O3	6.10	3.50	4.83	4.50	4.65	7.22	11.28	8.88	10.78	10.92	10.78
FeO	15.32	13.47	13.26	9.09	17.09	17.01	17.49	11.80	19.03	13.07	20.36
MnO	0.20	0.26	0.28	0.25	0.27	0.40	0.32	0.15	0.28	0.25	0.52
NiO	0.04	0.07	0.09	0.05	0.08	0.20	0.12	0.10	0.14	0.06	0.08
MgO	18.85	13.46	13.56	20.34	11.24	10.19	9.94	15.66	10.13	17.86	12.54
TOTAL	100.08	98.42	99.56	99.03	97.40	99.17	99.34	99.17	98.60	99.22	100.79
Ti	0.196		0.000			0.230	0.196	0.000			0.022
Al	9.842		4.748			1.015	1.206	7.751			13.018
Cr	4.737		10.333			13.030	12.068	6.648			1.142
Fe3+	1.029		0.919			1.495	2.333	1.601			1.797
Fe2+	1.846		2.807			3.914	4.022	2.362			3.771
Mn	0.038		0.060			0.093	0.075	0.030			0.098
Ni	0.007		0.018			0.044	0.027	0.019			0.014
Mg	6.305		5.115			4.178	4.073	5.588			4.139
TOTAL	24.000		24.000			24.000	24.000	24.000			24.000

SAMPLE	(266)	(258)	(18)	(19B)	(19C)	(71)	(107)
ROCK TYPE	CP	GD	GD	D	D	D	D
n	6	4	3	4	1	4	4
TiO2	0.74	0.01	2.56	1.92	1.49	0.05	1.28
Al2O3	12.06	17.27	0.19	0.26	0.31	23.81	0.38
Cr2O3	45.47	50.70	36.39	34.47	49.90	43.08	54.50
Fe2O3	12.80	3.31	28.78	30.74	17.47	3.92	13.50
FeO	18.98	14.04	24.89	22.16	21.63	12.94	20.57
MnO	0.49	0.29	0.45	0.51	0.47	0.27	0.50
NiO	0.07	0.04	0.25	0.25	0.14	0.09	0.13
MgO	9.84	13.06	5.22	6.08	6.79	14.42	7.41
TOTAL	100.45	98.71	98.73	96.39	98.20	98.58	98.27
Ti		0.002					
Al		5.175					
Cr		10.188					
Fe3+		0.633					
Fe2+		2.984					
Mn		0.062					
Ni		0.040					
Mg		4.948					
TOTAL		24.000					

- Cations calculated on the basis of 32 oxygens.

APPENDIX 3F: Fe/Ti-OXIDE COMPOSITIONS

SAMPLE	(72)	(264)	(283a)	(283b)	(147)	(273)
ROCK TYPE	GW	GW	GW	GW	GOP	E
n	2	5	3	8	3	1
TiO2	1.69	1.32	20.90	1.58	24.13	51.95
Al2O3	3.98	4.34	0.63	3.93	0.41	0.39
Cr2O3	5.23	6.63	1.81	4.61	2.59	0.38
Fe2O3	57.50	58.00	28.07	58.92	18.74	-
FeO	26.60	25.88	47.17	26.64	51.18	37.10
MnO	0.16	0.19	0.06	0.19	0.14	0.27
NiO	1.44	1.41	0.21	1.52	0.05	0.09
MgO	3.39	4.06	2.29	3.37	1.11	8.88
TOTAL	99.99	101.82	101.14	100.75	98.35	99.06
Ti			4.595	0.346		
Al			0.217	1.348		
Cr			0.418	1.060		
Fe3+			6.175	12.900		
Fe2+			11.533	6.482		
Mn			0.015	0.047		
Ni			0.998	0.308		
Mg			0.049	1.470		
TOTAL			24.000	24.000		

- Cations calculated on the basis of 32 oxygens.

APPENDIX 3G: AMPHIBOLE COMPOSITIONS

SAMPLE	(143)	(72)	(264)	(280)	(275)	(18)	(19B)
ROCK TYPE	GH	GW	GW	GW	E	GD	D
n	6	3	3	4	4	4	4
SiO2	45.67	42.98	44.87	44.28	41.26	54.30	55.11
TiO2	0.02	0.62	0.34	1.24	2.01	0.15	0.10
Al2O3	11.17	12.12	12.00	12.14	15.33	0.43	0.28
FeO	2.37	4.86	4.67	5.76	10.27	2.59	2.51
MnO	0.03	0.03	0.04	0.05	0.12	0.04	0.07
MgO	19.67	18.00	18.86	16.75	14.46	21.94	22.08
CaO	10.14	10.75	12.05	10.69	9.45	5.56	5.61
Na2O	3.35	2.28	2.45	2.67	3.62	4.36	4.60
K2O	0.93	1.53	0.32	1.69	1.07	4.37	4.33
TOTAL	93.34	93.19	95.58	95.28	97.58	93.74	94.69

APPENDIX 3H: PHLOGOPITE COMPOSITIONS

SAMPLE	(280)	(275)	(19A)	(19B)	(107)	(267)
ROCK TYPE	GW	E	D	D	D	D
n	4	4	4	2	4	4
SiO2	44.28	40.05	44.88	40.04	41.43	41.99
TiO2	1.24	1.26	0.12	0.08	0.19	0.49
Al2O3	12.14	15.97	6.54	8.12	9.80	10.93
FeO	5.76	10.30	4.92	7.84	4.76	3.67
MnO	0.05	0.08	0.03	0.04	0.03	0.01
MgO	16.75	16.91	24.61	25.12	25.75	25.50
CaO	10.69	4.50	1.12	0.26	0.00	0.02
Na2O	2.67	2.32	1.06	0.14	0.21	0.27
K2O	1.69	5.04	8.75	10.22	10.40	10.01
TOTAL	95.28	96.44	92.03	91.86	92.55	92.88

APPENDIX 4: THERMOBAROMETRY EQUATIONS USED FOR THIS STUDY

GEOTHERMOMETERS

WELLS, 1977 (pyroxene solvus)

$$T = \frac{7341}{[3.355 + 2.44(X^{Opx.Fe}) - \ln K]} \qquad (1)$$

where: $X^{Opx.Fe} = Fe^{2+}/(Fe^{2+} + Mg^{2+})$ in orthopyroxene.

K = (activity of $Mg_2Si_2O_6$ in Cpx)/(activity of $Mg_2Si_2O_6$ in Opx)

The activity of $Mg_2Si_2O_6$ in ortho- and clinopyroxene is estimated using the ideal two-site solution model of Wood and Banno (1973).

FINNERTY AND BOYD, 1987 (pyroxene solvus)

$$X^{Cpx.En} = [T/(2116 + 0.63P)]^{4.75} \qquad (2)$$

where: $X^{Cpx.En} = 1 - [2Ca/(Ca+Mg)]$ in clinopyroxene.

HARLEY, 1984 (Fe-Mg exchange between garnet and orthopyroxene)

$$T = \frac{3740 + 1400(X^{Gt.Ca}) + 22.86P}{R\ln K_D + 1.96} \qquad (3)$$

where: $K_D = (Fe/Mg)^{Gt}/((Fe/Mg)^{Opx}$

$X^{Gt.Ca} = Ca/(Ca + Mg + Fe)$ in garnet.

In all cases temperature is in ^{o}K and pressure is in kb.

APPENDIX 4 CONTINUED:

O'NEILL AND WOOD, 1979, 1980 (Fe-Mg exchange between garnet and olivine)

$$T = \frac{902 + DV + (X^{Ol.Mg} - X^{Ol.Fe})[498 + 1.51(P - 30)] - 98(X^{Gt.Mg} - X^{Gt.Fe}) + 1347(X^{Gt.Ca})}{\ln K_D + 0.357} \qquad (4)$$

where: $DV = -\{462.5[1.0191 + (T - 1073)(2.87 \times 10^{-5})][P - (2.63 \times 10^{-4})P^2 - 29.76]\}$
$-\{262.4[1.0292 + (T - 1073)(4.5 \times 10^{-5})][P - (3.9 \times 10^{-4})P^2 - 29.65]\}$
$+\{454[1.020 + (T - 1073)(2.84 \times 10^{-5})][P - (2.36 \times 10^{-4})P^2 - 29.79]\}$
$+\{278.3[1.0234 + (T - 1073)(2.3 \times 10^{-5})][P - (4.5 \times 10^{-4})P^2 - 29.6]\}$

$K^D = (X^{Ol.Mg}.X^{Gt.Fe})/(X^{Ol.Fe}.X^{Gt.Mg})$
$X^{Ol.Mg} = Mg/(Mg + Fe)$ in olivine
$X^{Ol.Fe} = Fe/(Mg + Fe)$ in olivine
$X^{Gt.Mg} = Mg/(Mg + Fe + Ca)$ in garnet
$X^{Gt.Fe} = Fe/(Mg + Fe + Ca)$ in garnet
$X^{Gt.Ca} = Ca/(Mg + Fe + Ca)$ in garnet

Because the DV term involves temperature, equation (4) is best solved using an iterative procedure, starting with an estimated temperature (T^0) and a pressure value calculated by substituting T^0 into a suitable barometric equation (e.g. 6 and 7 below).

ELLIS AND GREEN, 1979 (Fe-Mg exchange between garnet and clinopyroxene)

$$T = \frac{3104(X^{Gt.Ca}) + 3030 + 10.86P}{\ln K_D + 1.9034} \qquad (5)$$

where: $K_D = \frac{[(Fe^{2+}/Mg^{2+})^{Gt}]}{[(Fe^{2+}/Mg^{2+})^{Cpx}]}$

$X^{Gt.Ca} = Ca/(Ca + Mg + Fe + Mn)$ in garnet.

In all cases temperature is in ^oK and pressure is in kb.

APPENDIX 4 CONTINUED:

GEOBAROMETERS

NICKEL AND GREEN, 1985 (Al content of orthopyroxene)

$$P = \{1/-[183.3 + 178.98X^{M1.Al}(1 - X^{M1.Al})]\}\{-RT\ln[(1 - X^{Gt.Ca})^3(X^{Gt.Al})^2 \quad (6)$$
$$(X^{M1.Mg.Fe}(X^{M2.Mg.Fe})^2X^{M1.Al})^{-1}] - 9000(X^{Gt.Ca})^2$$
$$- 3400[2(X^{Gt.Cr})^2 - (X^{M1.Mg})(X^{M1.Cr})] - (X^{Gt.Ca})(X^{Gt.Cr})(90853 - 52.1T)$$
$$- 7590(X^{Gt.Fe})(X^{Gt.Ca}) + 5157(X^{M1.Mg})(X^{M1.Fe}) + 6047 - 3.23T\}$$

where: $X^{M1.Al} = (Al - Cr - 2Ti + Na)/2$ in orthopyroxene.

$X^{M1.Mg.Fe} = 1 - X^{M1.Al} - Cr - Ti$ " " .

$X^{M2.Mg.Fe} = 1 - Ca - Na - Mn$ " " .

$X^{M1.Mg} = [Mg/(Mg + Fe)]X^{M1.Mg.Fe}$ " " .

$X^{M1.Fe} = [Fe/(Mg + Fe)]X^{M1.Mg.Fe}$ " " .

$X^{M1.Cr} = Cr/(Cr + X^{M1.Al} + X^{M1.Mg.Fe})$ " " .

$X^{M2.Mg} = [Mg/(Mg + Fe)]X^{M2.Mg.Fe}$ " " .

$X^{Gt.Ca} = Ca/(Ca + Mg + Fe + Mn)$ in garnet.

$X^{Gt.Al} = Al/(Al + Cr)$ " " .

$X^{Gt.Cr} = Cr/Al + Cr)$ " " .

$X^{Gt.Ca} = Fe/(Ca + Mg + Fe + Mn)$ " " .

FINNERTY AND BOYD, 1984 (Al content of orthopyroxene)

$$P = \frac{1.46T - 3736 - \ln(Al_2O_3/100)T}{97.1} \quad (7)$$

where: Al_2O_3 = weight percent Al_2O_3 in orthopyroxene coexisting with garnet.

In all cases temperature is in ^oK and pressure is in kb.